Chemical Neurobiology of the Histone Lysine Demethylase KDM1A

Chemical Neurobiology of the Histone Lysine Demethylase KDM1A

A dissertation presented

by

Emily Ricq

to

The Department of Chemistry and Chemical Biology

in partial fulfillment of the requirements

for the degree of

Doctor of Philosophy

in the subject of

Chemistry

Harvard University

Cambridge, Massachusetts

May, 2016

Dissertation advisors: Dr. Stephen Haggarty, Dr. Jacob Hooker Emily Ricq

Chemical Neurobiology of the Histone Lysine Demethylase KDM1A

Abstract

Epigenetic mechanisms regulate gene expression and mediate interactions between genetic factors and environmental exposures. The enzymes responsible for epigenetic regulation may thus be important therapeutic targets for multifactorial neurological syndromes. KDM1A, the first histone lysine demethylase to be discovered, regulates the maturation of neurons and is inactivated by non-selective monoamine oxidase inhibitors such as the antidepressant tranylcypromine. This thesis entails the development of small-molecule tools to study KDM1A in a neurobiological context, with application towards the development of new therapeutic agents.

We leveraged the chemical scaffold of tranylcypromine to generate novel KDM1A inhibitors. In chapter 2, we profile these analogs using biochemical, cellular, and *in vivo* assays. We show that RN1 potently inhibits KDM1A, exhibits high brain uptake, and affects the behavior of mice in a novel object recognition assay. Thermal shift assays reveal engagement of KDM1A by tranylcypromine in the brains of systemically-treated rats, suggesting that inhibition of KDM1A by non-selective antidepressants in a clinical setting warrants further examination.

We sought to discover new mechanisms of KDM1A inhibition in order to gain further selectivity versus the monoamine oxidases. In chapter 3, we present outcomes of a high-throughput screen and secondary assays which reveal a predominant mode of KDM1A inhibition based on thiol-reactivity, and widespread contamination of test compounds by elemental sulfur. We show that KDM1A is inhibited by the FDA-approved drug disulfiram, and disclose two novel scaffolds for medicinal chemistry development.

In chapter 4, we further profile the thiol-reactivity of KDM1A and show that catalytically-generated hydrogen peroxide negatively regulates demethylase activity. MALDI-TOF mass spectrometry

indicates that hydrogen peroxide blocks labeling of cysteine 600, which we propose forms an intramolecular disulfide bond with cysteine 618. This activity-dependent regulation is unique among histone-modifying enzymes but consistent with redox sensitivity of epigenetic regulators. KDM1A may use this thiol/disulfide switch as a mechanism to sense other cellular oxidants, such as the monoamine neurotransmitter dopamine.

CONTENTS

LIST OF FIGURES vii
LIST OF TABLES viii
CONTRIBUTIONS ix
ACKNOWLEDGEMENTS xi
CHAPTER 1 1
1 KDM1A is a candidate target for neurological disease 1
1.1 Abstract 1
1.2 Rationale for targeting histone lysine methylation 1
1.3 KDM1A is inactivated by antidepressant monoamine oxidase inhibitors 3
1.3.1 Monoamine oxidase neuropharmacology – a historical perspective 3
1.3.2 KDM1A is a lysine demethylase and nuclear amine oxidase 5
1.3.3 Molecular pharmacology of the lysine and monoamine oxidases 6
1.4 KDM1A regulates neuronal development 8
1.4.1 Distinct KDM1A complexes regulate neuronal gene expression programs 8
1.4.2 Neurospecific isoforms of KDM1A regulate neurite growth and excitability 10
1.4.3 Human genetics implicate KDM1A mutations in neurodevelopmental disorders 11
1.5 Conclusion 12
1.6 References 12
CHAPTER 2 18
2 Neuropharmacology of FAD-directed KDM1A inhibitors 18
2.1 Abstract 18
2.2 Introduction 19
2.3 Results and Discussion 20
2.3.1 Development of orthogonal KDM1A/B and MAO-A/B inhibition assays 20
2.3.2 Identification of TCP-derivative RN1 as a highly potent KDM1A inhibitor 23
2.3.3 Kinetics of RN1-inactivation of KDM1A 25
2.3.4 Functional inhibition of cellular KDM1A by RN1 27
2.3.5 The cellular thermal shift assay reveals target engagement of KDM1A inhibitors 29
2.3.6 RN1 is brain-penetrant and affects novel object preference in behaving rodents 34
2.4 Conclusions 36

2.5 Materials and Methods 37
2.6 References 46
CHAPTER 3 51
3 Screening efforts towards the discovery of novel KDM1A inhibitors 51
3.1 Abstract 51
3.2 Introduction 51
3.3 Results and Discussion 53
3.3.1 High throughput screening strategy 53
3.3.2 Discovery of contamination of lead compounds by elemental sulfur (S_8) 55
3.3.3 Multiple classes of thiol-reactive compounds potently inhibit KDM1A 57
3.3.4 Assessment of non-thiol reactive KDM1A inhibitors in cellular assays 60
3.3.5 Assessment of KDM1A inhibitors in Wnt signaling pathway reporter assay 61
3.4 Conclusion 63
3.5 Materials and Methods 64
3.6 References 71
CHAPTER 4 75
4 Activity-Dependent Regulation of KDM1A by a Putative Thiol/Disulfide Switch 75
4.1 Abstract 75
4.2 Introduction 75
4.3 Results and Discussion 77
4.3.1 KDM1A is reversibly inhibited by thiol-reactive compounds 77
4.3.2 Cysteine Modification alters KDM1A conformation 82
4.3.3 Cys600 is Modified by Biotin-Mal and Forms a Putative Disulfide with Cys618 84
4.3.4 KDM1A is reversibly inhibited by H_2O_2 in vitro 86
4.3.5 Activity-dependent oxidation of KDM1A 88
4.3.6 Exogenous dopamine synergizes with KDM1A inhibitors and oxidizes KDM1A 90
4.4 Conclusion 92
4.5 Materials and Methods 95
4.6 References 102
APPENDIX A 106
Supplementary Material 106

LIST OF FIGURES

Figure 1.1 Chemical structures of select irreversible monoamine oxidase inhibitors. 4
Figure 1.2 The FAD-dependent amine oxidases oxidatively deaminate their substrates. 6
Figure 1.3 Crystal structures of KDM1A, KDM1B, MAO-A, and MAO-B. 7
Figure 1.4 KDM1A-RCOR1 complexes critical to the regulation of neuronal genes. 9
Figure 2.1 Schematic representation of KDM1A/B and MAOA/B in vitro enzymatic assays. 21
Figure 2.2 Covalent inactivation of KDM1A by TCP and RN1 26
Figure 2.3 RN1 inhibits full-length KDM1A but does not increase cellular H3K4me2 levels 29
Figure 2.4 Live-cell CETSA profiling of KDM1A and RCOR1. 30
Figure 2.5 TCP potently engages KDM1A by live-cell CETSA. 32
Figure 2.6 TCP engages KDM1A by in vivo CETSA 33
Figure 2.7 RN1 is brain-penetrant and affects rodent behavior. 34
Figure 3.1 Summary of screening strategy to discover novel inhibitors of KDM1A. 54
Figure 3.2 KDM1A is potently inhibited by elemental sulfur. 57
Figure 3.3 Representative structures of eliminated high throughput screening hits. 58
Figure 3.4 Counterscreening reveals two DTT-insensitive inhibitors of KDM1A. 59
Figure 3.5 Cellular assays with KDM-009 and KDM-093 61
Figure 3.6 KDM1A inhibitors in the Wnt signaling pathway 62
Figure 4.1 Chemical structures of thiol-reactive KDM1A inhibitors. 78
Figure 4.2 KDM1A is reversibly inhibited by thiol-reactive small molecules 80
Figure 4.3 Thiol-reactive inhibitors increase the fluorescence of KDM1A-bound FAD. 82
Figure 4.4 KDM1A forms a putative intramolecular disulfide bond. 85
Figure 4.5 Recombinant KDM1A is inhibited by hydrogen peroxide 88
Figure 4.6 Activity-dependent regulation of KDM1A. 89
Figure 4.7 Working model of KDM1A activity-dependent regulation by a thiol/disulfide redox switch. 90
Figure 4.8 Exogenous dopamine synergizes with KDM1A inhibitors and oxidizes KDM1A. 92
Supplementary Figure A.1 ^{1}H NMR spectrum of KDM-103 107
Supplementary Figure A.2 ^{13}C NMR spectrum of KDM-103 108
Supplementary Figure A.3 LC-MS of KDM-103 and elemental sulfur standard 109

LIST OF TABLES

Table 2.1 IC_{50} values for inhibition of KDM1A/B and MAO-A/B by TCP and the RN1 series of TCP-derivatives. 24
Supplementary Table A.1 Summary of thiol-reactive properties of KDM1A inhibitors 106
Supplementary Table A.2 KDM1A tryptic peptides identified by MALDI-TOF..... 110
Supplementary Table A.3 Summary of sequence coverage of KDM1A tryptic peptides. 113

CONTRIBUTIONS

Chapter 1

Emily Louise Ricq (ELR) wrote the text.

Chapter 2

Ramesh Neelamegam (RN) synthesized the RN series of inhibitors. Debasis Patnaik (DP), Stephanie Norton (SN) and ELR designed and performed the *in vitro* selectivity assays. Melissa Malvaez and Marcelo A. Wood performed and analyzed the novel object recognition assay. ELR performed all kinetic, cellular, and thermal shift assays, and wrote the text. Genevieve van der Bittner and Frederick Schroeder are thanked for their assistance with the *in vivo* CETSA. ELR, Stephen J. Haggarty (SJH), and Jacob M. Hooker (JMH) designed the project. Portions of this chapter have been published with significant changes as the following paper:

Neelamegam, R., Ricq, E. L., Malvaez, M., Patnaik, D., Norton, S., Carlin, S. M., Hill, I. T., Wood, M. A., Haggarty, S. J., and Hooker, J. M. (2011) Brain-penetrant LSD1 inhibitors can block memory consolidation. *ACS chemical neuroscience* **3**, 120-128.

Chapter 3

SN conducted the initial high-throughput screen. ELR, DP, and Krista Hennig performed secondary screening. ELR conducted all counterscreening, synthesis and characterization of KDM-103, LC-MS analysis, cellular assays, and wrote the text. Wendy Zhao is thanked for her assistance with the Wnt signaling reporter assay. ELR, JMH, and SJH designed the project.

Chapter 4

ELR designed and conducted all experiments and wrote the text. ELR, JMH, and SJH designed the project.

Portions of this chapter with minor changes have been submitted for publication as the following paper:

Ricq, E. L., Hooker, J.M, and Haggarty, S.J. (2016) Activity-Dependent Regulation of Histone Lysine Demethylase KDM1A by a Putative Thiol/Disulfide Switch. *Submitted to the Journal of Biological Chemistry.*

ACKNOWLEDGEMENTS

During graduate school I have had the privilege of working with exceptional colleagues. First, I would like to thank my advisors, Jacob Hooker and Steve Haggarty, for their support, guidance, and for providing a dynamic environment in which I was exposed to many disciplines, from synthetic chemistry to functional neuroimaging. I learned tremendously from both Jacob and Steve's approaches to science and have gained a unique appreciation for the scope of translation neurobiology research.

I would also like to thank Ralph Mazitschek, Jack Szostak, and Tobias Ritter for serving on my graduate advisory committee, for advice and for stimulating discussions.

In the Hooker lab, I would like to especially thank Ramesh Neelamegam and Himashinie Diyabalanage for their guidance with my rotation project and for their roles in establishing the Hooker lab. I also learned tremendously from working and writing with Genevieve van der Bittner and Al Schroeder and thank them for being excellent colleagues. It has been incredible to witness the Hooker lab blossom into a full-fledged research group.

Most of what I now know about biology was learned in the Haggarty lab and is due in large part to fantastic training by Debasis Patnaik, Krista Hennig, Wendy Zhao, and Surya Reis. From showing me how to run enzymatic assays, culture cells, and run western blots, their patience and expertise was instrumental to my project. I would also like to thank Stephanie Norton for her pioneering work on the KDM1A inhibitor screen.

Outside of the lab, Cambridge has been a wonderful home thanks to my delightfully eccentric friends. Thanks to Hannah, Yuri, Carolyn, David, Noam, Chelsea, Red, Steve and Mike for the intergalactic abbey, onesie karaoke, dino island, and many other happy memories. I'm looking forward to many more game nights (and lab days) with Sonia and Eric.

I would like to thank my parents, Philippe and Susan, for encouraging me to pursue my interests and for providing me support and motivation for my work. In particular, I would like to thank my brother Jeremy for being my inspiration for this dissertation. Finally, none of this would have been possible without constant love and companionship from my most excellent partner, Kyle. Truly, you are the better half of this horse.

CHAPTER 1

1 KDM1A is a candidate target for neurological disease

1.1 Abstract

Epigenetic mechanisms such as histone lysine methylation regulate gene expression and mediate interactions between genetic factors and environmental exposures. The enzymes responsible for epigenetic regulation may thus be important therapeutic targets for multifactorial neurological syndromes. Here, we review pharmacological, biochemical, and genetic evidence implicating lysine specific demethylase 1 (KDM1A, also known as LSD1) as a critical mediator of neuronal function. KDM1A is a nuclear amine oxidase, and is inhibited by non-selective antidepressants such as tranylcypromine. As part of multi-subunit complexes, KDM1A demethylase activity contributes to the coordinated control of neuronal gene expression programs. Alternative splicing generates a neurospecific isoform of KDM1A which dynamically regulates neurite growth and excitability. Human patients with mutations in *KDM1A* have a neurodevelopmental syndrome with cognitive impairment. Collectively, these observations motivate the development of small-molecule tools to study KDM1A in a neurobiological context, with application towards the development of new therapeutic agents.

1.2 Rationale for targeting histone lysine methylation

The mammalian brain dynamically activates or silences gene programs in response to environmental input and developmental cues. This neuroplasticity is controlled by signaling pathways that modify the activity, localization, and/or expressio°n of transcriptional-regulatory enzymes in combination with alterations in chromatin structure in the nucleus (1). Consistent with this conceptual framework, mutations in dozens of distinct chromatin regulators have been causally implicated in human

neurodevelopmental and psychiatric disorders (2). Furthermore, environmental factors including perinatal infection, malnutrition and neglect appear to increase the risk of the heterogeneous, multifactorial neurological disorders *via* epigenetic mechanisms (3). Alterations in chromatin state and transcriptional programs may also be relevant in adulthood, and are implicated in various aspects of experience-dependent plasticity, including learning and memory, stress responsivity, and cognition (4,5). Importantly, epigenetic regulation of gene expression is dynamic, and the enzymes responsible for chromatin modification may be targets for new and critically-needed therapeutic interventions. However, the control of gene expression is complex and multilayered, and the rational design of small-molecules to modulate epigenetic function is far from straightforward (6).

The best-characterized chromatin regulatory mechanism, both in and out of the brain, is the post-translational covalent modification of histone proteins (7). Such modifications include histone lysine methylation, which can either promote or repress gene activity depending on the extent of methylation and its context (8). Histone lysine methylation is maintained by dynamic opposition of methyltransferase and demethylase enzymes, both of which are implicated in neurodevelopmental and neuropsychiatric disease and in memory formation (9,10). Pathways regulating the methylation of one particular residue, lysine 4 of histone H3 (H3K4), have recently been identified to have the strongest genome-wide association across three adult psychiatric disorders: schizophrenia, major depression and bipolar disorder (11). Here, we profile one enzyme responsible for the removal of H3K4 methylation, the lysine specific demethylase 1 (KDM1A, also known as LSD1). KDM1A is found throughout the brain, with peak expression during embryonic development (12,13). Two lines of evidence have provoked our interest in KDM1A. First, KDM1A is inhibited by certain non-selective antidepressants. This observation may be clinically relevant and provides a framework for the development of chemical tools to profile KDM1A in the brain. Second, biochemical and genetic studies point towards a critical role for KDM1A in the regulation of neuronal development. The development of chemical tools to study KDM1A in a neurobiological context comprises

the body of this thesis. Other therapeutic indications for KDM1A, for example in cancer and viral replication, are reviewed elsewhere (14-17).

1.3 KDM1A is inactivated by antidepressant monoamine oxidase inhibitors

1.3.1 Monoamine oxidase neuropharmacology – a historical perspective

In the early 1950s, arylalkylhydrazines such as the drug iproniazid (Marsilid) were discovered to be anti-tuberculosis agents by phenotypic screening in infected mice (18). These compounds were synthetic intermediates to the thiosemicarbazones compounds known to kill *Mycobacterium tuberculosis*, but they were much more potent and quickly entered the clinic (19). Two decades earlier, the monoamine oxidase (MAO) was discovered to be responsible for oxidative deamination of biogenic amines in the central nervous system and periphery. It was quickly uncovered that iproniazid inhibits MAO, and that administration of iproniazid to laboratory animals produced a rapid increase in brain levels of serotonin (20). At the same time, tuberculosis patients treated with iproniazid were reported to have elevated mood, increased sociability, and improved quality of sleep (18). Several years elapsed until these side effects were recognized as representing a new class of drug, an antidepressant, and iproniazid found clinical success (21). The concurrent discovery of the antidepressant qualities of iproniazid and the antipsychotic properties of chlorpromazine and reserpine laid the foundation for much of modern neuropharmacology (22).

In the decades that followed, MAO was shown to use a flavin adenine dinucleotide (FAD) cofactor to oxidize its substrates, which include not only the biogenic amines, serotonin and the catecholamines, but other, sympathomimetic amines including tyramine, benzylamine, and phenylethylamine (18). In addition, two isozymes of MAO, MAO-A and MAO-B were described. Both flavoproteins are bound to the outer mitochondrial membrane and oxidize dopamine and tyramine. MAO-A preferentially deaminates adrenaline, noradrenaline and serotonin, and is implicated in the antidepressant properties of MAO

inhibitors; in contrast, MAO-B metabolizes benzylamine and phenylethylamine, and is a target for neurodegenerative disorders (19).

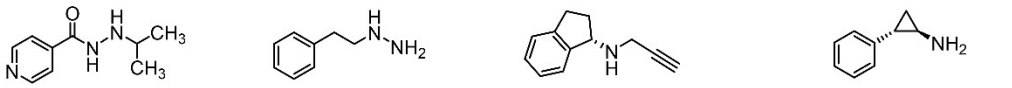

ipronaizid
(Marsilid)
hydrazine

phenelzine
(Nardil)
hydrazine

rasagiline
(Azilect)
propargylamine

tranylcypromine (TCP)
(Parnate)
cyclopropylamine

Figure 1.1 Chemical structures of select irreversible monoamine oxidase inhibitors.

Medicinal chemistry efforts to further improve the potency of iproniazid lead to the development of three main classes of irreversible monoamine oxidase inhibitors: hydrazines, propargylamines, and cyclopropylamines (Figure 1.1) (18). *A posteriori* biochemical analysis has revealed that these drugs function through covalent modification of flavin ring of the FAD cofactor (23). Hydrazines such as the antidepressant phenelzine (Nardil) are irreversible inhibitors of the MAOs, but oxidation and covalent attachment to flavin are not perfectly coupled and the precise mechanism of inhibition has yet to be fully defined (24). Propargylamines have been successfully modified to achieve selectivity between MAO-A and MAO-B, and the MAO-B selective rasaliline (Azilect) is used to treat the symptoms of early Parkinson's disease (25). The cyclopropylamine tranylcypromine (TCP; Parnate, a racemic mixture) forms a different flavin adduct through opening of the cyclopropyl ring, a mechanism distinct from the hydrazines and propargylamines, and the is a powerful antidepressant (20). Unfortunately, irreversible monoamine oxidase inhibition results in accumulation of trace sympathomimetic amines, and strict dietary restrictions to limit tyramine (found in most cheeses, chocolate, and fermented foods) are required to prevent hypertensive crisis. Newer classes of antidepressants, including reversible MAO inhibitors, have greatly improved safety profiles and have relegated TCP to the management of severe and treatment-resistant depression (20).

1.3.2 KDM1A is a lysine demethylase and nuclear amine oxidase

Protein lysine methylation is a ubiquitous cellular regulatory mechanism and plays critical roles in biology and pathobiology by regulating transcription, chromatin remodeling, cell signaling, viral pathogenesis, and protein recruitment, among other functions (17). Lysines can be mono-, di- or tri-methylated, with each modification resulting in different functional outcomes depending on the degree of methylation and its context (26). For decades, lysine methylation, as well as arginine and cytosine methylation, was presumed to be reversed only through protein turnover and degradation or cell division. This notion was challenged when KIAA0601 (aka KDM1A), a protein with homology to MAO-A/B, was found to associate with several histone deacetylase (HDAC)-containing complexes (27). In early 2004, Shi and coworkers provided the first direct evidence that KDM1A functions as an FAD-dependent histone lysine demethylase, with specificity for histone 3 lysine 4 mono- and di-methylated (H3K4me1/2) residues (28). Subsequently, another nuclear amine oxidase with H3K4me1/2 demethylase activity, KDM1B, was discovered by searching for homologous domains in genomic databases (29).

Like MAO-A/B, KDM1A and KDM1B couple the reduction of FAD to $FADH_2$ with the oxidation of the C-N methylamine bond to a hydrolytically labile iminium ion, a mechanism only compatible with mono- and di-methylated substrates (Figure 1.2) (28,30,31). Since their initial characterization as H3K4me1/2 demethylases, the substrate scope of KDM1A and KDM1B has been broadened to conditionally include H3K9me1/2 (29,32,33). Furthermore, KDM1A has been found to demethylate a small number of other nuclear proteins, including the tumor suppressor p53 (34), the maintenance DNA methyltransferase DNMT1 (35), and the HIV transactivator Tat (36). Dozens of other histone lysine demethylases have also been characterized; these demethylases belong to a separate class of JmjC domain-containing, iron (II) and α-ketoglutarate dependent oxygenases and are capable of demethylating mono-, di-, or tri-methylated substrates (37).

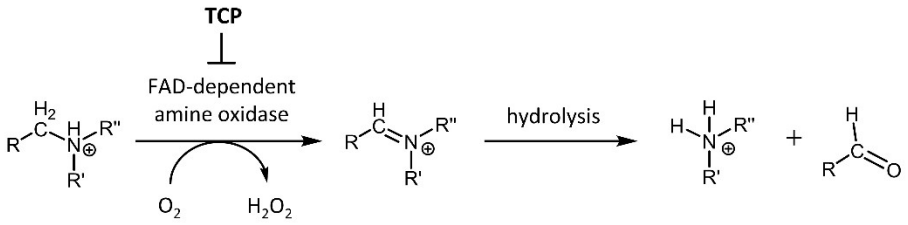

		KDM1A	KDM1B	MAO-A	MAO-B
Substrate specificity	R	H	H	dopamine, tyramine, serotonin, adrenaline	dopamine, tyramine, benzylamine, phenylethylamine
	R'	H, CH_3	H, CH_3	H	H
	R''	H3K4, H3K9, p53, DNMT1, HIV Tat	H3K4, H3K9	H	H
Subcellular localization		Nucleus	Nucleus	Mitochondria	Mitochondria
% AO Seq ID with KDM1A		-	37%	45%	39%

Figure 1.2 The FAD-dependent amine oxidases oxidatively deaminate their substrates.
The nuclear amine oxidases KDM1A/B remove methyl groups from lysine residues on histone H3, as well as other nuclear proteins. The mitochondrial amine oxidases MAO-A/B catabolize small molecule amines such as neurotransmitters. All four enzymes share considerable structural homology and sequence identity (% seq ID) in their amine oxidase catalytic domains, and all are inhibited by FAD-directed inhibitors such as TCP.

1.3.3 Molecular pharmacology of the lysine and monoamine oxidases

Motivated by the similarities in the enzymatic properties of KDM1A and MAO-A/B, McCafferty and coworkers screened a focused group of irreversible MAO inhibitors against KDM1A. The antidepressants TCP and phenelzine were found to weakly inhibit recombinant KDM1A demethylation of nucleosomes, whereas the propargylamines tested were inactive (38). Subsequent studies validated that TCP is a covalent, FAD-directed inhibitor of KDM1A and KDM1B with a mechanism of inactivation similar to that of MAO-A/B (39-41). Structural characterization of KDM1A/B and MAO-A/B by X-ray crystallography provided further evidence for the formation of TCP-FAD adducts, and provided insight to rational design of TCP analogs (Figure 1.3) (42-45)

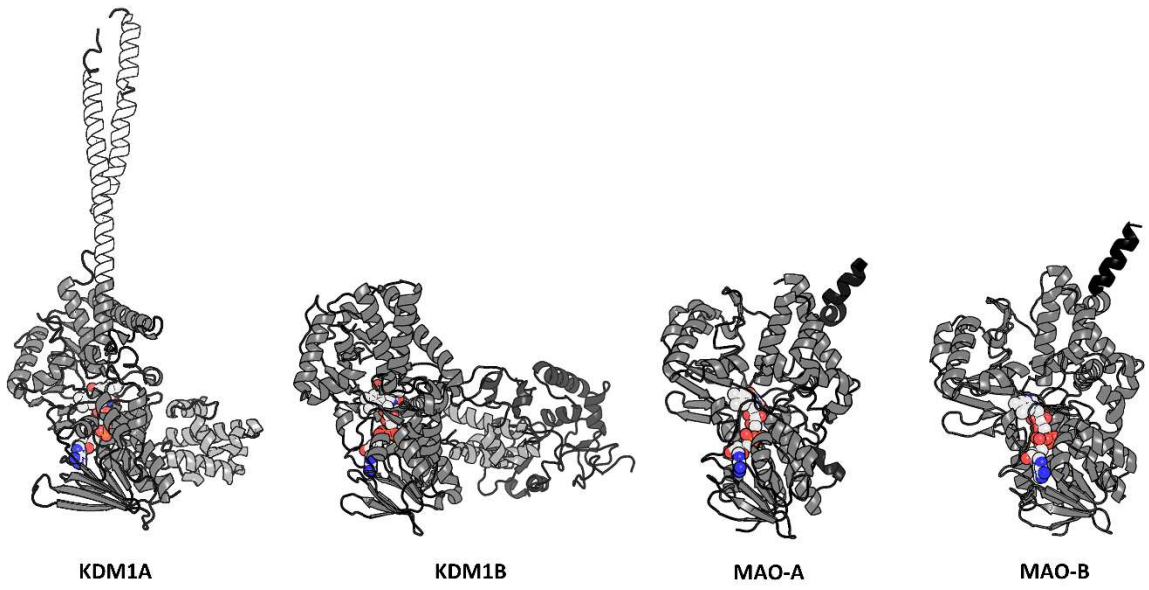

Figure 1.3 Crystal structures of KDM1A, KDM1B, MAO-A, and MAO-B.
A. Multidomain architecture. All four enzymes bind an FAD cofactor (colored spheres) in their homologous amine oxidase domains (aligned, in medium grey). The nuclear amine oxidases KDM1A and KDM1B feature a SWIRM domain (light grey). Additional protein interactions with the nuclear amine oxidases are mediated by the tower domain of KDM1A (white) and the zinc finger domain of KDM1B (dark grey). The mitochondrial amine oxidases MAO-A and MAO-B feature a helical domain (black) which enables insertion into the outer mitochondrial membrane. **B.** Substrate cavities. Surfaces are colored according to the Kyle-Doolittle hydrophobicity scale, -4.5 (most polar) = grey, 4.5 (most hydrophobic) = white. For A and B, crystal structures were accessed from the PDB: KDM1A with TCP (2EJR), KDM1B with TCP (4GUU), MAO-A with the propargylamine clorgyline (2BXS), MAO-B with TCP (2XFU).

The amine oxidase domains of KDM1A/B and MAO-A/B are homologous (37-45% sequence identity) (41,43). Both classes bind FAD through an expanded Rossmann fold, although the MAO proteins bind FAD covalently through thioether linkage between the 8α-methylene of the flavin ring and Cys406/397 in MAO-A/B, respectively, while the KDM1 proteins bind FAD non-covalently (46). The active sites of KDM1A/B feature an open cleft that accommodates the H3 N-terminal tail and other large substrates, whereas MAO-A/B feature internal cavities that are gated by surface loops (41). These structural differences have been exploited to design TCP analogs with improved potency and selectivity for KDM1A over MAO-A/B, which is paramount for studies of KDM1A function in a neurological context (15).

Packed against the amine oxidase domain in KDM1A/B is a Swi3p, Rsc8p and Moira (SWIRM) domain. SWIRM domains are mostly α-helical and are highly conserved amongst chromatin associating proteins, but the DNA-binding interface is partially blocked by amine oxidase domain in KDM1 proteins (47). Protruding from the top of the amine oxidase of KDM1A domain is a large, antiparallel coiled-coil tower domain insertion, which mediates interactions with RCOR1 (48). The N-terminal region of the enzyme has no predicted conserved structural elements, but does contain a nuclear localization signal (49). KDM1B features a unique N-terminal zinc-finger domain consisting of a C4H2C2-type zinc finger and a CW-type zinc finger (50). The multi-domain architecture of KDM1 proteins enables assembly of protein complexes and confers novel, nuclear functions for their amine oxidase chemistries.

1.4 KDM1A regulates neuronal development

1.4.1 Distinct KDM1A complexes regulate neuronal gene expression programs

KDM1A operates as a amine oxidase subunit within specific stable complexes that coordinate to perform regulatory functions (17). The identity of its binding partners directs KDM1A to specific substrates and influences the biological outcome of lysine demethylation. The earliest identified and most well-characterized interaction partner of KDM1A is RCOR1 (also known as CoREST), which acts as a scaffolding protein to link KDM1A to multiple distinct heteromeric complexes, including brain-specific complexes, and also facilitates binding to nucleosomes (28,51-55). RCOR1 frequently links KDM1A to the histone deacetylases (HDACS) 1 and 2 (17). Notably, modulation of HDAC activity with small molecules has been linked with altered memory, learning and cognition (6,56). Of about a dozen RCOR1-KDM1A complexes identified to date (17), the REST and TLX complexes are of particular importance for the regulation of neuronal genes and in the coordination of neurogenesis (Figure 1.4).

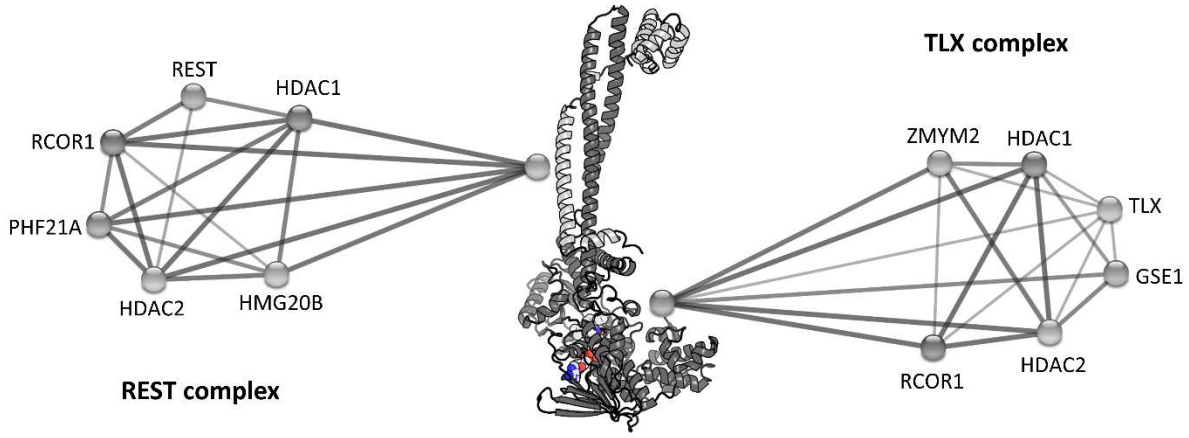

Figure 1.4 KDM1A-RCOR1 complexes critical to the regulation of neuronal genes.
KDM1A (dark grey) associates with RCOR1 (light grey). The REST complex is assembled *via* interactions with the tower domain of KDM1A and includes HDAC1/2, PHF21A, and HMG20B. The TLX complex associates with the amine oxidase and SWIRM domains of KDM1A and includes HDAC1/2, GSE1, and ZMYM2 (17). The crystal structure of KDM1A-RCOR1 was accessed from the PDB (2UXX). Diagrams of protein-protein interactions were generated using the STRING database. Lines between nodes indicate experimentally-determined interactions, and bolder line widths represent greater relative confidence for each interaction (57).

RE1-silencing transcription factor (REST) represses neuron-specific genes, such as ion channels, synaptic vesicle proteins, and neurotransmitter receptors, during cell fate decisions (58). REST jointly recruits a KDM1A-RCOR1-HDAC1/2 complex as well as a Sin3-HDAC1/2 complex to RE1 binding sites at the promoters of neuronal genes to maintain a repressed state that, in progenitor cells, is primed for activation upon neuronal differentiation (59). REST is degraded upon commitment to neuronal cell fate. Notably, the RCOR1-KDM1A complex transitions to a non-RE1 binding site to temper the expression of a subset of genes previously silenced by REST, including brain-derived neurotrophic factor (*BDNF*) (60). Alternately, upon differentiation into a non-neuronal cell type, the REST repressor complexes persist on RE1 binding sites and recruits additional corepressors to permanently silence expression of neuronal genes (17).

The orphan nuclear hormone receptor TLX maintains the proliferative and self-renewal properties of adult neural stem cells and regulates neurogenesis (61). TLX recruits KDM1A-RCOR1-HDAC1/2 *via* interactions with the amine oxidase and SWIRM domains of KDM1A, and histone lysine demethylation is

associated with transcriptional repression of TLX target genes such as *PTEN* to promote progenitor proliferation (62,63). The brain-enriched microRNA miR-137 targets *KDM1A* mRNA to accelerate neural differentiation of embryonic neural stem cells and acts as a tumor suppressor in neuroblastoma (64). In turn, TLX recruits KDM1A to genomic regions of miR-137, repressing its expression and thus forming a feedback regulatory loop to control the dynamics between neural stem cell proliferation and differentiation during neural development (65). Although both REST and TLX KDM1A-RCOR1 complexes are proposed to positively regulate neurogenesis, depletion of either RCOR1 or KDM1A by RNAi *in utero* delayed the radial migration and maturation of newborn cortical pyramidal neurons and increased the fraction of cells remaining in the progenitor state (66). Feedback loops such as the that between miR-137 and the TLX-KDM1A-RCOR1 complex may underlie this unexpected phenotype.

In contrast to KDM1A, relatively little is known about the interactions and biological significance of KDM1B, which associates with the histone binding protein NPAC but does not possess a tower domain and does not interact with RCOR1 (17). To the best of our knowledge, the role of KDM1B in neurological function has not been examined.

1.4.2 Neurospecific isoforms of KDM1A regulate neurite growth and excitability

Four mammalian isoforms of KDM1A have been described as resulting from single or double inclusion of two alternatively spliced exons, E2a and E8a. Intriguingly, the isoform retaining the E8a exon (KDM1A+8a) displays a neurospecific pattern of expression, representing one of the few examples of a chromatin-modifying enzyme devoted to neurons (67). The E8a exon is internal to the amine oxidase domain, and encodes the tetrapeptide Asp-Thr-Val-Lys. KDM1A+8a is dynamically regulated during brain development and enhances cortical neuronal maturation when overexpressed (68). Phosphorylation of the threonine residue of E8a was observed in rat brain, and a Thr369bAsp phosphomimetic fails to associate with RCOR1 and HDAC1/2 (67). Overexpression of this phosphomimetic promotes neurite

outgrowth and branching, suggesting that phosphorylation switches KDM1A+8a into a dominant negative isoform to derepress genes required for neuronal maturation. Consistent with this model, KDM1A+8a is unable to repress transcription and lacks H3K4 demethylase activity, but can act as transcriptional activator by binding the supervillin (SVIL) protein and acquiring H3K9 demethylase activity (33). In adult mice, KDM1A+8a is downregulated in response to epileptogenic stimuli, and animals lacking KDM1A+8a are hypoexcitable and have a decreased susceptibility for seizures (69). Furthermore, mice with reduced levels of KDM1A+8a display a low-anxiety phenotype in a panel of behavioral tests (70). Alternative splicing thus appears to be an important mechanism through which KDM1A can acquire switchable histone substrate specificity to fine-tuned control over gene expression programs governing neuronal differentiation.

1.4.3 Human genetics implicate KDM1A mutations in neurodevelopmental disorders

Recently, dominant missense point mutations in *KDM1A* have been identified and correlated with a new genetic disorder that phenotypically resembles Kabuki syndrome. Mutations in *KDM1A* result in skeletal abnormalities and significant cognitive impairment (71). Three cases have been reported, each with a different missense point mutation in the amine oxidase domain (Glu403Lys, Asp580Gly, and Tyr785His). All mutations are heterozygous, indicating that mutant KDM1A results in a dominant phenotype. Notably, mice with heterozygous *KDM1A* deletion appear normal, whereas homozygous *KDM1A*$^{-/-}$embryos are not viable (72). Biochemical analyses of all three KDM1A mutants found in human disease revealed weaker substrate binding and substantially reduced cellular protein stability (73). However, all KDM1A mutants retained binding to RCOR1 and HDAC1/2, and maintained their ability to repress a synthetic reporter gene. Thus, subtle mutations in KDM1A are associated with cognitive impairment, but additional studies will be required to clarify the mechanisms resulting in developmental neuropathology.

1.5 Conclusion

KDM1A is critical for brain development and for the coordination of neuronal gene expression programs. Pharmacological inhibition of KDM1A may be partially responsible for the therapeutic efficacy of the antidepressant TCP, and genetic reduction of a neurospecific isoform of KDM1A is associated with reduced anxiety and reduced susceptibility to seizures. However, the regulation of gene expression by epigenetic machinery is multilayered and involves feedback loops, complicating the rational design of small-molecules tool compounds. Collectively, these observations motivate the development of new small-molecule probes to empirically study KDM1A in a neurobiological context, with application towards the development of new therapeutic agents.

1.6 References

1. McClung, C. A., and Nestler, E. J. (2008) Neuroplasticity mediated by altered gene expression. *Neuropsychopharmacology* **33**, 3-17

2. Ronan, J. L., Wu, W., and Crabtree, G. R. (2013) From neural development to cognition: unexpected roles for chromatin. *Nature Reviews Genetics* **14**, 347-359

3. Millan, M. J. (2013) An epigenetic framework for neurodevelopmental disorders: from pathogenesis to potential therapy. *Neuropharmacology* **68**, 2-82

4. Maze, I., Noh, K.-M., and Allis, C. D. (2013) Histone regulation in the CNS: basic principles of epigenetic plasticity. *Neuropsychopharmacology* **38**, 3-22

5. Nestler, E. J., Peña, C. J., Kundakovic, M., Mitchell, A., and Akbarian, S. (2015) Epigenetic Basis of Mental Illness. *The Neuroscientist*, 1073858415608147

6. Szyf, M. (2015) Prospects for the development of epigenetic drugs for CNS conditions. *Nature Reviews Drug Discovery* **14**, 461-474

7. Jenuwein, T., and Allis, C. D. (2001) Translating the histone code. *Science* **293**, 1074-1080

8. Black, J. C., Van Rechem, C., and Whetstine, J. R. (2012) Histone lysine methylation dynamics: establishment, regulation, and biological impact. *Molecular cell* **48**, 491-507

9. Akbarian, S., and Huang, H.-S. (2009) Epigenetic regulation in human brain—focus on histone lysine methylation. *Biological psychiatry* **65**, 198-203

10. Gupta, S., Kim, S. Y., Artis, S., Molfese, D. L., Schumacher, A., Sweatt, J. D., Paylor, R. E., and Lubin, F. D. (2010) Histone methylation regulates memory formation. *The Journal of neuroscience* **30**, 3589-3599

11. Network, T., and Consortium, P. A. S. o. t. P. G. (2015) Psychiatric genome-wide association study analyses implicate neuronal, immune and histone pathways. *Nature neuroscience* **18**, 199-209

12. Hawrylycz, M. J., Lein, E. S., Guillozet-Bongaarts, A. L., Shen, E. H., Ng, L., Miller, J. A., van de Lagemaat, L. N., Smith, K. A., Ebbert, A., and Riley, Z. L. (2012) An anatomically comprehensive atlas of the adult human brain transcriptome. *Nature* **489**, 391-399

13. Sáez, J. E., Gómez, A. V., Barrios, Á. P., Parada, G. E., Galdames, L., González, M., and Andrés, M. E. (2015) Decreased expression of CoREST1 and CoREST2 together with LSD1 and HDAC1/2 during neuronal differentiation. *PloS one* **10**, e0131760

14. Højfeldt, J. W., Agger, K., and Helin, K. (2013) Histone lysine demethylases as targets for anticancer therapy. *Nature reviews Drug discovery* **12**, 917-930

15. Zheng, Y. C., Ma, J., Wang, Z., Li, J., Jiang, B., Zhou, W., Shi, X., Wang, X., Zhao, W., and Liu, H. M. (2015) A Systematic Review of Histone Lysine-Specific Demethylase 1 and Its Inhibitors. *Medicinal research reviews* **35**, 1032-1071

16. Amente, S., Lania, L., and Majello, B. (2013) The histone LSD1 demethylase in stemness and cancer transcription programs. *Biochimica et Biophysica Acta (BBA)-Gene Regulatory Mechanisms* **1829**, 981-986

17. Burg, J. M., Link, J. E., Morgan, B. S., Heller, F. J., Hargrove, A. E., and McCafferty, D. G. (2015) KDM1 class flavin-dependent protein lysine demethylases. *Peptide Science* **104**, 213-246

18. López-Muñoz, F., and Alamo, C. (2009) Monoaminergic neurotransmission: the history of the discovery of antidepressants from 1950s until today. *Current pharmaceutical design* **15**, 1563-1586

19. Khan, M. N. A., Suzuki, T., and Miyata, N. (2013) An overview of phenylcyclopropylamine derivatives: biochemical and biological significance and recent developments. *Medicinal research reviews* **33**, 873-910

20. Frieling, H., and Bleich, S. (2006) Tranylcypromine. *European archives of psychiatry and clinical neuroscience* **256**, 268-273

21. Sandler, M. (1990) Monoamine oxidase inhibitors in depression: history and mythology. *Journal of Psychopharmacology*

22. Shen, W. W. (1999) A history of antipsychotic drug development. *Comprehensive psychiatry* **40**, 407-414

23. Binda, C., Edmondson, D. E., and Mattevi, A. (2013) Monoamine Oxidase Inhibitors: Diverse and Surprising Chemistry with Expanding Pharmacological Potential. in *Advancing Methods for Biomolecular Crystallography*, Springer. pp 309-312

24. Binda, C., Wang, J., Li, M., Hubalek, F., Mattevi, A., and Edmondson, D. E. (2008) Structural and Mechanistic Studies of Arylalkylhydrazine Inhibition of Human Monoamine Oxidases A and B†‡. *Biochemistry* **47**, 5616-5625

25. Chen, J. J., Swope, D. M., and Dashtipour, K. (2007) Comprehensive review of rasagiline, a second-generation monoamine oxidase inhibitor, for the treatment of Parkinson's disease. *Clinical therapeutics* **29**, 1825-1849

26. Mosammaparast, N., and Shi, Y. (2010) Reversal of histone methylation: biochemical and molecular mechanisms of histone demethylases. *Annu. Rev. Biochem.* **79**, 155-179

27. Shi, Y. G., and Tsukada, Y.-i. (2013) The discovery of histone demethylases. *Cold Spring Harbor perspectives in biology* **5**, a017947

28. Shi, Y., Lan, F., Matson, C., Mulligan, P., Whetstine, J. R., Cole, P. A., Casero, R. A., and Shi, Y. (2004) Histone demethylation mediated by the nuclear amine oxidase homolog LSD1. *Cell* **119**, 941-953

29. Metzger, E., Wissmann, M., Yin, N., Müller, J. M., Schneider, R., Peters, A. H., Günther, T., Buettner, R., and Schüle, R. (2005) LSD1 demethylates repressive histone marks to promote androgen-receptor-dependent transcription. *Nature* **437**, 436-439

30. Gaweska, H., Henderson Pozzi, M., Schmidt, D. M., McCafferty, D. G., and Fitzpatrick, P. F. (2009) Use of pH and kinetic isotope effects to establish chemistry as rate-limiting in oxidation of a peptide substrate by LSD1. *Biochemistry* **48**, 5440-5445

31. Karytinos, A., Forneris, F., Profumo, A., Ciossani, G., Battaglioli, E., Binda, C., and Mattevi, A. (2009) A novel mammalian flavin-dependent histone demethylase. *J. Biol. Chem.* **284**, 17775-17782

32. van Essen, D., Zhu, Y., and Saccani, S. (2010) A feed-forward circuit controlling inducible NF-κB target gene activation by promoter histone demethylation. *Molecular cell* **39**, 750-760

33. Laurent, B., Ruitu, L., Murn, J., Hempel, K., Ferrao, R., Xiang, Y., Liu, S., Garcia, B. A., Wu, H., and Wu, F. (2015) A specific LSD1/KDM1A isoform regulates neuronal differentiation through H3K9 demethylation. *Molecular cell* **57**, 957-970

34. Huang, J., Sengupta, R., Espejo, A. B., Lee, M. G., Dorsey, J. A., Richter, M., Opravil, S., Shiekhattar, R., Bedford, M. T., and Jenuwein, T. (2007) p53 is regulated by the lysine demethylase LSD1. *Nature* **449**, 105-108

35. Wang, J., Hevi, S., Kurash, J. K., Lei, H., Gay, F., Bajko, J., Su, H., Sun, W., Chang, H., and Xu, G. (2009) The lysine demethylase LSD1 (KDM1) is required for maintenance of global DNA methylation. *Nature genetics* **41**, 125-129

36. Sakane, N., Kwon, H.-S., Pagans, S., Kaehlcke, K., Mizusawa, Y., Kamada, M., Lassen, K. G., Chan, J., Greene, W. C., and Schnoelzer, M. (2011) Activation of HIV transcription by the viral Tat protein requires a demethylation step mediated by lysine-specific demethylase 1 (LSD1/KDM1). *PLoS Pathog* **7**, e1002184

37. Walport, L. J., Hopkinson, R. J., and Schofield, C. J. (2012) Mechanisms of human histone and nucleic acid demethylases. *Curr. Opin. Chem. Biol.* **16**, 525-534

38. Lee, M. G., Wynder, C., Schmidt, D. M., McCafferty, D. G., and Shiekhattar, R. (2006) Histone H3 lysine 4 demethylation is a target of nonselective antidepressive medications. *Chemistry & biology* **13**, 563-567

39. Schmidt, D. M., and McCafferty, D. G. (2007) trans-2-Phenylcyclopropylamine is a mechanism-based inactivator of the histone demethylase LSD1. *Biochemistry* **46**, 4408-4416

40. Yang, M., Culhane, J. C., Szewczuk, L. M., Jalili, P., Ball, H. L., Machius, M., Cole, P. A., and Yu, H. (2007) Structural basis for the inhibition of the LSD1 histone demethylase by the antidepressant trans-2-phenylcyclopropylamine. *Biochemistry* **46**, 8058-8065

41. Binda, C., Valente, S., Romanenghi, M., Pilotto, S., Cirilli, R., Karytinos, A., Ciossani, G., Botrugno, O. A., Forneris, F., and Tardugno, M. (2010) Biochemical, structural, and biological evaluation of tranylcypromine derivatives as inhibitors of histone demethylases LSD1 and LSD2. *Journal of the American Chemical Society* **132**, 6827-6833

42. Mimasu, S., Sengoku, T., Fukuzawa, S., Umehara, T., and Yokoyama, S. (2008) Crystal structure of histone demethylase LSD1 and tranylcypromine at 2.25 Å. *Biochemical and biophysical research communications* **366**, 15-22

43. Fang, R., Chen, F., Dong, Z., Hu, D., Barbera, A. J., Clark, E. A., Fang, J., Yang, Y., Mei, P., and Rutenberg, M. (2013) LSD2/KDM1B and its cofactor NPAC/GLYR1 endow a structural and molecular model for regulation of H3K4 demethylation. *Molecular cell* **49**, 558-570

44. De Colibus, L., Li, M., Binda, C., Lustig, A., Edmondson, D. E., and Mattevi, A. (2005) Three-dimensional structure of human monoamine oxidase A (MAO A): relation to the structures of rat MAO A and human MAO B. *Proceedings of the National Academy of Sciences of the United States of America* **102**, 12684-12689

45. Binda, C., Li, M., Hubálek, F., Restelli, N., Edmondson, D. E., and Mattevi, A. (2003) Insights into the mode of inhibition of human mitochondrial monoamine oxidase B from high-resolution crystal structures. *Proceedings of the National Academy of Sciences* **100**, 9750-9755

46. Edmondson, D., Mattevi, A., Binda, C., Li, M., and Hubalek, F. (2003) Structure and mechanism of monoamine oxidase. *Burger's Medicinal Chemistry and Drug Discovery*

47. Stavropoulos, P., Blobel, G., and Hoelz, A. (2006) Crystal structure and mechanism of human lysine-specific demethylase-1. *Nature structural & molecular biology* **13**, 626-632

48. Yang, M., Culhane, J. C., Szewczuk, L. M., Gocke, C. B., Brautigam, C. A., Tomchick, D. R., Machius, M., Cole, P. A., and Yu, H. (2007) Structural basis of histone demethylation by LSD1 revealed by suicide inactivation. *Nature structural & molecular biology* **14**, 535-539

49. Jin, Y., Kim, T. Y., Kim, M. S., Kim, M. A., Park, S. H., and Jang, Y. K. (2014) Nuclear import of human histone lysine-specific demethylase LSD1. *Journal of biochemistry*, mvu042

50. Schroeder, F. A., Lewis, M. C., Fass, D. M., Wagner, F. F., Zhang, Y.-L., Hennig, K. M., Gale, J., Zhao, W.-N., Reis, S., and Barker, D. D. (2013) A selective HDAC 1/2 inhibitor modulates chromatin and gene expression in brain and alters mouse behavior in two mood-related tests. *PloS one* **8**, e71323

51. You, A., Tong, J. K., Grozinger, C. M., and Schreiber, S. L. (2001) CoREST is an integral component of the CoREST-human histone deacetylase complex. *Proceedings of the National Academy of Sciences* **98**, 1454-1458

52. Humphrey, G. W., Wang, Y., Russanova, V. R., Hirai, T., Qin, J., Nakatani, Y., and Howard, B. H. (2001) Stable histone deacetylase complexes distinguished by the presence of SANT domain proteins CoREST/kiaa0071 and Mta-L1. *Journal of Biological Chemistry* **276**, 6817-6824

53. Shi, Y., Sawada, J.-i., Sui, G., Affar, E. B., Whetstine, J. R., Lan, F., Ogawa, H., Luke, M. P.-S., Nakatani, Y., and Shi, Y. (2003) Coordinated histone modifications mediated by a CtBP co-repressor complex. *Nature* **422**, 735-738

54. Hakimi, M.-A., Bochar, D. A., Chenoweth, J., Lane, W. S., Mandel, G., and Shiekhattar, R. (2002) A core–BRAF35 complex containing histone deacetylase mediates repression of neuronal-specific genes. *Proceedings of the National Academy of Sciences* **99**, 7420-7425

55. Yokoyama, A., Igarashi, K., Sato, T., Takagi, K., Otsuka, M., Shishido, Y., Baba, T., Ito, R., Kanno, J., and Ohkawa, Y. (2014) Identification of myelin transcription factor 1 (MyT1) as a subunit of the neural cell type-specific lysine-specific demethylase 1 (LSD1) complex. *Journal of Biological Chemistry* **289**, 18152-18162

56. Fass, D. M., Schroeder, F. A., Perlis, R. H., and Haggarty, S. J. (2014) Epigenetic mechanisms in mood disorders: targeting neuroplasticity. *Neuroscience* **264**, 112-130

57. Jensen, L. J., Kuhn, M., Stark, M., Chaffron, S., Creevey, C., Muller, J., Doerks, T., Julien, P., Roth, A., and Simonovic, M. (2009) STRING 8—a global view on proteins and their functional interactions in 630 organisms. *Nucleic acids research* **37**, D412-D416

58. Ballas, N., and Mandel, G. (2005) The many faces of REST oversee epigenetic programming of neuronal genes. *Current opinion in neurobiology* **15**, 500-506

59. Lunyak, V. V., Burgess, R., Prefontaine, G. G., Nelson, C., Sze, S.-H., Chenoweth, J., Schwartz, P., Pevzner, P. A., Glass, C., and Mandel, G. (2002) Corepressor-dependent silencing of chromosomal regions encoding neuronal genes. *Science* **298**, 1747-1752

60. Ballas, N., Grunseich, C., Lu, D. D., Speh, J. C., and Mandel, G. (2005) REST and its corepressors mediate plasticity of neuronal gene chromatin throughout neurogenesis. *Cell* **121**, 645-657

61. Islam, M. M., and Zhang, C.-L. (2015) TLX: A master regulator for neural stem cell maintenance and neurogenesis. *Biochimica et Biophysica Acta (BBA)-Gene Regulatory Mechanisms* **1849**, 210-216

62. Yokoyama, A., Takezawa, S., Schüle, R., Kitagawa, H., and Kato, S. (2008) Transrepressive function of TLX requires the histone demethylase LSD1. *Molecular and cellular biology* **28**, 3995-4003

63. Sun, G., Alzayady, K., Stewart, R., Ye, P., Yang, S., Li, W., and Shi, Y. (2010) Histone demethylase LSD1 regulates neural stem cell proliferation. *Molecular and cellular biology* **30**, 1997-2005

64. Althoff, K., Beckers, A., Odersky, A., Mestdagh, P., Köster, J., Bray, I. M., Bryan, K., Vandesompele, J., Speleman, F., and Stallings, R. L. (2013) MiR-137 functions as a tumor suppressor in neuroblastoma by downregulating KDM1A. *International Journal of Cancer* **133**, 1064-1073

65. Sun, G., Ye, P., Murai, K., Lang, M.-F., Li, S., Zhang, H., Li, W., Fu, C., Yin, J., and Wang, A. (2011) miR-137 forms a regulatory loop with nuclear receptor TLX and LSD1 in neural stem cells. *Nature communications* **2**, 529

66. Fuentes, P., Cánovas, J., Berndt, F. A., Noctor, S. C., and Kukuljan, M. (2011) CoREST/LSD1 control the development of pyramidal cortical neurons. *Cerebral cortex*, bhr218

67. Toffolo, E., Rusconi, F., Paganini, L., Tortorici, M., Pilotto, S., Heise, C., Verpelli, C., Tedeschi, G., Maffioli, E., and Sala, C. (2014) Phosphorylation of neuronal Lysine-Specific Demethylase 1LSD1/KDM1A impairs transcriptional repression by regulating interaction with CoREST and histone deacetylases HDAC1/2. *Journal of neurochemistry* **128**, 603-616

68. Zibetti, C., Adamo, A., Binda, C., Forneris, F., Toffolo, E., Verpelli, C., Ginelli, E., Mattevi, A., Sala, C., and Battaglioli, E. (2010) Alternative splicing of the histone demethylase LSD1/KDM1 contributes to the modulation of neurite morphogenesis in the mammalian nervous system. *The Journal of Neuroscience* **30**, 2521-2532

69. Rusconi, F., Paganini, L., Braida, D., Ponzoni, L., Toffolo, E., Maroli, A., Landsberger, N., Bedogni, F., Turco, E., and Pattini, L. (2014) LSD1 neurospecific alternative splicing controls neuronal excitability in mouse models of epilepsy. *Cerebral Cortex*, bhu070

70. Rusconi, F., Grillo, B., Ponzoni, L., Bassani, S., Toffolo, E., Paganini, L., Mallei, A., Braida, D., Passafaro, M., and Popoli, M. (2016) LSD1 modulates stress-evoked transcription of immediate early genes and emotional behavior. *Proceedings of the National Academy of Sciences* **113**, 3651-3656

71. Tunovic, S., Barkovich, J., Sherr, E. H., and Slavotinek, A. M. (2014) De novo ANKRD11 and KDM1A gene mutations in a male with features of KBG syndrome and Kabuki syndrome. *American Journal of Medical Genetics Part A* **164**, 1744-1749

72. Wang, J., Scully, K., Zhu, X., Cai, L., Zhang, J., Prefontaine, G. G., Krones, A., Ohgi, K. A., Zhu, P., and Garcia-Bassets, I. (2007) Opposing LSD1 complexes function in developmental gene activation and repression programmes. *Nature* **446**, 882-887

73. Pilotto, S., Speranzini, V., Marabelli, C., Rusconi, F., Toffolo, E., Grillo, B., Battaglioli, E., and Mattevi, A. (2016) LSD1/KDM1A mutations associated to a newly described form of intellectual disability impair demethylase activity and binding to transcription factors. *Human Molecular Genetics*, ddw120

CHAPTER 2

2 Neuropharmacology of FAD-directed KDM1A inhibitors

2.1 Abstract

The FDA-approved antidepressant tranylcypromine (TCP; Parnate) inhibits MAO-A/B by covalent inactivation of their respective FAD cofactors. TCP similarly inhibits the histone lysine demethylase KDM1A, albeit with low potency and selectivity *in vitro.* In previous work, we leveraged the FAD-directed scaffold of TCP to prepare the RN series of analogs. Here, we describe biochemical, cellular, and *in vivo* assays to determine the selectivity of these derivatives for KDM1A. Orthogonal biochemical assays were developed to profile KDM1A inhibition and selectivity versus KDM1B and MAO-A/B. Relative to TCP, the derivative RN1 had greatly increased potency for KDM1A and excellent selectivity versus KDM1B, while potency towards MAO-A/B remained relatively unchanged. Dilution studies and spectroscopic analysis support a mechanism where RN1 covalently and irreversibly inactivates the flavin ring of KDM1A's FAD cofactor. Although RN1 inhibited full-length, immunoprecipitated KDM1A, no reproducible changes in bulk H3K4 dimethylation levels were observed in cells treated with FAD-directed inhibitors. However, the cellular thermal shift assay (CETSA) revealed potent engagement of KDM1A by TCP both in live SH-SY5Y cells and in the brains of systemically-treated rats. RN1 also engaged KDM1A in cells, and conferred thermal stability to RCOR1 (CoREST1). Finally, RN1 was found to be highly brain penetrant, and to affect the behavior of mice in a novel object recognition assay. These data are the first to profile the behavioral effects of a highly potent KDM1A inhibitor in rodents, and suggest that target engagement of KDM1A by TCP in a clinical setting warrants further examination.

2.2 Introduction

Chromatin modification is not only crucial to differentiation and maintenance of cellular states, but also mammalian neurobiology, including cognition, mood, and behavior (1-3). Epigenetic dysfunction is a common factor in neuropsychiatric and neurodegenerative disorders, and targeting of epigenetic regulators may present new opportunities for therapeutic intervention (4,5). In particular, pathways regulating histone 3 lysine 4 (H3K4) methylation have been identified to have strong genetic association with major psychiatric disease in analysis of large patient cohorts (6). Intriguingly, a key modulator of this epigenetic mark, the FAD-dependent histone lysine demethylase KDM1A, is weakly inhibited by monoamine oxidase (MAO) inhibitors used to treat depression and Parkinson's disease (7-9). Furthermore, KDM1A demethylates its substrates as part of a complex including the histone deacetylases (HDAC)1/2, CtBP, RCOR1, and BHC80, many of which are also implicated in neurological function (10-13). Thus, KDM1A has emerged as an attractive and tractable target for potential therapeutic development in neuropsychiatric disease. Interest in other therapeutic applications for KMD1A have been reviewed elsewhere (14).

KDM1A and its homolog KDM1B share considerable structural similarity with the catalytic domains of MAO-A and MAO-B; furthermore, all four enzymes use an FAD cofactor to oxidatively deaminate their substrates and all are irreversibly inactivated by FAD-directed inhibitors (15). Three structural classes of FAD-directed antidepressants have been described: hydrazines (phenelzine; Nardil), propargylamines (pargyline; Eutonyl), and cyclopropylamines (tranylcypromine or TCP; Parnate) (16). These drugs inhibit KDM1A weakly and with poor selectivity, but their core scaffolds can be readily modified to generate tool compounds optimized for the study of KDM1A in a neurological context. To this end, we and others have prepared analogs of these irreversible inhibitors with the goal of increasing potency and selectivity for KDM1A (14,15,17-20). Here, we describe biochemical, cellular, and *in vivo*

assays to determine the selectivity of TCP-derivatives for KDM1A, and provide the first insights into the neuropharmacology of these tool compounds.

2.3 Results and Discussion

2.3.1 Development of orthogonal KDM1A/B and MAO-A/B inhibition assays

Recombinant KDM1A has robust demethylase activity *in vitro,* and various biochemical assays to measure enzyme inhibition have been developed (21-23). To provide orthogonal validation of assay results and to help inform future inhibitor studies, KDM1A inhibition was profiled using three biochemical assay formats: a horseradish peroxidase (HRP)-coupled assay, a time-resolved fluorescence energy transfer (TR-FRET) assay, and a label free, direct mass spectrometry (MS) assay (Figure 2.1) (24). All assays utilized34 a synthetic 21-mer dimethylated H3K4 peptide (H3K4me2) or a biotinylated derivate as a substrate. After assessment of KDM1A demethylase activity by this panel of assays, the most robust assay was adapted to measure KDM1B activity. In addition, selectivity of the inhibitors for KDM1A versus MAO-A/B was assessed using a commercially-available luciferase-coupled assay (25).

The HRP-coupled assay has been the high throughput method of choice to profile novel KDM1A inhibitors due to its low cost, convenience and robustness to support structure-activity-relationship (SAR) efforts (26). In the coupled assay (Figure 2.1A), the H_2O_2 generated as a byproduct of KDM1A catalysis is detected through an HRP-catalyzed reaction with ADHP (10-acetyl-3,7-dihydroxyphenoxazine) to produce a fluorescent oxidation product, resorufin, in proportion to enzyme activity (24). In our hands, this HRP-coupled assay for measuring LSD1 was robust and reproducible, but resulted in many false positives and negatives through the interaction of small molecules with H_2O_2, HRP, or ADPH. This assay is also incompatible with the concentration of reducing agents required to eliminate KDM1A thiol-reactivity (Chapter 3).

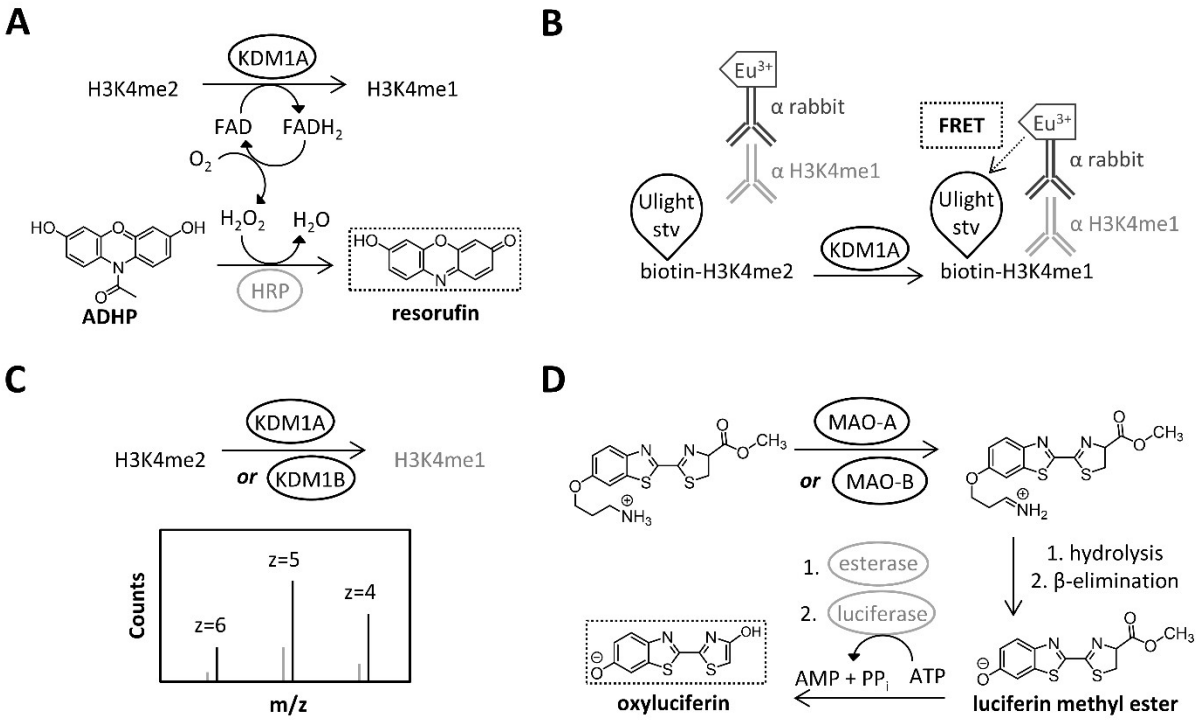

Figure 2.1 Schematic representation of KDM1A/B and MAOA/B *in vitro* enzymatic assays.
In all schemes, the rate-limiting enzyme is outlined in black, while the coupled enzyme, if present, is outlined in grey. Fluorescent or luminescent species are outlined in dashed lines. **A.** The HRP-coupled assay detects the H_2O_2 byproduct of KDM1A catalysis by enzymatic conversion of ADHP to the fluorescent resorufin. **B.** The TR-FRET assay relies on antibody binding to the demethylated peptide product, H3K4me1, to bring the donor and acceptor fluorophores in sufficient proximity for energy transfer. **C.** MS-based assays detect the highly charged peptide substrate and demethylated products, and their relative peak areas can be used to determine enzyme activity. **D.** The MAO-glo assay uses an amine luciferin derivative that, upon oxidation by MAO-A/B, can be converted to the luminescent oxyluciferin in a multi-step reaction.

Results from the HRP-coupled KDM1A assays were validated in-house by assessing demethylation using a TR-FRET assay for KDM1A inhibition as previously described (23,27). The TR-FRET assay directly detects peptide methylation state by measuring gain of energy transfer between donor and acceptor fluorophores targeted to the biotinylated peptide substrate and to an anti-H3K4me1 antibody (Figure 2.1B). While this assay produced fewer false positives from fluorescent or redox active compounds than the HRP-coupled assay, consistent apparent IC_{50} values for time-dependent FAD-directed inhibitors could only be obtained if the KDM1A demethylation was quenched with RN1 before addition of the detection reagents. Another limitation of the TR-FRET assay was variability in the quality of the H3K4me1 primary

antibody which, unlike the H3K4me2 antibody, was observed to vary from lot to lot by western blotting (data not shown).

Ultimately, mass spectrometry-based assays were favored as the most direct and reproducible means to measure KDM1A and KDM1B demethylase activity. For analysis of 384-well plates, the high-throughput RapidFire MS assay was adapted for label-free detection of H3K4me2 peptide demethylation (28,29). Using identical assay conditions to those used for the HRP-coupled assay, H3K4me1 was the major product of the demethylation reaction (Figure 2.1C). Since the RapidFire MS assay requires dedicated and specialized instrumentation, an in-house LC-MS assay was later developed and used to monitor the activity of KDM1A and KDM1B on a medium-throughput scale. Detection of H3K4me1 and H3K4me0 products by electrospray ionization (ESI) is identical for both the RapidFire and LC-MS assays, but the former separates the peptide from the other reaction components by solid-phase extraction, whereas the latter relies on reverse-phase column chromatography. For both MS assays, substrate conversion values were used to calculate the apparent IC_{50} values for each test compound. The LC-MS assay was adapted to monitor demethylation of the H4K3me2 peptide substrate by KDM1B when the recombinant enzyme became available.

Selectivity of novel KDM1A inhibitors over MAO-A/B is paramount given that the MAOs are highly expressed in the brain and both families of enzymes are targeted by TCP (7). Inhibition of recombinant MAO-A/B was determined using the commercially-available, luciferase-coupled MAO-Glo® assays (25). The substrate for this coupled reaction is a luciferin derivative bearing an alkyl amine which can be oxidized by both monoamine oxidases (Figure 2.1D). Upon hydrolysis to the aldehyde and β-elimination of acrolein, the resulting product can be sequentially processed by an esterase and luciferase to generate luminescence proportional to MAO enzymatic activity.

2.3.2 Identification of TCP-derivative RN1 as a highly potent KDM1A inhibitor

We have previously described the synthesis of FAD-directed KDM1A inhibitors based on the core structure of TCP. Briefly, the RN series of N-alkylated TCP-analogs was prepared from transformation of cinnamic acid or cinnamate ester derivatives by cyclopropanation, hydrolysis and Curtius rearrangement, as well as Suzuki cross-coupling of a bromo-derivative (17). The compounds were assessed as *trans* racemic mixtures. The potency and selectivity of this small library of compounds was assessed using our panel of orthogonal *in vitro* activity assays (Table 2.1). For these experiments, TCP was used as a positive control of inhibition, and was found to inhibit KDM1A with an apparent IC_{50} value of 14-37 μM. This value is within the range of IC_{50} values previously reported by others using similar assay formats (32-271 μM) (15,19,23). Inactivity of TCP in the TR-FRET assay may be due to the shorter reaction time relative to the HRP-coupled or MS assays (8 minutes versus 20 minutes). Comparison of apparent IC_{50} values at a set endpoint was sufficient to compare the relative potencies of compounds in the RN series; however, future studies will be required to compare the rate of inactivation of KDM1A by these time-dependent inhibitors. The most potent compounds identified by our orthogonal KDM1A assays were RN1 and RN7 (Table 2.1), with apparent IC_{50} values between 3 and 70 nM. There was overall good agreement both between assays and between replicates within an assay.

Our studies confirmed that TCP exhibits modest selectivity for MAO-A and MAO-B versus KDM1A *in vitro* (2.4- and 16-fold, respectively) (7). Unexpectedly, N-alkylation and phenyl ring modification in the RN series did not diminish potency towards MAO-A/B (Table 2.1, the structure of RN1 is shown in Figure 2.2B). Although the overall amine oxidase domains of the KDM1 and MAO families of enzymes are highly homologous, the catalytic active site of MAO-A/B is small, closed, and hydrophobic relative to that of KDM1A/B (30). Based on this observation, we and others hypothesized that functionalization of the TCP core structure would prevent MAO A/B FAD-adduct formation; instead, gains in selectivity were made by increasing the potency of KDM1A inactivation. Thus, the most potent KDM1A inhibitors, RN7 and RN1,

were also the most selective. To the best of our knowledge, these compounds are among two of the most potent and selective KDM1A inhibitors described to date (14,18). Initial experiments with [^{18}F]-radiolabeled RN7 indicated that uptake of this compound into rat brain is not saturable, suggestive of high levels of non-specific binding ((17) and data not shown). On this basis, and on that of additional data presented below, we selected RN1 as a lead compound for further studies of KDM1A inhibition.

Table 2.1 IC_{50} values for inhibition of KDM1A/B and MAO-A/B by TCP and the RN1 series of TCP-derivatives.

	KDM1A IC_{50} (μM)			KDM1B IC_{50} (μM)	MAO IC_{50} (μM)	
	HRP	TR-FRET	MS	MS	MAO-A	MAO-B
TCP	37	>100	13.7	>400	0.48	4.9
RN1	0.070	0.01	0.02	150	0.51	2.8
RN5	0.20	0.10	-----	-----	2.0	-----
RN7	0.031	0.003	0.007	-----	13	11
RN11	0.60	0.20	0.65	-----	0.10	-----
RN21	0.034	0.002	0.015	-----	3.7	11
RN22	0.047	0.30	8.4	-----	1.2	23
RN23	2.0	0.72	0.37	-----	0.15	-----
RN24	0.047	0.004	0.019	-----	0.51	-----
RN27	0.055	0.009	0.033	-----	1.5	1.3

TCP and TCP-derivatives have previously been shown to inhibit KDM1B (15). As MS-based assays were found to be the most reproducible means to measure KDM1A inactivation, the LC-MS was modified to assess KDM1B inhibition. As others have reported, the enzymatic activity of recombinant human KDM1B was substantially lower than recombinant KDM1A *in vitro*, and demethylation was only detectable at elevated pH (31). Under these conditions, TCP only partially inhibited KDM1B at the highest dose tested (400 μM), precluding apparent IC_{50} determination by nonlinear regression. RN1 inhibited human KDM1B with an apparent IC_{50} of 150 μM, several orders of magnitude above the potencies observed for MAO-A/B, which were in turn an order of magnitude greater than that for KDM1A. This pattern of selectivity is consistent with that of the TCP derivative ORY-1001 (18). In contrast, studies with recombinant mouse KDM1B have indicated only modest selectivity of TCP analogs for KDM1A (15). The relative potencies of

MAO inhibitors are known to be highly species-dependent (32); thus, preparations of human KDM1B with more robust activity would greatly facilitate the future studies that are needed to determine the kinetics of inactivation of by RN1 and to validate the observed pattern of selectivity in orthogonal assays. Taken together, these data suggest that RN1 is an excellent tool compound to probe the role of KDM1A inhibition in a cellular and behavioral context.

2.3.3 Kinetics of RN1-inactivation of KDM1A

Multiple mechanisms of covalent attachment of TCP to the flavin ring of FAD have been proposed for the monoamine oxidases (33). Similarly, several distinct adducts of TCP to the flavin ring of KDM1A have been observed in mass spectrometry and x-ray crystallography experiments (15). The prevailing view in the literature is that inactivation is initiated by single electron transfer from the amine of TCP to FAD, followed by cyclopropyl ring opening and recombination of radicals to form a covalent adduct (9). However, the site of attachment to the flavin ring remains unclear, and evidence for both N(5) and C(4a) adducts has been found (Figure 2.2A). C(4a) adducts have been proposed to cyclize with the N(5) atom upon iminium hydrolysis and dehydration; this cyclized adduct is challenging to differentiate from an N(5) adduct on the basis of electron density maps generated by x-ray diffraction (19). An additional subtlety is that the two stereoisomers of TCP have been observed to form unique N(5) adducts with different atoms of their cyclopropyl rings (15).

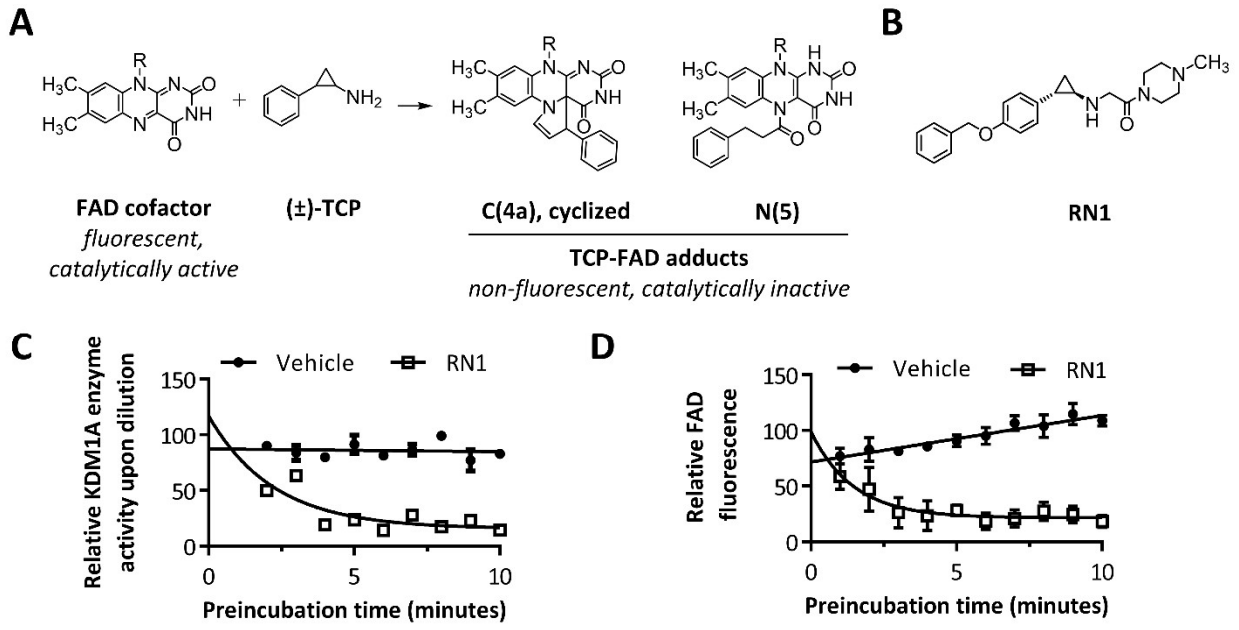

Figure 2.2 Covalent inactivation of KDM1A by TCP and RN1

A. Representative structures of proposed TCP-flavin ring adducts and their respective spectroscopic properties. **B.** Chemical structure of TCP-analog RN1. **C.** Kinetics of KDM1A enzymatic inhibition by RN1. KDM1A (3.2 μM) was pre-incubated with 6 μM RN1 for the duration of time indicated on the x-axis, then diluted 100-fold to promote dissociation and assayed for demethylase activity. **D.** Kinetics of loss of FAD fluorescence upon treatment of 5 μM KDM1A with 10 μM RN1. For C and D, error bars indicate SD.

Regardless of the precise mechanism, covalent inactivation of FAD by TCP is irreversible, and loss of characteristic flavin absorbance and fluorescence properties upon adduct formation can be monitored spectroscopically (7). As a structural analog of TCP, RN1 was predicted to inhibit KDM1A in a similar manner (Figure 2.2B). To assess the reversibility of inhibition, a concentrated solution of KDM1A (3.2 μM) was pre-incubated with a slight excess of RN1 (6 μM) for various durations, followed by 100-fold dilution into assay buffer containing the H3K4me2 substrate. This dilution results in a concentration of KDM1A equal to that under standard assay conditions and a concentration of RN1 concentration slightly below its IC_{50} value for those same conditions. Partial inhibition of KDM1A relative to vehicle control was observed with pre-incubation times up to 4 minutes, after which enzyme activity plateaued at a minimum value (Figure 2.2C). This behavior is consistent with an inhibitor with a slow or zero off-rate, such that enzyme inactivation is not rescued by dilution-promoted dissociation. In a separate experiment, the FAD

fluorescence of a concentration solution of KDM1A (5 μM) was monitored immediately after addition of RN1 (10 μM) or vehicle control (7,34). The FAD fluorescence of RN1-treated KDM1A plateaued at a minimum value after a 4-minute incubation (Figure 2.2D). Additional spectroscopic support for covalent modification of FAD by RN1 is discussed in Chapter 4. Taken together, these data are consistent with irreversible inhibition of KDM1A *via* FAD-adduct formation by RN1, as is expected based on its structural similarity to TCP. Future studies to identify an FAD-RN1 adduct by LC-MS/MS could provide additional support for this putative mechanism and may shed light on the position of flavin attachment. Although a direct comparison was not made, these data suggest that RN1 inactivates KDM1A at a faster rate than TCP, which requires up to an hour for covalent modification under similar conditions (7). The difference in the rates of inactivation may be partially responsible for the apparent increased potency of RN1 versus TCP in the end point assays described above, which profiled KDM1A activity after a total of 23 minutes (TR-FRET) or 30 minutes (HRP-coupled, MS) of exposure to test compound.

2.3.4 Functional inhibition of cellular KDM1A by RN1

Having profiled RN1 *in vitro,* we next turned to assess the consequence of KDM1A inhibition in cellular models. Although KDM1A is known to demethylate around a dozen non-histone substrates, analysis of bulk histone H3K4me2 levels (or H3K9me2 levels in breast and testicular cancer cell lines) remains the most frequently used assay to profile enzyme inhibitors (14,35). Comparable assays to monitor bulk histone acetylation levels have been invaluable to the development of novel histone deacetylase (HDAC) inhibitors and their assessment at the systems level (for example, (36)). Many HDAC inhibitors are known to significantly increase H4K4me2 levels, suggesting that this modification is dynamic and may be a suitable marker for KDM1A activity (37). However, dozens of experimental conditions in tested in numerous cell lines over several years failed to show robust and reproducible increases in bulk H3K4me2 levels by western blotting (Figure 2.3A-C) or by immunofluorescence (data not shown) in

response to TCP or RN1 treatment. In contrast, RN1 clearly inhibits the demethylation of a peptide substrate by full-length KDM1A immunoprecipitated from HeLa nuclei in a cell-free assay (Figures 2.3D-F). This result suggests that RN1 can inhibit native KDM1A, but either does not reach its target in a cellular context and/or the consequence of KDM1A inhibition cannot be readily detected at the level of global histone methylation. Small changes in H3K4me2 levels (ie. 1.2 - 1.5-fold increase) have been reported in response to other FAD-directed inhibitors, such as the phenelzine analog bizine (20); however, this dynamic range is far too narrow for reliable detection by immunoblotting techniques and cannot support the discovery of novel, non-covalent KDM1A inhibitors. Consequently, the field has largely turned to inhibition of cancer cell line proliferation or measurement of cell- or tissue-specific target gene expression as a measure of KDM1A inhibition (14).

Several general explanations can be invoked to explain the observation that bulk H3K4 methylation is a poor biomarker for KDM1A activity. Many classes of histone lysine demethylases have been described, each opposed by numerous histone lysine methyltransferases (Figure 2.3A), such that the contribution of KDM1A to the maintenance of overall histone methylation may be minor and/or compensated for by partially redundant mechanisms. Furthermore, the activity of KDM1A is highly dependent on adjacent post-translational modification of the histone H3 tail (38), which could render pharmacological inhibition insignificant if the 'upstream' marks remain unaffected, as implicated in crosstalk mechanisms of histone modification (39,40). This view of KDM1A as a highly specific regulator of gene expression is supported by the robust changes in histone methylation observed at the promoters of REST target genes despite no global changes in H3K4me2 levels upon knockdown of KDM1A by RNA interference (8). Unfortunately, the target genes profiled in genetic and pharmacological studies of KDM1A vary widely from cell-type to cell-type, and no standardized metric for meaningful KDM1A inhibition has yet to be established.

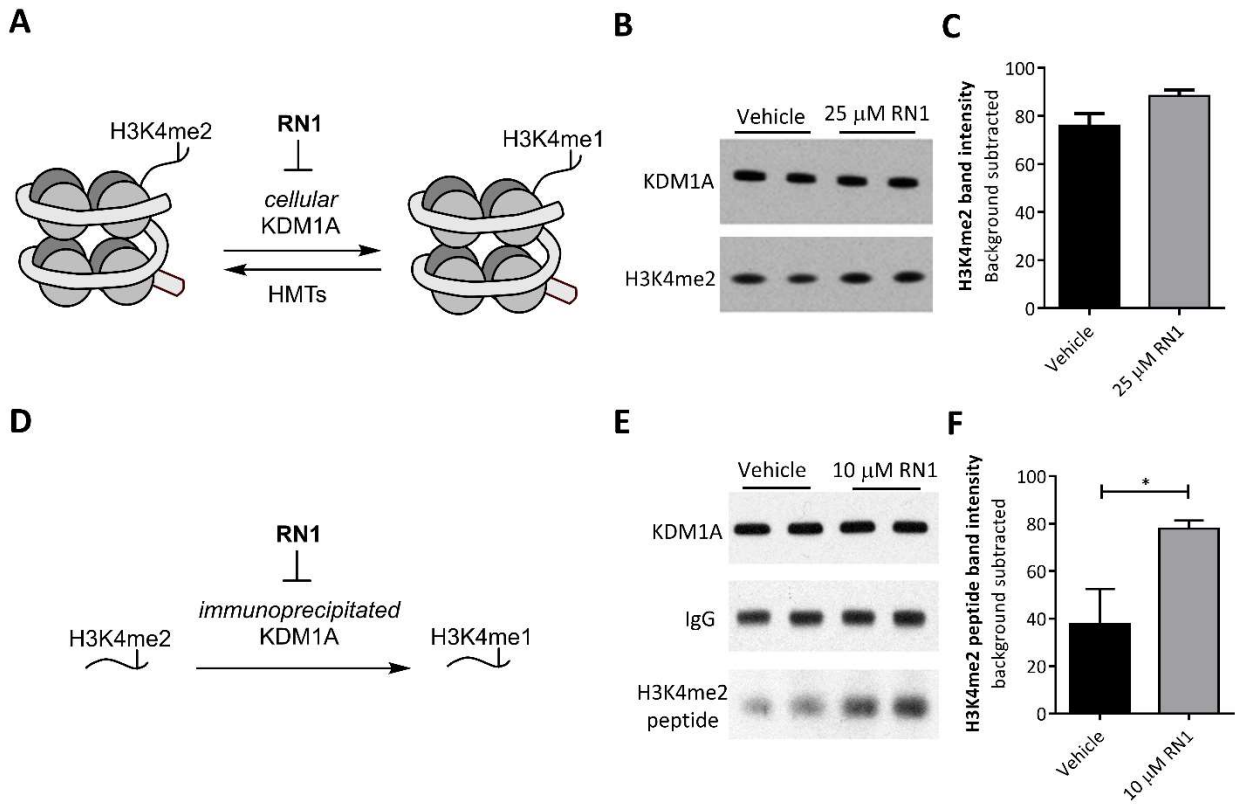

Figure 2.3 RN1 inhibits full-length KDM1A but does not increase cellular H3K4me2 levels.
A. Schematic of histone demethylation by KDM1A and methylation by histone methyltransferases in living cells. Inhibition of KDM1A is predicted to increase H3K4me2 levels. **B & C.** SH-SY5Y cells treated with RN1 for 24 hours do not have significantly increased H3K4me2 levels. Data representative of > 10 experiments, error bars indicate SD. **D.** Schematic of H3K4me2 peptide demethylation by immunoprecipitated KDM1A. **E & F.** Immunoprecipitated KDM1A is inhibited by 10 μM RN1 in a cell-free assay. Error bars indicate SD, * $p < 0.5$ by 2-tailed Student's *t* test.

2.3.5 The cellular thermal shift assay reveals target engagement of KDM1A inhibitors

The lack of a standard cell-based assay by which to assess novel inhibitors precludes the optimization of lead compounds for factors such as cellular/nuclear permeability and potency against native KDM1A complexes. To overcome this limitation, the recently described cellular thermal shift assay (CETSA) was adapted to analyze KDM1A target engagement in intact SH-SY5Y cells (41,42). The CETSA assay is a broadly-applicable and label-free strategy to measure target engagement in a variety of living cells and tissues and does not depend on knowledge of the functional outcome of the drug-target interaction. Cells (or tissues, or live animals) are treated with test compound, then samples are subjected

to a temperature gradient (Figure 2.4A). After cell lysis, denatured and aggregated proteins are pelleted by centrifugation and the soluble fractions are assayed to generate a melting curve indicative of the protein thermal stability. Extensively studied *in vitro* thermal shift assays have firmly established that ligand binding typically increases the thermal stability of target proteins; CETSA extends this concept to a cellular context (43).

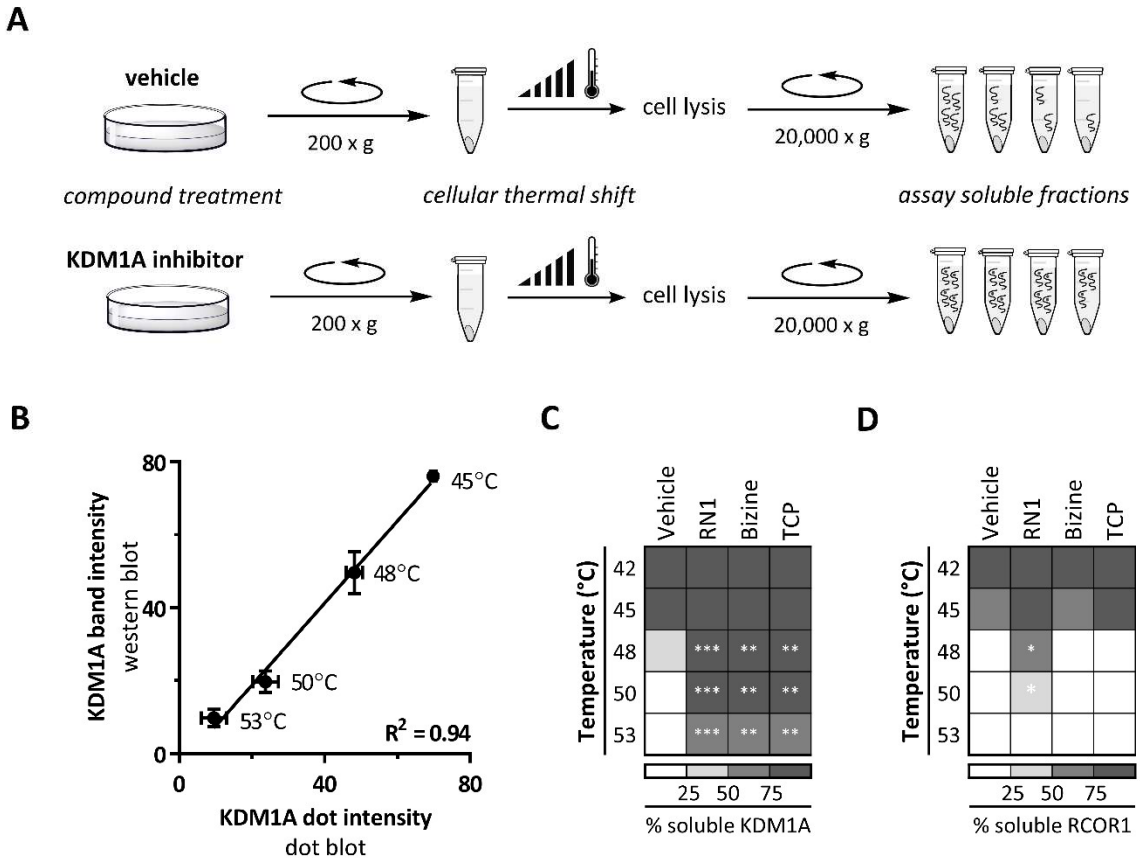

Figure 2.4 Live-cell CETSA profiling of KDM1A and RCOR1.
A. Schematic representation of the live-cell CETSA method. **B.** Soluble KDM1A decreases as a function of temperature. The same samples (n=4 from biological duplicates) were analyzed by western blotting and dot blotting. Good correlation between these detection methods was observed for a subset of antibodies (R^2 = 0.94 for KDM1A). **C.** FAD-directed inhibitors thermally stabilize KDM1A. **D.** RN1 thermally stabilizes RCOR1. For C and D, the heat map represents the relative soluble KDM1A in cells pre-treated with test compounds (25 µM) for 30 minutes prior to CETSA analysis. The same samples were analyzed for both KDM1A and RCOR1 (n=3 from biological duplicates). Statistical significance was assessed by 2-way ANOVA with Dunnett correction for multiple comparisons, * $p < 0.05$, ** $p < 0.01$, *** $p < 0.001$.

In initial experiments, live SH-SY5Y cells were heated using a gradient method in a thermal cycler, and the temperature at which soluble KDM1A was reduced by 50%, the apparent T_M, was determined to be 47 °C by western blotting (Figure 2.4B and data not shown). The biggest limitation of CETSA stems from the detection method used to assay the soluble protein of interest. To address the bottleneck imposed by SDS-PAGE, a dot blot assay was developed with good correlation to results obtained by western blotting for KDM1A (Figure 2.4B) and RCOR1 (data not shown). All FAD-directed inhibitors tested resulted significant (>8 °C) thermal stabilization of KDM1A in SH-SY5Y cells, the clearest phenotype of cellular target engagement determined to date (Figure 2.4C). Additionally, inactivation of KDM1A by RN1, but not TCP or bizine, resulted in significant thermal stabilization of RCOR1 (Figure 2.4D). RCOR1 tightly associates with KDM1A, and the stabilization of RCOR1 conferred by RN1 is presumed to be mediated by the extensive contacts formed between this co-repressor and the tower domain of KDM1A (9,10). This finding raises the intriguing possibility that the CETSA method may be used to profile the selectivity of compounds for distinct KDM1A complexes. GAPDH and actin were not thermally stabilized by KMD1A inhibitors (data not shown); however, these negative control proteins have very different T_M values than KDM1A and so are not ideal standards. Technical limitations involving the immunodetection of KDM1B and the optimization of detergents required to solubilize the membrane-bound MAO-A/B were not overcome prior to writing. These data will be important to future studies designed to assess the selectivity of FAD-directed inhibitors against these homologous amine oxidases in a cellular context.

The low potency and slow kinetics of TCP inactivation of KDM1A *in vitro* motivated the development of more selective analogs. It was thus surprising to observe that TCP thermally stabilized KDM1A to approximately the same extent as RN1 in live SH-SY5Y cells. To further analyze this result, a variant of the live-cell CETSA was run holding the temperature constant and varying the concentration of TCP to generate an effective CETSA IC_{50} value. Importantly, cells were pelleted and washed twice after 30-minute treatment with TCP to minimize compound binding after cell lysis. Under these conditions, TCP

was found to thermally stabilize KDM1A with a CETSA IC_{50} of 0.25 μM (Figure 2.5A), a potency two orders of magnitude below that observed in the HRP-coupled (Figure 2.5B) or MS (Figure 2.5C) assays. As described above, further experiments are required to extend this analysis to KDM1B and MAO-A/B, and to determine if TCP is also unexpectedly potent against these flavoproteins in a cellular context.

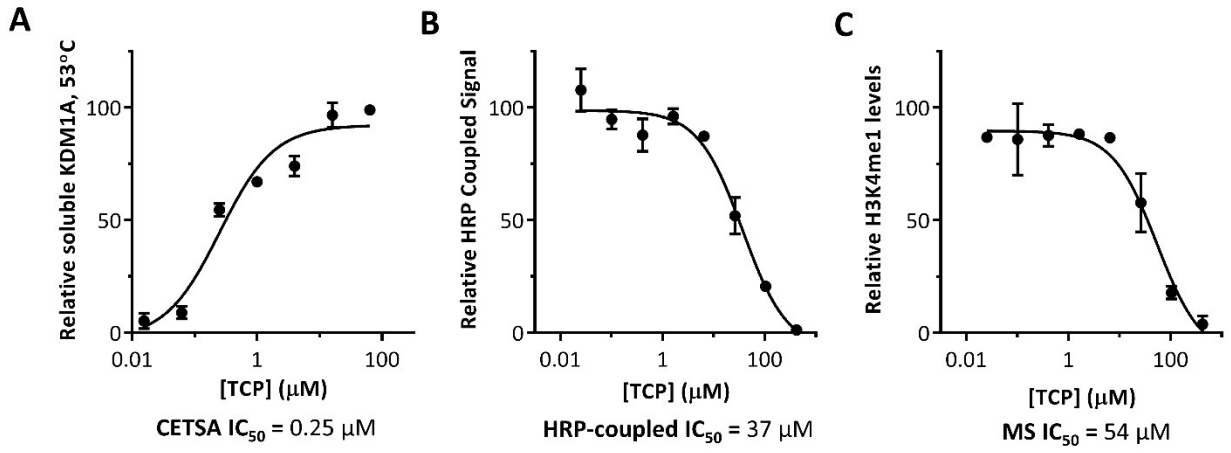

Figure 2.5 TCP potently engages KDM1A by live-cell CETSA.
A. Dose-response curve of TCP in the live-cell CETSA assay. SH-SY5Y cells were treated for 30 minutes, then washed twice before heating to 53 °C and analysis by the CETSA method. Soluble KDM1A was detected by dot blotting from biological duplicates (n=2). **B.** Representative dose-response curves for TCP in the HRP-coupled and **C.** MS assays indicate an *in vitro* potency for recombinant KDM1A far weaker than that observed for cellular KDM1A. Demethylation reactions were allowed to proceed for 20 minutes after a 10-minute pre-incubation period, such that the total duration of TCP exposure is matched in all 3 sets of experiments.

Based on its low potency and selectivity *in vitro*, the prevailing view in the literature is that TCP is unlikely to meaningfully engage KDM1A in a clinical setting (9). However, this assumption warrants testing given the apparent potency of TCP in a cellular context. In addition to live cells, the CETSA method can be applied to study the effects of test compounds added to tissue lysate (*ex vivo* CETSA). Furthermore, tissue harvested from animals treated with test compounds while still alive can also be assessed by this technique (*in vivo* CETSA). TCP is an excellent candidate for *in vivo* CETSA based on its covalent mechanism of inhibition, such that dilution of tissue for analysis should not promote dissociation. In a preliminary

experiment, rats were treated intraperitoneally with 15 mg/kg TCP or saline vehicle control (2 animals per group) for 2 hours. This dose of TCP has been shown to inhibit monoamine oxidase activity in rats and is within the high end of doses prescribed to humans for treatment of refractory depression (44-46). Rodent brains were bisected and a powderized homogenate was prepared that enabled CETSA analysis from tissue representative of the whole brain. TCP thermally stabilized KDM1A in rat brain by ~5 °C as determined by western blotting (Figure 2.6A and 2.6B). To the best of our knowledge, this is the first evidence of *in vivo* KDM1A target engagement by TCP. Although many additional studies are required to validate and interpret this finding, these initial data suggest that inhibition of KDM1A may be relevant in clinical application of TCP.

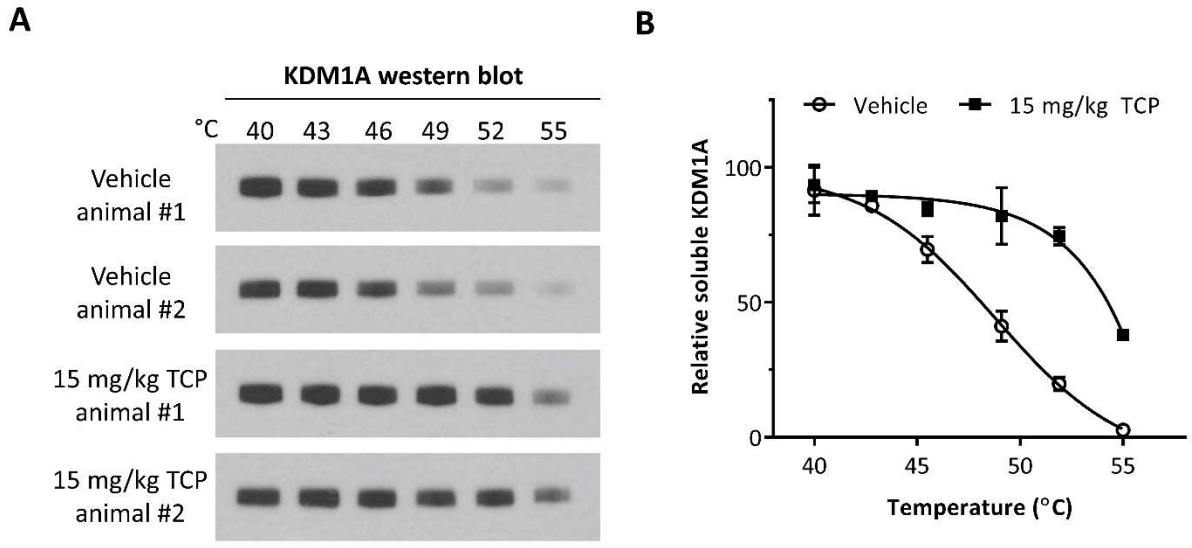

Figure 2.6 TCP engages KDM1A by *in vivo* CETSA.
A. Western blot of soluble KDM1A from CETSA analysis of whole brain homogenate prepared from rats treated with TCP (15 mg/kg) or saline vehicle for 2 hours *in vivo*. **B.** Quantification of relative soluble KDM1A reveals thermal stabilization of ~5 °C.

2.3.6 RN1 is brain-penetrant and affects novel object preference in behaving rodents

Although therapeutically relevant doses of TCP might engage KDM1A, they also result in profound inhibition of monoamine oxidase function. Thus, TCP analogs with improved selectivity for KDM1A over MAO-A/B may be valuable tools compounds to study the contribution of this histone lysine demethylase to cognition and mood. Although the *in vivo* selectivity of RN1 remains to be determined, our *in vitro* results suggest 10-100-fold selectivity versus MAO-A/B, with much greater selectivity versus KDM1B. Furthermore, pharmacokinetic analysis of intraperitoneally administered RN1 revealed excellent brain uptake and retention as measured by LC-MS/MS (Figure 2.7A). Based on these data, we prioritized RN1 for evaluation in behaving animals.

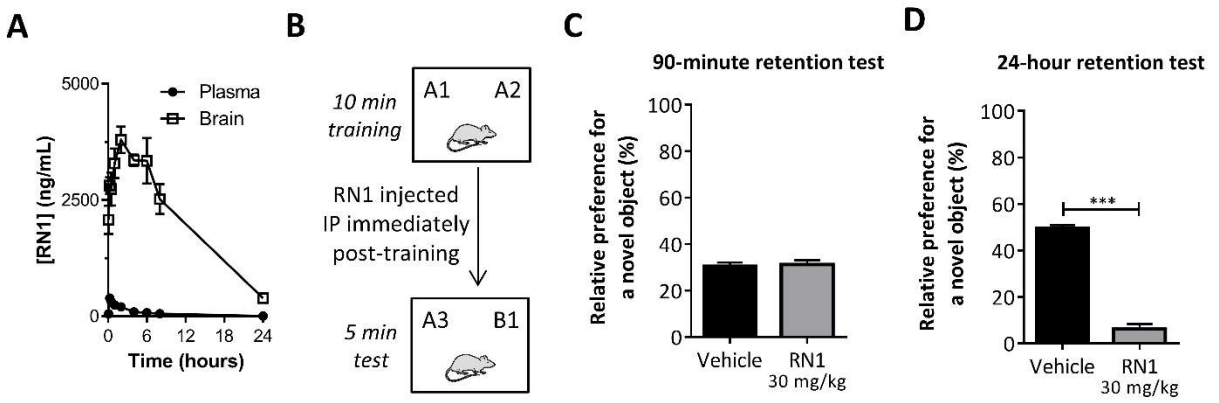

Figure 2.7 RN1 is brain-penetrant and affects rodent behavior.
A. Concentration of RN1 as determined by LC-MS/MS in plasma and brain over time following a single intraperitoneal injection (10 mg/kg) in mice. **B.** Schematic of the novel object recognition task. **C.** Mice treated with RN1 immediately following novel object recognition training exhibit normal discrimination for a novel object as compared to vehicle-treated mice (n=7 for each group). **C.** RN1-treated mice have impaired long-term memory for novel object recognition 24 hours after training (n=10 for each group). Error bars indicate SD, *** $p < 0.001$ by 2-tailed Student's *t* test.

To begin to understand the role of KDM1A in behavior, we examined the effect of RN1 administration on novel object recognition (NOR) in collaboration with the Wood lab at UC Irvine. The novel object recognition task is an excellent initial behavioral test, as it measures complex cognitive processes involving memory, attention, anxiety, and preference for novelty; in addition, NOR does not

require external motivation (reward or punishment), and little training or habituation is required (47). In the NOR task, mice were habituated to a chamber containing two identical objects for 10 minutes (Figure 2.7B). Immediately after habituation, RN1 (30 mg/kg) or vehicle control was administered by intraperitoneal injection. One of the objects was exchanged for a new type of object, then the mice were returned to the chamber after either 90 minutes or 24 hours had elapsed since RN1 administration. Object preference was measured by the difference in time spent exploring the novel object versus the familiar object, normalized to the total time spent investigating. All vehicle-treated mice show a significant preference for the novel object. At 90 minutes after treatment, RN1 concentration in the brain is near its peak (~10 μM for a 10 mg/kg injection, or 1,000-fold greater than the apparent *in vitro* IC_{50}). At this time, RN1-treated mice did not differ from vehicle-treated animals in their preference for the novel object (Figure 2.7C). However, generalized hyper- or hypo-activity resulting from compound treatment might not be captured by this behavior metric, which is normalized by the total time spend investigating either object. Rats treated with 15 mg/kg of TCP for *in vivo* CETSA analysis were altered in their behavior and appearance within 90 minutes of treatment, but these changes were not quantified. At 24 hours, mice treated with RN1 show nearly equal preference for both the novel and familiar objects, differing significantly from the novel-object seeking control mice (Figure 2.7D). Several possibilities exist for this lack of novel object preference, including impaired memory consolidation (a process associated with many structural and post-translational modifications of chromatin, including histone methylation (48)), or decreased motivation for exploration. These effects may be attributable to MAO-A/B and/or KDM1B inhibition in addition to other off-targets (49). Nonetheless, these data are the first to profile the behavioral effects of a highly potent KDM1A inhibitor in rodents and set the stage for future studies of KDM1A neuropharmacology.

2.4 Conclusions

TCP analogs potently inhibit KDM1A *in vitro* and engage KDM1A in living cells, and are thus excellent compounds for future studies of the biological roles of this histone lysine demethylase. In particular, these validated tool compounds will be critical to the development of functional assays of KDM1A inhibition in cells, as bulk histone methylation is not a reliable surrogate measure of demethylase activity. While the panel of orthogonal enzymatic assays was helpful to rank the relative end-point potencies of FAD-directed inhibitors, the obvious discrepancy between the *in vitro* and cellular behavior of TCP suggest that translation of these assays may be limited. The substrate preference of KDM1A is known to be modulated by its co-regulators (10,50); thus, the active-site of cellular KDM1A may be more optimally configured for binding and/or electron transfer by TCP. In addition, TCP can act as a substrate for KDM1A and may be released prior to covalent linkage, suggesting that binding events (as measured by CETSA) and flavin-inactivating events (as measured by enzymatic assays) may be partially decoupled (15). Adapting the CETSA method for analysis of the recombinant enzyme may clarify this distinction. Regardless of mechanism, our data suggest that the possibility of target engagement of KDM1A by TCP in a clinical setting warrants revisiting, particularly as the first wave of TCP analogs enters clinical trials (18).

Our studies are the first to show changes in behavior associated with a brain-penetrant, potent KDM1A inhibitor. Specifically, RN1 alters novel-object seeking in rodents, a complex phenotype which may reflect impaired memory consolidation or decreased motivation for exploration. Alteration of mood and cognition has been associated with inhibitors of the histone deacetylases, and can vary substantially with the pharmacological agent applied (51); these studies motivate and provide a conceptual framework to guide future efforts to validate a role for KDM1A in behavior. Finally, although translation of the *in vitro* assay results to *in vivo* experiments may be limited, our data suggest that TCP analogs such as RN1 retain potency against the monoamine oxidases. Inhibitors of KDM1A that do not target the FAD cofactor may thus be valuable tool compounds to study this histone lysine demethylase in a neurological context.

2.5 Materials and Methods

Inhibitors and Reagents– TCP was purchased from Sigma Aldrich (catalog #P8511) and stored as a 50 mM stock solution in DMSO at -20 °C for biochemical and cell-based experiments, and stored as a powder at -20 °C for animal injection. Bizine was purchased from Axon MedChem (catalog #2306) and was stored as a 25 mM stock solution in DMSO at -20 °C. RN1 was synthesized as previously described (17). Dilutions in aqueous buffer were prepared immediately prior to use.

Recombinant Enzymes and Substrates - Recombinant KDM1A (GenBank Accession No. NM_015013, human amino acids 158-end with N-terminal GST tag, BPS Biosciences, catalog #50100, lot # 91006) was expressed in E. coli and purified as previously described (17,24). KDM1B (GenBank Accession No. XM_005248926.1, human full length with N-terminal GST tag, Active Motif catalog #31470, lot #21814001) was expressed in Sf9 insect cells and purified by the manufacturer. The 21-mer peptide corresponding to the histone H3 dimethylated lysine 4 tail (NH_2-ARTK(me2)QTARKSTGGKAPRKQKA-COOH, abbreviated H3K4me2) was synthesized by the Massachusetts Institute of Technology Biopolymers Laboratory and the purity was confirmed by high performance liquid chromatography (HPLC) and matrix-assisted laser desorption/ionization time-of-flight (MALDI-TOF) mass spectrometry (expected $[M+H^+]$= 2297.71, observed ion= 2298.30). Monoamine oxidase A (human, Sigma Aldrich, catalog #M7316, lot #047K1130) and monoamine oxidase B (human, Sigma Aldrich, catalog #M7441, lot #021M2162) were expressed in BTI insect cells and purified by the manufacturer.

IC_{50} determination and statistical analysis – Nonlinear regression, statistical testing and graph preparation were performed using GraphPad Prism 6 (GraphPad Software, Inc.). The log[inhibitor] was plotted versus the assay response and fitted with a three-parameter non-linear regression to determine the apparent IC_{50} values. Statistical analysis of enzyme activity and blot densitometry data were performed using unpaired, two-tailed Student's t tests with post hoc Holm-Sidak correction for multiple comparisons determine p values or 2-way ANOVA with Dunnett correction for multiple comparisons as

indicated in each figure legend. All error bars indicate standard deviation (SD). A *p* value of <0.05 was considered significant. Relative degree of significance is indicated in figures by the number of asterisks and is defined in each figure legend.

HRP-Coupled Assay – Previous experiments determined that 100 ng of KDM1A in a reaction volume of 30 µL (ie. 30 nM) afforded satisfactory signal over background; subsequently, the substrate K_m for 30 nM KDM1A was determined to be 10 µM, and this concentration was used for all HRP-coupled and mass spectrometry assays unless otherwise specified (data not shown). In addition, the assay was determined to be linear over at least 30 minutes, although enzymatic activity was observed to degrade at reactions longer than 1 hour (Chapter 4). Only a minimal change in background fluorescence was observed upon leaving out of the H3K4me2 peptide. Unless otherwise specified, reactions were run as follows. KDM1A activity was profiled in 50 mM sodium phosphate buffer (Boston BioProducts #BB-185, pH 7.4) with 0.01% BRIJ35 detergent (Calbiochem #203728) in 383-well black non-sterile plates (Corning #3573). To 100 ng of KDM1A in 20 µL of buffer was added inhibitor stock solution in DMSO. Typical volumes of DMSO were 50-500 nL. After pre-incubation of the enzyme and inhibitor for 10 minutes, 10 µL of substrate in buffer was added to a final concentration of 10 µM. The reaction was allowed to proceed for 20 minutes at room temperature, during which time the detection reagent was prepared. HRP (Sigma, #P2088, 5KU) and ADHP (ABD Bioquest #11000, in DMSO) were diluted in buffer, then 30 µL was added to each well for a final concentration of 0.06 U HRP and 40 µM ADHP. The plates were immediately read on a PerkinElmer Wallac Envision 2103 Multilabel plate reader (excitation filter: 485 nm; emission filter: 595 nm). For each compound, the assay was repeated at least 3 times to determine reproducibility. The IC_{50} values reported in Table 2.1 were collected during one single parallel experiment (including TCP) so that direct comparisons can be made.

TR-FRET assay – The assay was performed as previously described (17). Briefly, KDM1A enzymatic reactions were performed in duplicate in a 10 µl reaction volume using an assay buffer of 50 mM Tris, pH

7.5, 0.01% Brij-35 in Proxiplate 384 Plus white plates (Perkin Elmer). Test compounds were pre-incubated for 15 minutes with 25 nM recombinant KDM1A, then the reaction was initiated by addition of 0.0625 µM biotinylated H3K4Me2 substrate peptide (Anaspec # 64356-1). Reactions were terminated after 8 minutes by addition of 10 µl of reaction termination and detection reagents consisting of 50 µM RN1 in 1X LANCE detection buffer, 2 nM Mono-Methyl-Histone H3 (lys4) D1A9 Rabbit mAb (Cell Signaling Technology, catalog # 9723, various lots used), 2 nM LANCE Eu-W1024 anti-rabbit IgG (Perkin Elmer, catalog # AD0082) and 50 nM streptavidin-Ulight in (Perkin Elmer, catalog # TRF0102). Following incubation for one hour at room temperature, the samples were read using a PerkinElmer Wallac Envision 2103 Multilabel plate reader (excitation filter: 337 nm; emission filter: 665 nm).

MS assays – For detection with RapidFire MS, the KDM1A demethylation reaction was performed under identical assay conditions to those used for the HRP-coupled assay and reactions were quenched by the addition of formic acid. Detection of the H3K4me1 and H3K4me0 products were accomplished on an Agilent RF300 Mass Spectrometry System with RapidFire chromatography in line with a triple stage quadrapole mass spectrometer. Using our assay conditions, H3K4me1 was the major product of the demethylation reaction, and was used to calculate the apparent IC_{50} values for each test compound. For detection with LC-MS, KDM1A (30 nM) or KDM1B (60 nM) was pre-incubated with test compounds for 10 min in 50 mM sodium phosphate buffer (pH 7.4 for KDM1A, pH 8.1 for KDM1B) without detergent followed by addition of H3K4me2 peptide substrate (5 µM) in a total reaction volume of 15 µL. The demethylation reaction was quenched with 1% formic acid after 1 hour, then detection of substrate conversion to H3K4me1 and H3K4me0 was accomplished using an Agilent 6310 ion trap mass spectrometer with an ESI source connected to an Agilent 1200 series HPLC with isocratic elution of 5% acetonitrile (ACN) in 0.1% formic acid (FA) at a flow rate of 0.5 mL/min through an Agilent Eclipse XBD-C8 reversed-phase column. Percent enzyme activity was calculated from ratio of H3K4me1 to H3K4me2 peak area in inhibited wells relative to control wells.

MAO-Glo assay – The assays were performed as previously described (17,25). Briefly, activity assays were performed using a MAO-Glo® assay kit (Promega, catalog #V1401), according to the manufacturer's protocol in 384 well Proxiplate 384 Plus white plates (Perkin Elmer) with miniaturization of final assay volume to 20 µL. Amine oxidation was quenched after 1 hour by addition of the reconstituted luciferin detection reagent (50 µL/well), which includes the esterase, luciferase, and ATP. After 20-minute incubation at room temperature in the dark, the luminescence was read using a PerkinElmer Wallac Envision 2103 Multilabel plate reader (emission filter: 570 nm).

Activity-based assay for FAD-inactivation kinetics – Recombinant KDM1A was diluted to 3.2 µM in assay buffer and incubated with RN-1 (final concentration of 6 µM) or vehicle control for various durations. At one minute intervals, 0.3 µL of pre-incubated RN1-KDM1A solution was diluted to 30 µL in assay buffer containing 10 µM H3K4me2 peptide substrate. The demethylation reaction was allowed to proceed for 20 minutes, then the HRP and amplite detection reagents were added and the resorufin fluorescence was detected as described for the HRP-coupled reactions above. The experiment was performed in triplicate.

Fluorescence-based assay for FAD-inactivation kinetics: Recombinant KDM1A was diluted to a final concentration of 5 µM in 50 mM pH 7.4 sodium phosphate buffer and added to black 384-well plate (Corning #3573). Immediately prior to fluorescence measurements, 5 µL of RN1 or vehicle control pre-diluted in buffer from a 25 mM stock solution was added to a final volume of 25 µL and a final inhibitor concentration of 10 µM. Fluorescence measurements were performed every minute for 10 minutes until the change in fluorescence plateaued using a PerkinElmer Wallac Envision 2103 Multilabel plate reader (excitation filter: 485 nm; emission filter: 535 nm). The experiment was performed in triplicate.

Cell lines – HeLa and SH-SY5Y cells were purchased from ATCC (CCL-2) and subcultured according to manufacturer's guidelines in Minimum Essential Eagle's medium (ATCC, #30-2003) supplemented with 10% fetal bovine serum (Gibco, #10437) and 1% penicillin-streptomycin dual antibiotic solution (Fisher,

#ICN1670249) at 37 °C and 5% CO_2 in a humidified incubator. Cells were collected at near confluence by brief (1-2 minute) treatment with 0.05% trypsin-EDTA (Gibco, #25300). Trypsin was quenched with 5 volumes of medium, cells were pelleted by centrifugation for 5 minutes at 1,000 rpm, then media was aspirated and the cells were washed 2x with 5 volumes of PBS prior to subsequent experimentation.

Analysis of bulk histone H3K4me2 levels by western blotting – A large number of variables, including cell type (HeLa, SH-SY5Y, and primary murine embryonic forebrain cultures), treatment duration (6, 12, 24, and 48 hours), cell seeding density, compound dose, and omission of serum from media were tested in an attempt to find conditions resulting in robust and reproducible increases in H3K4me2 as detected by western blot using RN1 and TCP as positive controls. All permutations tested resulted in small (<2-fold) increases in histone methylation and had limited reproducibility, likely due to the inherent variability and semi-quantitative nature of immunodetection techniques. For the data presented here, nearly confluent SH-SY5Y cells subcultured in T-75 flasks (Falcon, catalog #353136) were passaged and density and viabilty were determined using Trypan Blue dye (Life Technologies, catalog #T10282) and an automate cell counter according to manufacturer specifications (Countess, Invitrogen). Cells were diluted to 120,000 cells/mL in media, then 50 µL was added to each well of a 24-well plate (Falcon, catalog #353047). Cells were grown in a 37 ° C incubator with 5% CO_2 overnight until 70-80% confluent. Inhibitor stock solutions in tissue culture-grade DMSO (Sigma, #D2650) were diluted in culture media to a desired concentration such that addition of 5 uL to each well resulted in a final concentration of no more than 0.1% v/v DMSO. An equal volume of DMSO was added as vehicle control. After 24-hour incubation with 10 µM RN1 or DMSO control, the media was gently removed by aspiration and cells were immediately lysed with 150 µL of sample loading buffer (New England BioLabs, catalog #B7703) supplemented with DTT (New England BioLabs, catalog #B7705, final concentration of 40 mM) diluted to 1x in DPBS (Gibco, catalog #14190). Lysates were transferred to Eppendorf tubes and heated to 95 °C for 10 minutes in a heat block before gel electrophoresis, and were thereafter stored at -80 °C. Proteins were separated on

pre-cast 4-12% Bis-Tris Nu-PAGE gels (Invitrogen) with MES running buffer (Invitrogen) for 30 minutes at 200 V, transferred to PVDF membrane (Millipore Immobilon-P, 0.45 µm pore size, catalog #IPVH00010), blocked with 5% non-fat milk in TBST then co-probed overnight with 1:1,000 anti-KDM1A (Abcam, catalog #129195, lot # YI120618DS or Cell Signaling, catalog #2184S, lot #1) and 1:1,000 anti-H3K4me2 (Cell Signaling, catalog #9725S, lot #1) at 4 °C. Detection was achieved with an HRP-linked anti-rabbit secondary antibody and ECL substrate (Thermo Scientific) and captured on autoradiography film (LabScientific). Films were scanned and band intensities from exposures within a linear range were quantified in ImageJ (NIH). Percent enzyme activity was calculated from the remaining H3K4me2 starting material of inhibited lanes relative to control lanes.

Immunoprecipitation assay - HeLa cells were lysed with sonication at 4 °C (Fischer FB120, 50% power for 30 seconds, alternating 1 second on and 2 seconds off) in ice-cold PBS containing 0.15% Ipegal CA-630 (Sigma Aldrich) and 1x protease inhibitors (Roche, complete, EDTA-free, prepared just prior to use). Lysate was pre-cleared for 1 hour, nutated with anti-KDM1A antibody (Abcam, catalog #129195, lot #YI120618DS) for 1 hour, then immunoprecipitated overnight at 4 °C at a ratio of 12 million HeLa cells per 50 µL packed protein agarose A beads (Roche) per 5 µL antibody per tube. KDM1A-bound beads were pooled, washed three times with 50 mM phosphate buffer, pH 7.4 with 0.1% Brij-35 (Calbiochem), then divided into Eppendorf tubes (25 µL of 1:1 bead slurry per reaction). Immunoprecipitated KDM1A was pre-incubated with 10 µM RN1 or vehicle control for 10 minutes before addition of 10 µM H3K4me2 substrate for a final reaction volume of 30 µL. Reactions were incubated at 37 °C for 1 hour, then quenched by addition of sample loading buffer + DTT. Reactions were run in technical replicates, and the entire procedure was repeated twice. Proteins were separated and detected by western blotting as described above. The IgG band resulting from the KDM1A antibody used for immunoprecipitation was readily detected and used as an additional loading control. Specificity of the H3K4me2 antibody for the recombinant H3K4me2 substrate starting material was confirmed with a substrate-only control and an

unmethylated peptide substrate control (data not shown). MES was determined to be the optimal running buffer to resolve the highly cationic synthetic peptide, which ran with an apparent mass of around 10 kDa.

Live-cell cellular thermal shift assay (CETSA) – The CETSA method was closely adapted from previous reports (41,42). SH-SY5Y cells were grown to near confluence in T-75 flasks as described above. Cell were collected with a cell lifter (Corning, catalog #3008) and the cell density was determined using Trypan Blue as described above. Trypsinization was avoided to minimize effects on membrane permeability. The cell suspension was adjusted to a density of 1 million cells per mL of culture media, then 3 mL of gently mixed suspension was transferred a 15-mL conical tube (Falcon, catalog #352196), with one tube per compound treatment. Test compounds or DMSO vehicle control were pre-diluted in 37 °C cell culture media then added to the cell suspension, with a final amount of DMSO not exceeding 0.1% v/v. During the 30-minute exposure to test compounds, cells were kept in a humidified incubator with the lids of the conical tubes loosened to allow for gas exchange. In experiments not fully described here, adherent SH-SY5Y cells were treated with test compounds in 6-well plates (Falcon, catalog #353226) and then scraped and collected for CETSA analysis. This method yielded comparable results for KDM1A T_M determination and for the magnitude of thermal stabilization by FAD-directed inhibitors, but greater variability in cell density from well to well was observed by western blot. As the CETSA method relies on aggregation of denatured proteins, which depends on protein concentration, normalization of cell density prior to application of test compounds and a thermal gradient was favored (42). In both methods, cells were pelleted after exposure to test compound, washed twice with 37 °C PBS, then suspended at a density of 1 million cells per 0.1 mL of PBS. To each tube of a PCR strip (Axygen Scientific, catalog #22-705) was added 25 µL of cell suspension, then samples were heated in a gradient method in a BioRad MyCycler thermal cycler with a hold time of 3 minutes prior to cooling to room temperature for 5 minutes. Cells were lysed by 3 cycles of freeze-thawing on dry ice, then aggregated proteins were pelleted with by high speed (20,000 x g) centrifugation for 20 minutes at 4 °C in a refrigerated Eppendorf centrifuge (model

#5417R). Supernatant (15 µL) was carefully removed and mixed with 7.5 µL of sample loading buffer + DT for analysis by western blotting as described above, or by dot blotting. Both methods used 1:1000 KDM1A (Cell Signaling, catalog #2184S, lot #1) or 1:1000 RCOR1 (Upstate, catalog #07-455, lot # JBC1368011) and overnight incubation at 4 °C.

Dot blot assay - PVDF membrane (Millipore Immobilon-P, 0.45 µm pore size, catalog #IPVH00010) was activated by immersion in methanol for 30 seconds, then briefly rinsed in DI water. The membrane and a comparably sized, thick sheet of filter paper were equilibrated in transfer buffer (25 mM Tris glycine with 12.5% methanol) while samples were heated to 95 °C then cooled to room temperature. The soaked filter paper was placed on a Kimwipe, then the PVDF membrane was placed on top of the filter paper and allowed to briefly air dry until the surface was no longer reflective. Then, 1.5 µL of protein samples were deposited onto the membrane using a multichannel pipette 16-channel 0.5 – 12.5 µL Matrix electronic multichannel pipettor (Thermo Scientific). A slight decrease in protein adsorption was observed as the membrane dried. To account for this effect, samples from the same temperature were deposited simultaneously with the multichannel pipettor such that comparison across compound treatments could be made. Additionally, samples for dot blotting were stored in PCR strips to facilitate rapid application to the PVDF membrane. After proteins had absorbed, the membrane was allowed to fully dry, then blocked in 5% non-fat milk in TBST then probed with antibodies in an identical fashion to western blotting. Dot blotting requires very specific antibody binding, as there is no separation of proteins by SDS-PAGE, thus limiting the general applicability of this technique. In addition, some antibodies that were very clean by western blotting, such as anti-KDM1A from Abcam, catalog #129195, lot # YI120618DS, did not appear to recognize KDM1A by dot blot. For all dot blot data, anti-KDM1A from Cell Signaling, catalog #2184S, lot #1 was used. To generate the heat maps represented in Figure 2.4, the measured dot intensities were normalized with the average background-subtracted dot intensity from the lowest temperature of the vehicle-treated samples set to 100% and the highest temperature of the vehicle-treated sample set to 0%.

These average normalized intensities were then binned into quartiles (0-25%, 25-50%, 50-75%, and 75-100%) and color-coded accordingly. Statistical analyses were performed on background subtracted but non-transformed data. The number of replicates is indicated in each figure legend.

In vivo CETSA – Male Sprague-Dawley rats (250 – 350 g, Charles River Labs) were treated with 15 mg/kg Parnate HCl (2 animals) or saline vehicle (2 animals) by intraperitoneal (IP) administration (total volume of 1-2 mL) with manual restraint. Animals were kept in their home cage for 2 hours, then sacrificed and their brains removed, bisected, and frozen on dry ice. Previous experiments indicated that homogenized brain lysate could not be frozen and used for CETSA analysis, as no melting curves were obtained. To overcome this limitation, the right hemisphere from each animal was powderized by mortar and pestle under liquid nitrogen and aliquoted for storage. For CETSA analysis, an aliquot of tissue from each animal was briefly thawed on ice, weighed, suspended in ice-cold PBS + 0.15% Ipegal CA-630 (Sigma Aldrich) and 1x protease inhibitors (Roche, complete, EDTA-free, prepared just prior to use) at a concentration of 50 mg wet tissue/mL lysis buffer, and lysed with sonication at 4 °C (Fischer FB120, 50% power for 30 seconds, alternating 1 second on and 2 seconds off). From here, brain lysate from each animal was processed following the same protocol as the live cell CETSA, with the omission of the free-thaw lysis step. Samples were analyzed by western blotting as described above.

Pharmacokinetics and Biodistribution studies of RN-1 – Biodistribution of RN1 was determined by the bioanalytical group of Sai Advantium Pharma Ltd (Pune, India) exactly a previously described (17). Briefly, 27 male mice were injected intraperitoneally with freshly prepared RN-1 solution formulation at 10 mg/kg dose. Blood was collected at the indicated time points, then the animals were sacrificed and their brain removed and homogenized. The concentration of RN1 in plasma and brain samples was determined by LC-MS/MS and quantified using internal standards.

Novel Object Recognition – Novel object recognition assays were performed in the laboratory of Dr. Marcelo Wood exactly as previously described (17). Briefly, before training, mice were handled 1-2

min for 4 days and then habituated to the experimental apparatus (white rectangular open field, 30 x 23 x 21.5 cm) 5 min a day for 6 consecutive days in the absence of objects. During training, mice were placed into the experimental apparatus with two identical objects (A1 and A2; either 100 ml beakers, 2.5 cm diameter, 4 cm height; or large blue Lego blocks, 2.5 x 2.5 x 5 cm) and were allowed to explore for 10 min (52). Immediately following training, mice were systemically administered either 30 mg/kg RN1, dissolved in a vehicle of 3% DMSO in ddH_2O, or vehicle alone (10 mL/kg volume; intraperitoneal). During the retention test, (90 minutes for short-term memory or 24 hours for long-term memory, tested in different sets of animals), mice explored the experimental apparatus for 5 min. For the novel object recognition task, one familiar object (A3) and one novel object (B1) were placed in the same location as during training. All combinations and locations of objects were used in a balanced manner to reduce potential biases due to preference for particular locations or objects. All training and testing trials were videotaped and analyzed by individuals blind to the treatment condition. A mouse was scored as exploring an object when its head was oriented toward the object within a distance of 1 cm or when the nose was touching the object. The relative exploration time was recorded and expressed by a discrimination index [DI = (t_{novel} – $t_{familiar}$)/(t_{novel} + $t_{familiar}$) X 100].

2.6 References

1. Kouzarides, T. (2007) Chromatin modifications and their function. *Cell* **128**, 693-705

2. Levenson, J. M., and Sweatt, J. D. (2005) Epigenetic mechanisms in memory formation. *Nature Reviews Neuroscience* **6**, 108-118

3. Fagiolini, M., Jensen, C. L., and Champagne, F. A. (2009) Epigenetic influences on brain development and plasticity. *Current opinion in neurobiology* **19**, 207-212

4. Deutsch, S. I., Rosse, R. B., Mastropaolo, J., Long, K. D., and Gaskins, B. L. (2008) Epigenetic therapeutic strategies for the treatment of neuropsychiatric disorders: ready for prime time? *Clinical neuropharmacology* **31**, 104-119

5. Tsankova, N., Renthal, W., Kumar, A., and Nestler, E. J. (2007) Epigenetic regulation in psychiatric disorders. *Nature Reviews Neuroscience* **8**, 355-367

6. Network, T., and Consortium, P. A. S. o. t. P. G. (2015) Psychiatric genome-wide association study analyses implicate neuronal, immune and histone pathways. *Nature neuroscience* **18**, 199-209

7. Schmidt, D. M., and McCafferty, D. G. (2007) trans-2-Phenylcyclopropylamine is a mechanism-based inactivator of the histone demethylase LSD1. *Biochemistry* **46**, 4408-4416

8. Shi, Y., Lan, F., Matson, C., Mulligan, P., Whetstine, J. R., Cole, P. A., Casero, R. A., and Shi, Y. (2004) Histone demethylation mediated by the nuclear amine oxidase homolog LSD1. *Cell* **119**, 941-953

9. Yang, M., Culhane, J. C., Szewczuk, L. M., Jalili, P., Ball, H. L., Machius, M., Cole, P. A., and Yu, H. (2007) Structural basis for the inhibition of the LSD1 histone demethylase by the antidepressant trans-2-phenylcyclopropylamine. *Biochemistry* **46**, 8058-8065

10. Shi, Y. J., Matson, C., Lan, F., Iwase, S., Baba, T., and Shi, Y. (2005) Regulation of LSD1 histone demethylase activity by its associated factors. *Molecular cell* **19**, 857-864

11. Humphrey, G. W., Wang, Y., Russanova, V. R., Hirai, T., Qin, J., Nakatani, Y., and Howard, B. H. (2001) Stable histone deacetylase complexes distinguished by the presence of SANT domain proteins CoREST/kiaa0071 and Mta-L1. *Journal of Biological Chemistry* **276**, 6817

12. Shi, Y., Sawada, J., Sui, G., Affar, E. B., Whetstine, J. R., Lan, F., Ogawa, H., Luke, M. P. S., and Nakatani, Y. (2003) Coordinated histone modifications mediated by a CtBP co-repressor complex. *Nature* **422**, 735-738

13. You, A., Tong, J. K., Grozinger, C. M., and Schreiber, S. L. (2001) CoREST is an integral component of the CoREST-human histone deacetylase complex. *Proceedings of the National Academy of Sciences* **98**, 1454

14. Zheng, Y. C., Ma, J., Wang, Z., Li, J., Jiang, B., Zhou, W., Shi, X., Wang, X., Zhao, W., and Liu, H. M. (2015) A Systematic Review of Histone Lysine-Specific Demethylase 1 and Its Inhibitors. *Medicinal research reviews* **35**, 1032-1071

15. Binda, C., Valente, S., Romanenghi, M., Pilotto, S., Cirilli, R., Karytinos, A., Ciossani, G., Botrugno, O. A., Forneris, F., and Tardugno, M. (2010) Biochemical, structural, and biological evaluation of tranylcypromine derivatives as inhibitors of histone demethylases LSD1 and LSD2. *Journal of the American Chemical Society* **132**, 6827-6833

16. Binda, C., Edmondson, D. E., and Mattevi, A. (2013) Monoamine Oxidase Inhibitors: Diverse and Surprising Chemistry with Expanding Pharmacological Potential. in *Advancing Methods for Biomolecular Crystallography*, Springer. pp 309-312

17. Neelamegam, R., Ricq, E. L., Malvaez, M., Patnaik, D., Norton, S., Carlin, S. M., Hill, I. T., Wood, M. A., Haggarty, S. J., and Hooker, J. M. (2011) Brain-penetrant LSD1 inhibitors can block memory consolidation. *ACS chemical neuroscience* **3**, 120-128

18. Maes, T., Carceller, E., Salas, J., Ortega, A., and Buesa, C. (2015) Advances in the development of histone lysine demethylase inhibitors. *Current opinion in pharmacology* **23**, 52-60

19. Mimasu, S., Umezawa, N., Sato, S., Higuchi, T., Umehara, T., and Yokoyama, S. (2010) Structurally designed trans-2-phenylcyclopropylamine derivatives potently inhibit histone demethylase LSD1/KDM1. *Biochemistry* **49**, 6494-6503

20. Prusevich, P., Kalin, J. H., Ming, S. A., Basso, M., Givens, J., Li, X., Hu, J., Taylor, M. S., Cieniewicz, A. M., and Hsiao, P.-Y. (2014) A selective phenelzine analogue inhibitor of histone demethylase LSD1. *ACS chemical biology* **9**, 1284-1293

21. Hauser, A. T., Bissinger, E. M., Metzger, E., Repenning, A., Bauer, U. M., Mai, A., Schüle, R., and Jung, M. (2011) Screening Assays for Epigenetic Targets Using Native Histones as Substrates. *Journal of Biomolecular Screening*

22. Wigle, T. J., Provencher, L. M., Norris, J. L., Jin, J., Brown, P. J., Frye, S. V., and Janzen, W. P. (2010) Accessing protein methyltransferase and demethylase enzymology using microfluidic capillary electrophoresis. *Chemistry & biology* **17**, 695-704

23. Gauthier, N., Caron, M., Pedro, L., Arcand, M., Blouin, J., Labonté, A., Normand, C., Paquet, V., Rodenbrock, A., and Roy, M. (2011) Development of Homogeneous Nonradioactive Methyltransferase and Demethylase Assays Targeting Histone H3 Lysine 4. *Journal of Biomolecular Screening*

24. Forneris, F., Binda, C., Adamo, A., Battaglioli, E., and Mattevi, A. (2007) Structural basis of LSD1-CoREST selectivity in histone H3 recognition. *The Journal of biological chemistry* **282**, 20070-20074

25. Zhou, W., Valley, M. P., Shultz, J., Hawkins, E. M., Bernad, L., Good, T., Good, D., Riss, T. L., Klaubert, D. H., and Wood, K. V. (2006) New bioluminogenic substrates for monoamine oxidase assays. *Journal of the American Chemical Society* **128**, 3122-3123

26. Hayward, D., and Cole, P. (2016) LSD1 Histone Demethylase Assays and Inhibition. *Methods in Enzymology*

27. Yu, V., Fisch, T., Long, A. M., Tang, J., Lee, J. H., Hierl, M., Chen, H., Yakowec, P., Schwandner, R., and Emkey, R. (2011) High-Throughput TR-FRET Assays for Identifying Inhibitors of LSD1 and JMJD2C Histone Lysine Demethylases. *J Biomol Screen*

28. Plant, M., Dineen, T., Cheng, A., Long, A. M., Chen, H., and Morgenstern, K. A. (2011) Screening for lysine-specific demethylase-1 inhibitors using a label-free high-throughput mass spectrometry assay. *Analytical biochemistry*

29. Rye, P., Frick, L., LaMarr, W., and Özbal, C. (November 2009) High-throughput Mass Spectrometric Detection of Histone 3 Demethylation. in *Society for Biomolecular Sciences Label Free Meeting*, San Diego, CA

30. Mimasu, S., Sengoku, T., Fukuzawa, S., Umehara, T., and Yokoyama, S. (2008) Crystal structure of histone demethylase LSD1 and tranylcypromine at 2.25 Å. *Biochemical and biophysical research communications* **366**, 15-22

31. Kakizawa, T., Mizukami, T., Itoh, Y., Hasegawa, M., Sasaki, R., and Suzuki, T. (2016) Evaluation of phenylcyclopropylamine compounds by enzymatic assay of lysine-specific demethylase 2 in the presence of NPAC peptide. *Bioorganic & Medicinal Chemistry Letters*

32. Egashira, T., Takayama, F., and Yamanaka, Y. (1999) The Inhibition of Monoamine Oxidase Activity by Various Antidepressants. Differences Found in Various Mammalian Species. *The Japanese Journal of Pharmacology* **81**, 115-121

33. Binda, C., Li, M., Hubálek, F., Restelli, N., Edmondson, D. E., and Mattevi, A. (2003) Insights into the mode of inhibition of human mitochondrial monoamine oxidase B from high-resolution crystal structures. *Proceedings of the National Academy of Sciences* **100**, 9750-9755

34. Forneris, F., Orru, R., Bonivento, D., Chiarelli, L. R., and Mattevi, A. (2009) ThermoFAD, a Thermofluor®-adapted flavin ad hoc detection system for protein folding and ligand binding. *FEBS journal* **276**, 2833-2840

35. Burg, J. M., Link, J. E., Morgan, B. S., Heller, F. J., Hargrove, A. E., and McCafferty, D. G. (2015) KDM1 class flavin-dependent protein lysine demethylases. *Peptide Science* **104**, 213-246

36. Schroeder, F. A., Lewis, M. C., Fass, D. M., Wagner, F. F., Zhang, Y.-L., Hennig, K. M., Gale, J., Zhao, W.-N., Reis, S., and Barker, D. D. (2013) A selective HDAC 1/2 inhibitor modulates chromatin and gene expression in brain and alters mouse behavior in two mood-related tests. *PloS one* **8**, e71323

37. Zhang, K., Siino, J. S., Jones, P. R., Yau, P. M., and Bradbury, E. M. (2004) A mass spectrometric "Western blot" to evaluate the correlations between histone methylation and histone acetylation. *Proteomics* **4**, 3765-3775

38. Forneris, F., Binda, C., Dall'Aglio, A., Fraaije, M. W., Battaglioli, E., and Mattevi, A. (2006) A highly specific mechanism of histone H3-K4 recognition by histone demethylase LSD1. *Journal of Biological Chemistry* **281**, 35289-35295

39. Ooi, L., and Wood, I. C. (2007) Chromatin crosstalk in development and disease: lessons from REST. *Nature Reviews Genetics* **8**, 544-554

40. Shi, Y.-J., Matson, C., Lan, F., Iwase, S., Baba, T., and Shi, Y. (2005) Regulation of LSD1 histone demethylase activity by its associated factors. *Molecular cell* **19**, 857-864

41. Molina, D. M., Jafari, R., Ignatushchenko, M., Seki, T., Larsson, E. A., Dan, C., Sreekumar, L., Cao, Y., and Nordlund, P. (2013) Monitoring drug target engagement in cells and tissues using the cellular thermal shift assay. *Science* **341**, 84-87

42. Franken, H., Mathieson, T., Childs, D., Sweetman, G. M., Werner, T., Tögel, I., Doce, C., Gade, S., Bantscheff, M., and Drewes, G. (2015) Thermal proteome profiling for unbiased identification of direct and indirect drug targets using multiplexed quantitative mass spectrometry. *Nature protocols* **10**, 1567-1593

43. Martinez Molina, D., and Nordlund, P. (2016) The cellular thermal shift assay: a novel biophysical assay for in situ drug target engagement and mechanistic biomarker studies. *Annual review of pharmacology and toxicology* **56**, 141-161

44. Maitre, L., and Wyss, E. (1967) Monoamine oxidase inhibiting properties of SU-11,739 in the rat. Comparison with pargyline, tranylcypromine and iproniazid. *Journal of Pharmacology and Experimental Therapeutics* **157**, 81-88

45. Reagan-Shaw, S., Nihal, M., and Ahmad, N. (2008) Dose translation from animal to human studies revisited. *The FASEB Journal* **22**, 659-661

46. Amsterdam, J. D., and Berwish, N. (1989) High dose tranylcypromine therapy for refractory depression. *Pharmacopsychiatry* **22**, 21-25

47. Antunes, M., and Biala, G. (2012) The novel object recognition memory: neurobiology, test procedure, and its modifications. *Cognitive processing* **13**, 93-110

48. Gupta, S., Kim, S. Y., Artis, S., Molfese, D. L., Schumacher, A., Sweatt, J. D., Paylor, R. E., and Lubin, F. D. (2010) Histone methylation regulates memory formation. *The Journal of neuroscience* **30**, 3589-3599

49. Salsali, M., Holt, A., and Baker, G. B. (2004) Inhibitory effects of the monoamine oxidase inhibitor tranylcypromine on the cytochrome P450 enzymes CYP2C19, CYP2C9, and CYP2D6. *Cellular and molecular neurobiology* **24**, 63-76

50. Metzger, E., Wissmann, M., Yin, N., Müller, J. M., Schneider, R., Peters, A. H., Günther, T., Buettner, R., and Schüle, R. (2005) LSD1 demethylates repressive histone marks to promote androgen-receptor-dependent transcription. *Nature* **437**, 436-439

51. Fass, D. M., Schroeder, F. A., Perlis, R. H., and Haggarty, S. J. (2014) Epigenetic mechanisms in mood disorders: targeting neuroplasticity. *Neuroscience* **264**, 112-130

52. Stefanko, D. P., Barrett, R. M., Ly, A. R., Reolon, G. K., and Wood, M. A. (2009) Modulation of long-term memory for object recognition via HDAC inhibition. *Proceedings of the National Academy of Sciences* **106**, 9447

CHAPTER 3

3 Screening efforts towards the discovery of novel KDM1A inhibitors

3.1 Abstract

Tremendous interest in the therapeutic targeting of KDM1A has motivated efforts to discover novel classes of small molecule inhibitors. However, inadequate assay validation and lack of a clear cellular phenotype of KDM1A engagement has hampered drug discovery. Here, we present outcomes of a high throughput screen and secondary assays which revealed a predominant mode of KDM1A inhibition based on thiol-reactivity, and widespread contamination of test compounds by elemental sulfur. Inhibition of KDM1A by multiple classes of thiol-reactive compounds, including the FDA-approved drug disulfiram, strongly suggests that cysteine modification antagonizes enzyme catalysis. Counterscreening in the presence of reducing agents revealed two novel scaffolds which may represent starting points for further medicinal chemistry development. However, these compounds do not appear to engage KDM1A in cells using assays developed with FAD-directed inhibitors, and are not active in a Wnt signaling reporter assay. Considerations for future probe development are discussed in light of the pronounced thiol-reactivity of KDM1A.

3.2 Introduction

KDM1A is implicated in diverse biological processes and may be therapeutically targeted in breast, prostate, colon, esophageal, brain, lung, bladder and blood cancer progression, HIV and HSV virus replication, adipose tissue energy expenditure, and neuropsychiatric disease (reviewed in (1-3)). Accordingly, tremendous drug discovery efforts have been made to identify novel small molecule inhibitors, primarily for application in oncology. The most potent and well-characterized KDM1A inhibitors

are derivatives of FAD-directed propargylamine, cyclopropylamine, and hydrazine chemical scaffolds, with two cyclopropylamine derivatives entering clinical trials at time of writing (4). The most selective KDM1A inhibitor described to date is a TCP-analog developed by GlaxoSmithKline, GSK2879552, which exerts antitumor effects against some small cell lung carcinoma cell lines without increasing histone methylation levels, although a DNA hypomethylation signature was observed in responsive lines (5). In addition to modifications made to increase selectivity for KDM1A, TCP has also been modified with core scaffolds targeting histone deacetylases or Jumonji C demethylases to generate dual function inhibitors (6,7), although these compounds tend to be less potent and less selective for KDM1A than typical TCP analogs. Although many FAD-directed inhibitors have been developed, their selectivity against the monoamine oxidases substantially limits their use for studies of KDM1A activity in the brain and other contexts in which neurotransmitters play a physiological role (1).

To overcome the inherently-limited selectivity of FAD-directed inhibitors, numerous screening efforts to identify non-covalent KDM1A inhibitors have been conducted, and with disappointing results. Although several non-covalent inhibitors have been reported, the *in vitro* potency of these compounds is weak (generally 1-20 μM), assay validation is typically lacking, and cellular activity is frequently assessed by toxicity in cancer lines without validation of KDM1A inhibition as the relevant mechanism of action (1). For example, by far the most potent non-covalent inhibitor reported is SP2509 (8), but its activity was only assessed by the HRP-coupled assay without orthogonal validation or counterscreening, despite the fact that N'-(2-hydroxybenzylidene)hydrazide core of the compound is known to interfere with numerous assays (9), and the primary cellular phenotype was toxicity. While these compounds may have utility in oncology, they are not suitable for studies of KDM1A function in the central nervous system. More thorough mechanistic characterization of oligamine and bisguanidine inhibitors of spermine oxidase (SMO/PAOh1) has revealed reversible inhibition of KDM1A (10-13), but these highly-charged, detergent-like species have limited potential for systemic administration. In short, pervasive methodological issues

and lack of a clear cellular phenotype of KDM1A engagement have plagued efforts to identify novel classes of KDM1A inhibitors. Herein, we report the outcomes of a high throughput screen and secondary assays which collectively revealed a predominant mode of KDM1A inhibition based on thiol-reactivity. Two novel scaffolds are described which may represent starting points for further medicinal chemistry development, but do not appear to engage KDM1A in cells.

3.3 Results and Discussion

3.3.1 High throughput screening strategy

High throughput screening was used to identify unique small-molecule scaffolds with KDM1A inhibitory potential that could serve as platforms for chemical optimization (Figure 3.1). The lead scaffolds identified through HTS were carried through a pipeline of experiments for validation as KDM1A inhibitors. The primary assay for KDM1A inhibition was an HRP-coupled assay as previously described (14,15), which was chosen because of its relatively low cost, operational simplicity, and high degree of reproducibility. For our experiments we used a truncated form of recombinant human KDM1A (Δ1 – 157) with robust demethylase activity (16) (BPS Biosciences) in conjunction with a synthetic H3K4me2 peptide substrate (1-21 aa). The action of KDM1A on this substrate produces one equivalent of peroxide (per demethylation and re-oxidation event), which can be detected and quantified through an HRP-catalyzed reaction with ADHP (10-acetyl-3,7-dihydroxyphenoxazine). The product of this coupled reaction, resorufin, can be readily detected with a fluorescence plate reader.

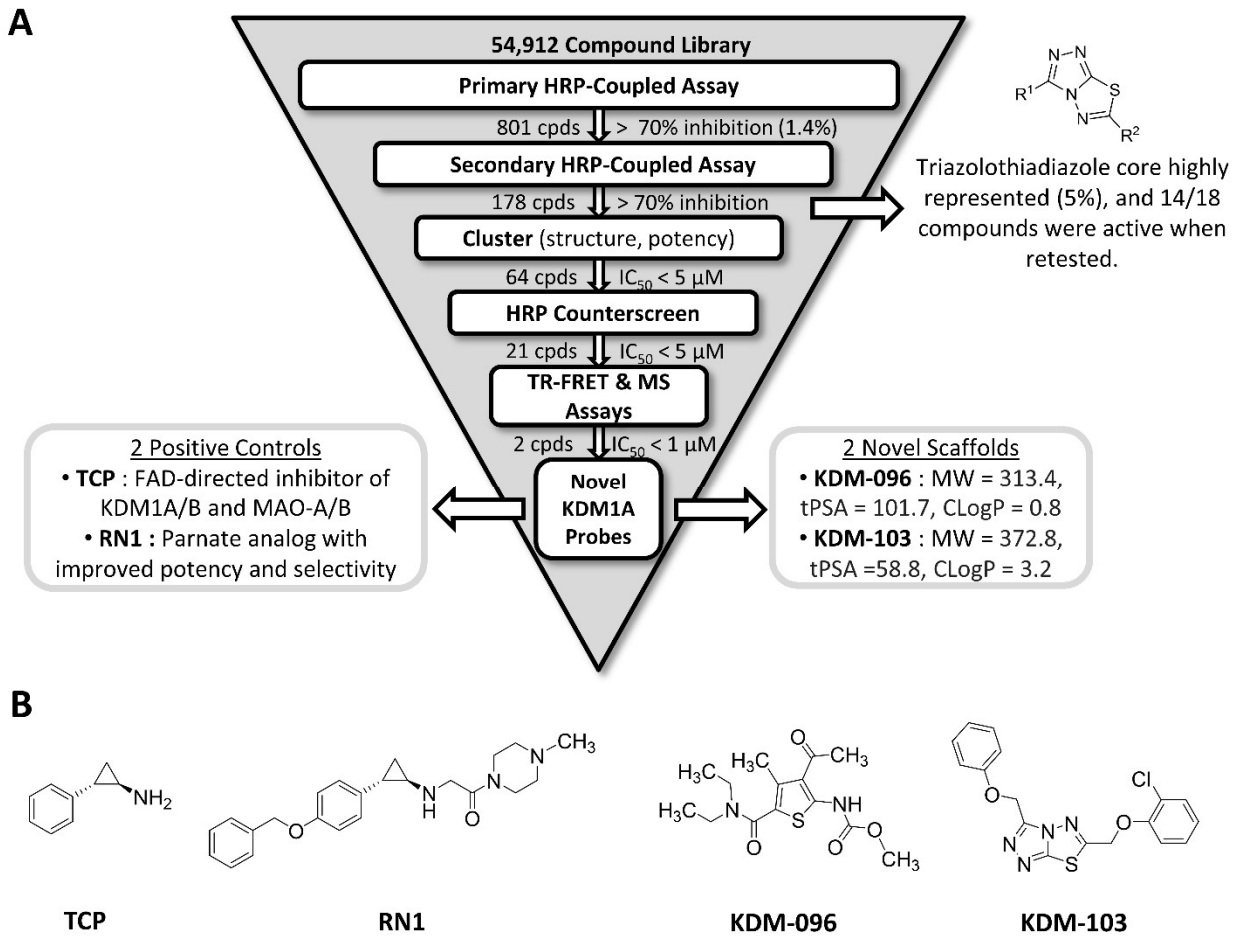

Figure 3.1 Summary of screening strategy to discover novel inhibitors of KDM1A.
A. Hits from high-throughput screening were validated by three orthogonal primary screens and five counter-screens. Two novel scaffolds, KDM-096 and KDM-103 were identified. KDM-103 features the triazolothiadiazole core highly enriched in active compounds identified in secondary screening. **B.** Chemical structures of FAD-directed positive control inhibitors, TCP and RN1, and novel inhibitor scaffolds, KDM-096 and KDM-103.

The small molecule library of 54,912 compounds was screened at an initial concentration of 13 µM. These compounds were obtained from the Prestwick Collection of FDA-approved drugs and bioactives and a commercially-available BPBio library, and were screened by the Partners Center for Drug Discovery (PCDD) at a single concentration of 13 µM. At a threshold of 70% inhibition or greater relative to DMSO, 810 compounds (1.4%) were considered as hits, and were subsequently tested in a 3-point dose-response assay. To assess whether the primary hit compounds interacted directly with hydrogen peroxide, ADHP,

resorufin, or HRP, a counter-screen was implemented in house whereby compounds were added to a reaction consisting of HRP and the ADHP substrate in the absence of KDM1A. Peroxide was added to match the signal generated by the activity of KDM1A. This additional counterscreen identified numerous compounds which inhibited HRP or reacted with the coupled assay components, often resulting in similar apparent IC_{50} values as measured with the coupled KDM1A assay. These results were used to eliminate approximately two-thirds of the primary hits. The remaining 21 compounds were then validated using the RapidFire MS and TR-FRET assays as previously described (Chapter 2, (15,17-20)). TCP and RN1 were used as positive controls in all assay formats. There was much greater variability between the HRP-coupled and MS assays for the compounds identified by screening relative to the panel of FAD-directed inhibitors, suggesting that many more of the screening compounds interacted with the HRP-detection reagents. The TR-FRET assay produced lower but qualitatively similar IC_{50} values to the MS results. Taken together, these assays identified 2 novel KDM1A scaffolds with IC_{50} values of less than 1 μM: KDM-094 and five structurally-related triazolothiadiazoles, of which KDM-103 was the most potent (Figure 3.1). Additionally, chlorhexidine (KDM-055), an FDA-approved antiseptic and structural analog of known bisguanidine KDM1A inhibitors (10,11,13) was identified as a less-potent (10 – 20 μM) inhibitor. The high incidence of false-positives in the initial hits highlights the limitations of coupled-assays and the need for stringent counter-screening and secondary assays in probe discovery.

3.3.2 Discovery of contamination of lead compounds by elemental sulfur (S_8)

The triazolothiadiazole core was highly represented in hits from the secondary HRP-coupled assay (~5% of the 178 secondary hits), is present in numerous bioactive molecules, and is synthetically tractable (21,22). Based on these attractive characteristics, a series of analogs was synthesized as an entryway to future SAR efforts (data not shown). The most potent of the initial series, KDM-103 (Figure 3.1B), was selected for additional studies of selectivity and binding kinetics. Upon re-synthesis and purification,

however, the inhibitory potency of KDM-103 was found to be negligible compared to the original stock solution, prompting an investigation to discover the active species (Figure 3.2). Puzzlingly, the ^{1}H and ^{13}C NMR spectra and LC-MS data for the original preparation of KDM-103 did not reveal obvious impurities (Supplementary Figure A1 – A3). A highly non-polar species was isolated by extraction into hexanes but eluded structural characterization until crystals were analyzed by X-ray crystallography and determined to consist of elemental sulfur (data not shown). Inhibition of KDM1A by commercial-grade sulfur (Sigma) was confirmed by both HRP-coupled and RapidFire MS assays (Figure 3.2). Importantly, the poor solubility of S_8 in DMSO and aqueous media suggest that the observed IC_{50} values (~100 nM) are almost certainly underestimates of the true potency. The mechanism by which elemental sulfur was synthetically produced remains unclear, but likely originates from the thiolate eliminated during the cyclization of the 1,2,4-triazole-3-thiol precursor to KDM-103 and other triazolothiadiazoles. Based on recovered masses isolated from extraction into hexanes, S_8 comprised about 5% w/w of crudely purified KDM-103, and appeared to have enhanced solubility in DMSO in the presence of the inactive triazolothiadiazole (Figure 3.2 and data not shown).

What is the significance of KDM1A inhibition by S_8? There are limited examples of polysulfanes, including elemental sulfur, inhibiting *in vitro* enzyme activity by sulfuration of critical cysteine thiols (23-25). However, the cellular relevance of this mechanism remains unclear. Elemental sulfur has extremely low solubility in aqueous solution, polysulfides are relatively unstable species with cysteine adducts expected to have poorly controlled regioselectivity, and the potential source of elemental sulfur and/or polysulfide species in mammals is unknown (26). Preliminary cell-based experiments with exogenously applied sulfur were plagued by precipitation of S_8 (10 µM – 1 mM) in culture media and cell death (data not shown).

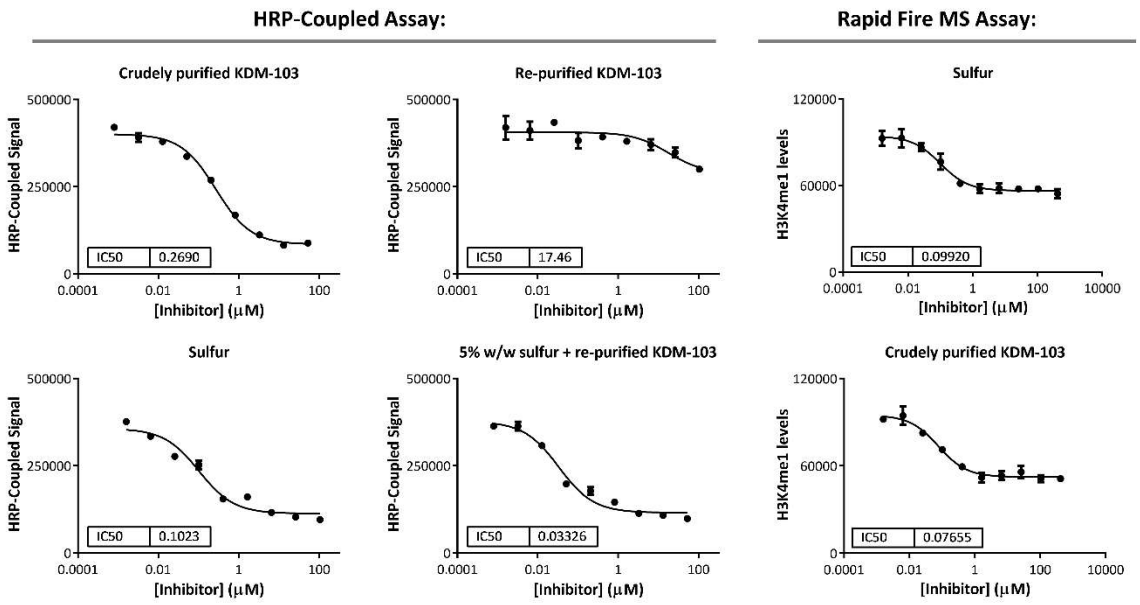

Figure 3.2 KDM1A is potently inhibited by elemental sulfur.
The activity of KDM-103 was lost upon re-synthesis and purification due to removal of contaminating S_8. Inhibition of KDM1A by commercial-grade S_8 was validated in both the HRP-coupled (left) and Rapid Fire MS assays (right).

3.3.3 Multiple classes of thiol-reactive compounds potently inhibit KDM1A

To gain further insight on the possible mechanisms of inhibition by S_8, we examined the structures of other KDM1A inhibitors identified in our screen and found that many are known to be thiol-reactive through more canonical sulfhydryl chemistries. For example, the FDA-approved drug disulfiram (KDM-094) and has been used clinically as an aldehyde dehydrogenase inhibitor, where it inhibits catalysis by modification of active-site cysteines (27). We found that disulfiram potently inhibits KDM1A. Maleimides such as KDM-037 (naphthylmaleimide, Np-Mal) and isothiazolinones such as KDM-028 are also well-known to trap reactive cysteine residues. A small library of other known thiol-reactive compounds was tested for KDM1A inhibition, leading to identification of the disulfide-forming 2,2-dithiodipyridine (2,2'-DPS, KDM-113) as another valuable tool compound. Notably, none of the vinyl sulfones or cyanoacrylates tested inhibited demethylase activity, suggesting that these compounds did not engage with KDM1A or were rapidly reversible (data not shown) (28). Taken together, inhibition of KDM1A by these thiol-reactive

compounds strongly suggested that cysteine modification antagonizes enzyme catalysis. Many of these tool compounds were later used to probe KDM1A cysteine reactivity in cells (Chapter 4).

The remaining hits that had been validated with the Rapid Fire MS assay were triaged with an LC-MS assay using negative ionization mode to detect elemental sulfur. This analysis revealed widespread sulfur contamination of commercially-available drug-like small molecules (Figure 3.3A). Troublingly, at least one compound containing no sulfur atoms was found to be contaminated by S_8, suggesting this impurity may be pervasive among reagents from medicinal chemistry vendors. Although redox- and cysteine-reactive 'bad actors' in high throughput academic screening libraries have received increased visibility (29), we are unaware of other examples of screens plagued by elemental sulfur contamination.

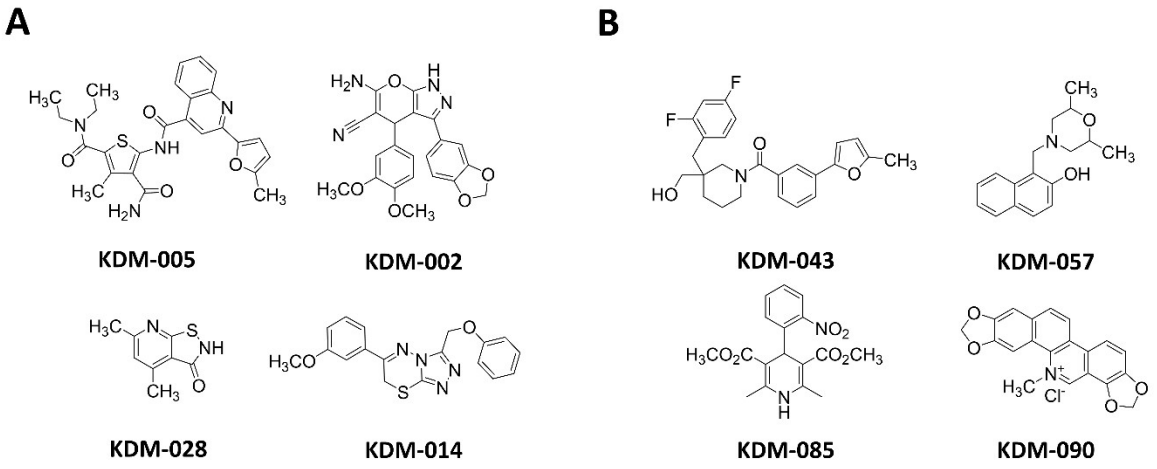

Figure 3.3 Representative structures of eliminated high throughput screening hits.
A. Structures of compounds that were contaminated with elemental sulfur as determined by LC-MS. **B.** Structures of compounds that failed to inhibit KDM1A in assay buffer supplemented with 1 mM DTT.

To determine if any hits uncovered by our screen inhibited KDM1A in a thiol-independent manner, a counterscreen was conducted with the thiol-selective reducing agent dithiothreitol (DTT) present in the assay buffer (Figure 3.4). Neither DTT nor tris(2-carboxyethyl)phosphine (TCEP) were compatible with the HRP-coupled assay reagents, as both dramatically increased the baseline fluorescence and overwhelmed the signal generated by KDM1A demethylase activity (data not shown). To overcome this limitation, a

western blot assay initially developed to probe the thiol-reactivity of immunoprecipitated KDM1A (Chapter 4) was adapted to study the recombinant enzyme. Demethylation of 21 aa synthethic peptide substrate can be monitored by loss of binding of an H3K4me2 antibody as in the TR-FRET assay; importantly, separation of proteins by SDS-PAGE and transfer to PVDF membrane rendered this assay compatible with any reducing agent and any detergent. As expected, disulfiram and Np-Mal were inactive in the presence of DTT, as was sulfur-contaminated KDM-103. Several other compounds were inactive in all conditions tested or were inactive in the presence of DTT (Figures 3.3B and 3.4A). As the compounds tested in this DTT counterscreen were not stringently selected and included many that had not been validated with the Rapid Fire MS assay nor assessed for S_8 contamination by LC-MS, further work is needed to clarify if this DTT-sensitivity stems from sulfur contamination or more direct interference by DTT. Importantly, two novel scaffolds, KDM-009 and KDM-093, were found to inhibit KDM1A demethylase activity in the presence of DTT, albeit with relatively low potency. Thus, these compounds were selected for further study.

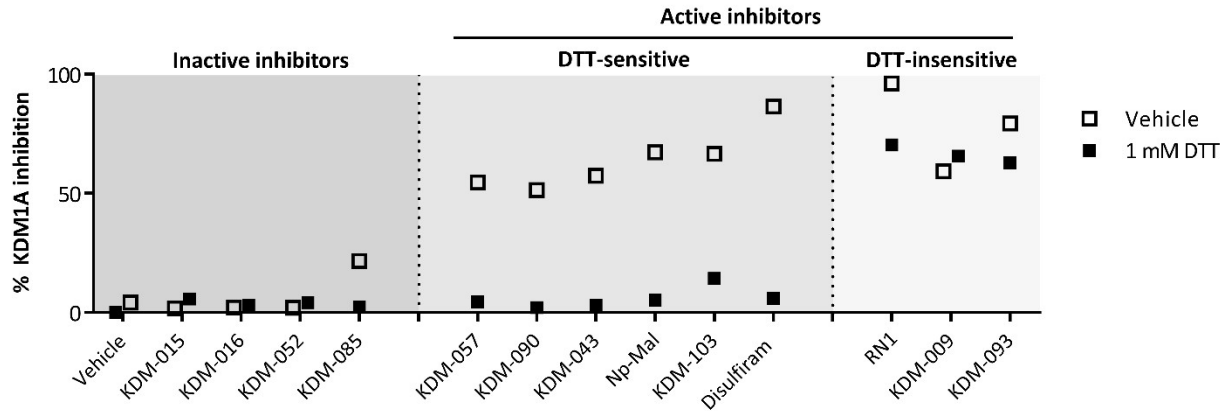

Figure 3.4 Counterscreening reveals two DTT-insensitive inhibitors of KDM1A.
KDM-009, KDM-093, and RN1 inhibit KDM1A when assay buffer is supplemented with 10 mM DTT. Samples of recombinant enzyme were treated with 25 µM inhibitor and demethylation of H3K4me2 peptide substrate after 1 hour was detected by western blotting.

3.3.4 Assessment of non-thiol reactive KDM1A inhibitors in cellular assays

KDM-009 is a dihydropyridine without previously reported biological activity but with considerable structural similarity to compounds our group has previously found to regulate the Wnt signaling pathway, as further discussed below (Figure 3.5A, (30)). KDM-093 is also known as benzbromarone, a uricosuric agent and non-competitive inhibitor of xanthine oxidase used in the treatment of gout (31). Neither KDM-009 nor KDM-093 inhibit recombinant KDM1A potently, with apparent IC_{50} values of 16 μM and 8 μM, respectively. However, we hoped to leverage the cellular assays developed using FAD-directed KDM1A inhibitors (Chapter 2) to profile these compounds and perhaps prioritize one structure for future development. Not surprisingly, neither compound resulted in increased bulk histone methylation levels in SH-SY5Y cells (Figure 3.5B). The results shown here reflect 24 hours of compound exposure, but shorter durations were also examined with similar results (6 hours, data not shown).

The CETSA assay has been the most robust measure of cellular KDM1A target engagement, but neither compound resulted in the pronounced thermal stabilization observed with the FAD-directed inhibitors (Figure 3.5C). Although a slight increase in soluble KDM1A was observed upon treatment of live cells with 25 μM KDM-009, this change did not reach statistical significance (Figure 3.5D). Finally, the effects of KDM-009 and KDM-093 on cell viability were measured using a commercially-available CellTiter Glo® assay, which measures the concentration of ATP in living cells. This assay revealed that KDM-093 resulted in significant cellular toxicity at the lowest tested dose, 5 μM (Figure 3.4E). However, lack of thermal stabilization by CETSA suggests that this toxicity is likely independent of KDM1A engagement. Lower doses of KDM-009 were tolerated, while RN1 had no effect on cellular viability.

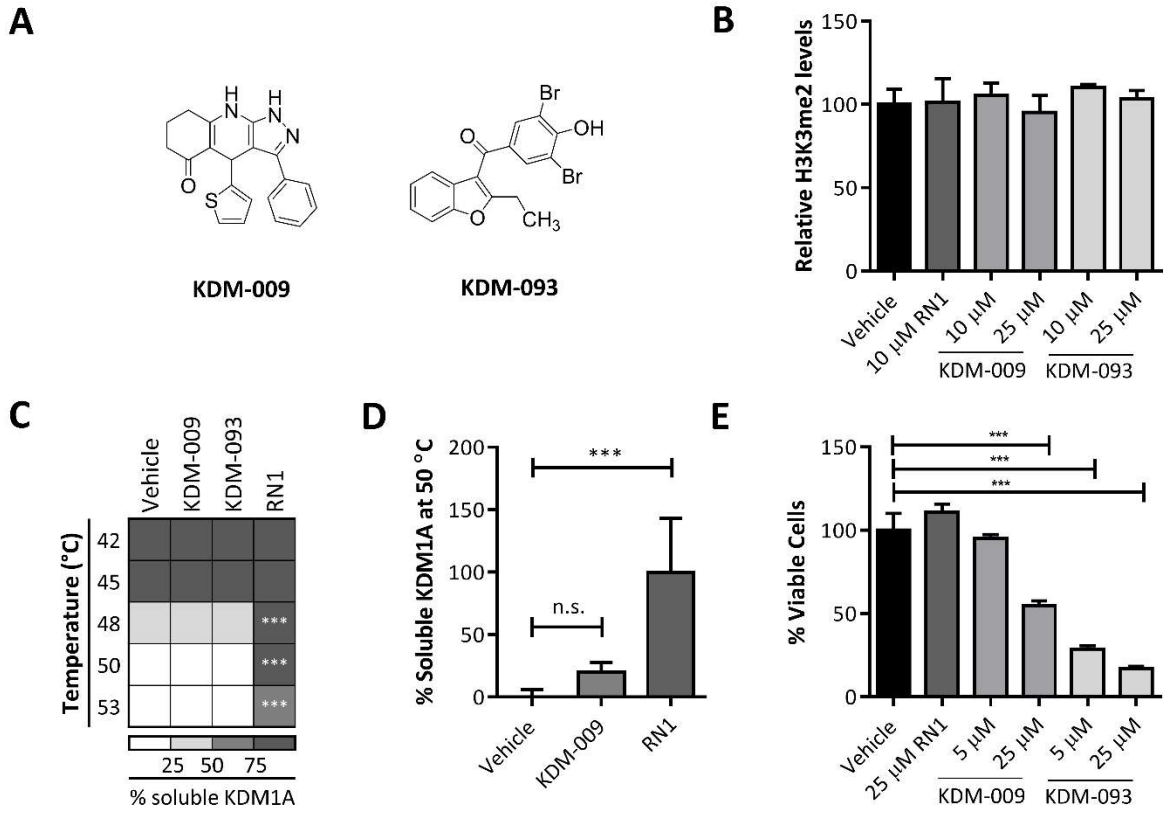

Figure 3.5 Cellular assays with KDM-009 and KDM-093.
A. Chemical structures of dihydropyridine KDM-009 and KDM-093, also known as the drug benzbromarone. **B.** Novel KDM1A inhibitors do not significantly increase bulk histone H3K4me2 levels. SH-SY5Y cells were treated with compounds at the indicated concentrations for 24 hours, then bulk histone methylation levels were determined by western blotting. **C.** Novel KDM1A inhibitors (25 μM) do not significantly shift the thermal stability of KDM1A in a whole-cell CETSA assay. **D.** Whole cell CETSA analysis (n = 4) does not indicate significant thermal stabilization by 25 μM KDM-009. **E.** Novel KDM1A inhibitors are cytotoxic as assessed by the CellTiter Glo® assay. For C-E, Error bars indicate SD, *** $p < 0.001$ by 1-way ANOVA with Dunnett's correction for multiple comparisons.

3.3.5 Assessment of KDM1A inhibitors in Wnt signaling pathway reporter assay

KDM1A was the first histone lysine demethylase to be discovered, and was identified as part of a complex with C-terminal binding protein 1 (CtBP1), a transcriptional regulator of Wnt signaling (32). The Wnt signaling pathways controls cell proliferation and body patterning throughout development, and dynamic chromatin remodeling is known to play a role in the regulation of Wnt target genes (33). Our interest in Wnt signaling arises from the observation that the mood stabilizer lithium enhances Wnt

signaling and promotes adult hippocampal neurogenesis by inhibiting a negative regulator of the pathway, glycogen synthase kinase-3β (GSK3β) (Figure 3.6, (34)). Additional support for a role of Wnt signaling in neuropsychiatric disease comes from a high incidence of mental illness in a family bearing a translocation in the *Disrupted-in-Schizophrenia (DISC)* locus, encoding a negative regulator of GSK3β (35,36). The interaction of KDM1A with CtBP1, as well as the structural similarity of KDM-009 to other inhibitors of GSK3β prompted us to examine a possible role for KDM1A inhibition in the regulation of Wnt signaling (30).

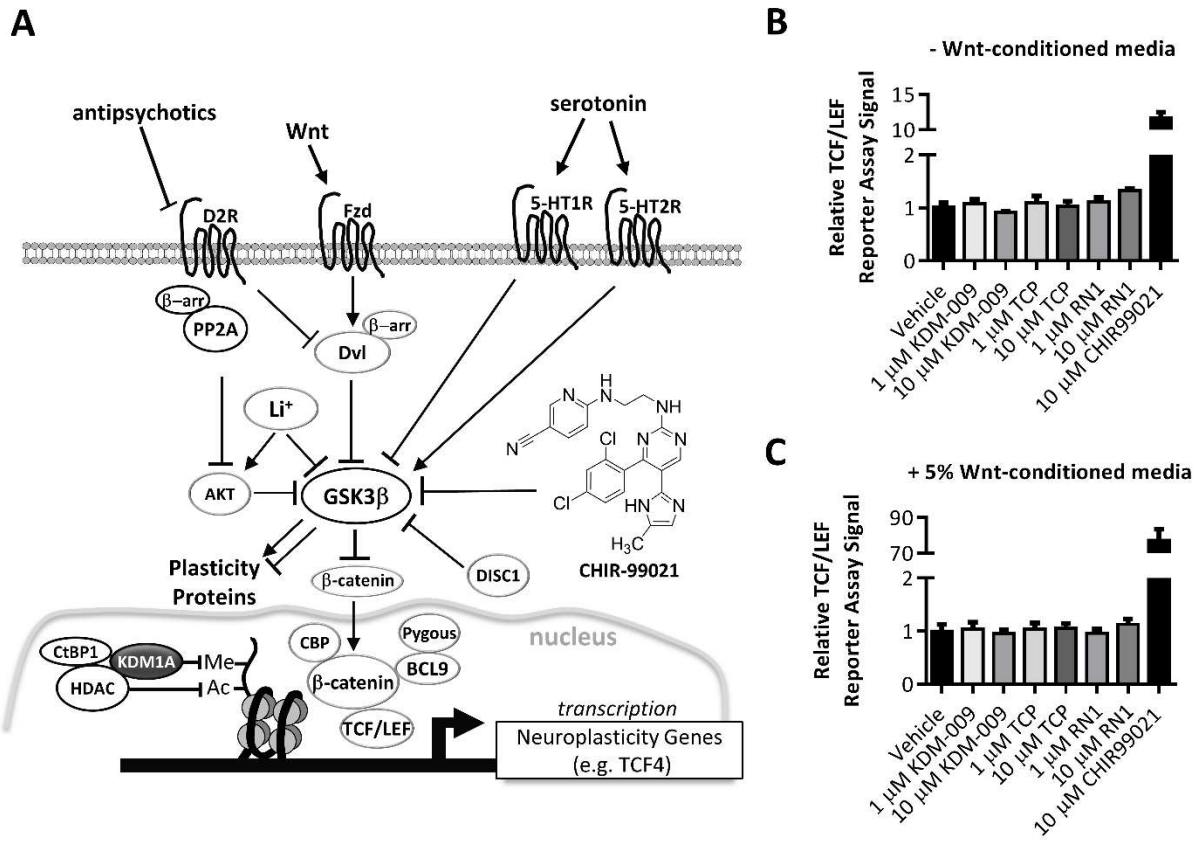

Figure 3.6 KDM1A inhibitors in the Wnt signaling pathway.
A. Simplified schematic of canonical Wnt signaling regulating the expression of genes important for regulation of neuroplasticity, modified from (37). Negative regulators of Wnt signaling are outlined in black, positive regulators in grey. KDM1A is known to interact with CtBP1 in a transcriptional complex that regulates gene expression. **B.** KDM1A inhibitors do not significantly increase expression of a TCF-LEF reporter gene in the absence of extracellular Wnt. **C.** KDM1A inhibitors do not significantly increase expression of a TCF-LEF reporter gene in the presence of 5% Wnt-conditioned media. For B and C, human iPSC-derived NPC cells transduced with a TCF/LEF luciferase reporter gene construct were treated with compounds for 24 hours prior to measurement of luminescence with the SteadyGlo® assay. CHIR99021 was used as a positive control. Error bars indicate SD.

To identify novel modulators of the Wnt signaling pathway that may have therapeutic relevance to neuropsychiatric disease, our lab previously has generated an induced pluripotent stem cell (iPSC)-derived human neural progenitor cell line expressing a firefly luciferase reporter driven by the T-cell factor/lymphoid enhancer factor (TCF/LFF) family transcription factor binding sites (38). To test for a potential role for KDM1A in regulation of Wnt signaling, these neural progenitors were treated with the novel scaffold KDM-009, as well as TCP and RN1, and luciferase production was measured one day later. The potent GSK3β inhibitor CHIR99021 was used as a positive control. Contrary to our expectations, KDM1A inhibitors did not affect Wnt signaling in this model system, neither under basal conditions (Figure 3.6B) nor when the pathway was stimulated with 5% Wnt-conditioned media (Figure 3.6C). CtBP1 is known to play dual roles as a transcriptional co-activator and co-repressor. Furthermore, the chromatin structure of transgenes may not be regulated with identical mechanisms as endogenous Wnt target genes (39). Thus, future studies monitoring the expression of endogenous Wnt target genes by qRT-PCR will be required to validate these findings.

3.4 Conclusion

In summary, all KDM1A inhibitors uncovered by our screen with a potency of less than 10 μM were contaminated with elemental sulfur or were thiol-reactive through some other mechanism (Supplementary Table A1), suggesting that this mode of inhibition was dominant in our chosen assay conditions. Our results as well as others' reports indicate that additional screening strategies are needed to overcome the predominant mode of inhibition (40). One potential approach could be to mutate candidate cysteine residues and repeat screening efforts with the modified enzyme. Subsequent mass spectrometry experiments implicate Cys600 as the reactive site (Chapter 4); mutation of this residue to an alanine or serine may greatly facilitate drug discovery. However, a more general solution would have

been to avoid the HRP-coupled assay altogether, as potential lead compounds were overwhelmed by the vastly more potent and more numerous false positives. In hindsight, a direct detection method such as the RapidFire MS would have likely saved time and expense, and is readily compatible with reducing agents. Thiol-reactive small molecules are known to be promiscuous enzyme inhibitors, and are generally disfavored for therapeutic development due to metabolic liability (29). However, a covalent approach for targeting non-catalytic cysteines has been proposed for kinase inhibitors, both to impart selectivity among enzymes with highly similar catalytic sites, but also to improve drug properties due to longer windows of target engagement without the toxicity associated with irreversible covalent modification (28). Additional cyanoacrylates should be screened, and may reveal therapeutically-relevant compounds that leverage the thiol-reactivity of KDM1A. Given the lack of cellular phenotype produced by FAD-directed inhibitors in histone methylation and Wnt signaling assays, the CETSA method remains the most robust assay by which such novel compounds should be assessed. Ultimately, the thiol-reactivity of KDM1A is intriguing due to an emerging understanding of the redox regulation of epigenetic modifiers (41). Application of cysteine-reactive small molecules probes, such as those uncovered by our screening efforts, may help to unravel the biochemical significance of this mode of reactivity.

3.5 Materials and Methods

Inhibitors and Reagents– All compounds were stored as 25 mM stock solutions in DMSO at -20 °C. TCP was purchased from Sigma Aldrich (catalog #P8511). RN1 was synthesized as previously described (42). Compounds identified by high-throughput screening were purchased from various small molecule vendors (ChemDiv, Vitas-M-Lab, BioMol, ChemBridge, Enamine, and Sigma Aldrich) and stored either in vials or in 384-well microarray plates (Thermo Scientific, #AB-1055) sealed with Thermowell sealing tape (Corning Costar, #6569). Dilutions in aqueous buffer were prepared immediately prior to use.

Recombinant Enzymes and Substrates – Enzymes and substrates were prepared exactly as previously described (Chapter 2).

IC_{50} determination and statistical analysis – Nonlinear regression, statistical testing and graph preparation were performed using GraphPad Prism 6 (GraphPad Software, Inc.) exactly as previously described (Chapter 2).

High Throughput Screening – Initial screening was performed using the BPBio and Prestwick bioactives library by the Partners Center for Drug Discovery at a single concentration of 13 μM. For secondary screening, a three-point dose response (14 μM, 1.4 μM, and 0.14 μM) was utilized. For in-house testing, KDM1A, H3K4me2 substrate, and HRP assay reagents were prepared as previously described (15). Under optimized conditions for screening, the HRP-coupled reactions were run in a final volume of 25 μl in 384-well plates with an amount of KDM1A (240 nM) in the reaction titrated that produced a linear increase in fluorescence over 30 min. By titrating the amount of substrate between 1-500 μM the, half-maximal velocity (K_m) was found to be 65 μM (data not shown). The optimal, non-rate limiting, concentration of HRP was found to be 10 μM, which is in significant excess so as to minimize the number of false positives identified due to HRP inhibition as determined by our pilot studies. Titration of the ADHP substrate indicated that 40 μM produced an optimal reaction without being limiting and having minimal background auto-fluorescence over the course of the reaction. Only a minimal change in background fluorescence was observed upon either leaving out of the H3K4me2 peptide substrate or enzyme. KDM1A activity assay produced a linear increase in fluorescence over 30 min. Using TCP as a positive control for inhibition, we determined that the average Z' value for the assay was 0.6 - 0.7 (data not shown). Data were collected on a PerkinElmer Wallac Envision 2103 Multilabel plate reader (excitation filter: 485, emission filter: 595). Follow-up HRP-coupled assays were run as previously described (Chapter 2 and (15)).

HRP Counterscreen - Reactions were run in duplicate in 50 mM sodium phosphate buffer (Boston BioProducts #BB-185, pH 7.4) with 0.01% BRIJ35 detergent (Calbiochem #203728) in 384-well black non-

sterile plates (Corning #3573). Hydrogen peroxide (Sigma, #95314, Urea adduct) was freshly dissolved in Milli-Q (Millipore) purified H_2O to a working concentration of 0.1 µM. Separately, the detection reagent used in the HRP-coupled assays was prepared. HRP (Sigma, #P2088, 5KU) and Amplite (ABD Bioquest #11000, in DMSO) were diluted in buffer, then 30 µL was added to each well using a Multidrop Combi Reagent Dispenser (Thermo Scientific). A CyBi-Well vario 384 Channel Simultaneous Pipettor (CyBio) was used to transfer 50 nL of inhibitor stock solutions in DMSO per well. Plates were briefly spun down, then 30 µL of the prepared hydrogen peroxide solution was added using the Multidrop Combi. The reagent dispenser tubing was flushed extensively with reaction buffer followed by warm water to remove residual peroxide. After addition of the peroxide solution, the plates were immediately read on a PerkinElmer Wallac Envision 2103 Multilabel plate reader (excitation filter: 485 nm, emission filter: 595 nm).

Secondary KDM1A assays – TR-FRET and Rapid Fire MS assays were performed exactly as previously described (Chapter 2 and (15)).

Preparation of KDM-103 and isolation of elemental sulfur – Extended synthetic methods omitted for brevity. To an oven-dried round-bottom flask under argon atmosphere was added 3-(2-chlorophenoxy)propanoic acid (1.0 equiv.) and 4-amino-5-(phenoxymethyl)-4H-1,2,4-triazole-3-thiol (1.0 equiv.). Phosphoryl chloride (Sigma, 1-3 mL) was added *via* syringe, then the suspension was heated to 100 °C and stirred overnight at reflux under inert atmosphere. After cooling to 0 °C in an ice bath, ice cold water was added dropwise to the reaction mixture until heat evolution ceased and precipitate began to form. For the initial preparation of KDM-103, the solution was poured over ice chips and allowed to stand for one hour. The resulting precipitate was filtered over a plug of silica gel in 100% EtOAc to afford the triazolothiadiazole product as an off-white powder. The NMR and LC-MS characterization of this compound is provided in Supplementary Figures A1-A3. ^{1}H and ^{13}C spectra were measured with a Varian 500 MHz spectrometer. ^{1}H NMR chemical shifts are reported as δ in units of parts per million (ppm)

relative to dimethylsulfoxide-d6 (δ 2.50, pentet). Multiplicities are reported as follows: s (singlet), d (doublet), t (triplet), q (quartet), dd (doublet of doublets), dt (doublet of triplets), or m (multiplet). Coupling constants are reported as a J value in Hertz (Hz). ^{13}C NMR chemical shifts are reported as δ in units of parts per million (ppm) relative to dimethyl sulfoxide-d6 (δ 39.5 septet). Re-synthesized KDM-103 was purified with gradient (30 – 70% EtOAc in hexanes) chromatography on an HP silica chromatography column by Teledyne Isco. The fractions corresponding to pure KDM-103 were pooled and concentrated by rotary evaporation. For isolation of elemental sulfur, crudely purified KDM-103 was triterated in solvents of varying polarities, then undissolved material was filtered and the extract was concentrated and tested for KDM1A inhibitory activity in the HRP-coupled assay. The residual material extracted into hexanes was found to potently inhibit KDM1A activity but did not contain KDM-103 as determined by LC-MS (data not shown). The material in the hexanes extraction was recrystallized twice from THF overnight at room temperature, then crystals were submitted for diffraction analysis by Dr. Shao-Liang Zheng at the Center for Crystallographic Studies in the Department of Chemistry and Chemical Biology at Harvard University. The structure of S_8 was confirmed using several crystals.

LC-MS assay for elemental sulfur contamination – Stock solutions of inhibitors (25 mM in DMSO) were diluted to 1 mM in acetonitrile. Then, 5 µL was injected *via* autosampler into an Agilent 1200 series HPLC, eluted with a 5-95% ACN gradient in 0.1% ammonium formate over 15 minutes through an Agilent Eclipse XBD-C8 reversed-phase column at a flow rate of 0.5 mL/min, and detected with an Agilent 6310 ion trap mass spectrometer with an ESI source in negative ion mode. Elemental sulfur eluted with a retention time of 14.2 minutes and had an observed mass of 255.3 m/z (Supplementary Figure S3). This retention time and mass were confirmed using an elemental sulfur standard (Sigma, reagent-grade, exact mass: 255.78 amu).

DTT-counterscreen – Recombinant KDM1A was diluted to a final concentration of 100 nM in assay buffer (50 mM pH 7.4 sodium phosphate buffer with 0.01% BRIJ35 detergent) with or without 1 mM DTT

(Sigma Aldrich, solution prepared from powder immediately prior to use). Inhibitors (25 mM stock solutions in DMSO) were diluted in assay buffer and added to a final concentration of 50 μM, with the equivalent volume of DMSO added to the vehicle control reaction. After 10-minute pre-incubation with inhibitors, H3K4me2 peptide substrate diluted to a final concentration of 5 μM in assay buffer with or without 1 mM DTT was added and the reaction (total volume of 15 μL) was allowed to proceed for 1 hour at room temperature. The reaction was quenched by addition of 7.5 μL of sample loading buffer + DTT. Reactions were run in singlicate and the entire procedure was repeated twice. Proteins were separated on pre-cast 4-12% Bis-Tris Nu-PAGE gels (Invitrogen) with MES running buffer (Invitrogen) for 30 minutes at 200 V, transferred to PVDF membrane (Millipore), blocked with 5% non-fat milk in TBST then probed overnight with 1:1,000 anti-H3K4me2 (Cell Signaling, catalog #9725S, lot #1) at 4 °C. Specificity of the H3K4me2 antibody for the recombinant H3K4me2 substrate starting material was confirmed with a substrate-only control and an unmethylated peptide substrate control (data not shown). Detection was achieved with an HRP-linked anti-rabbit secondary antibody and ECL substrate (Thermo Scientific) and captured on autoradiography film (LabScientific). Films were scanned and band intensities from exposures within a linear range were quantified in ImageJ (NIH). Percent enzyme inhibition was calculated from the remaining H3K4me2 starting material of RN1-inhibited lanes relative to vehicle control lanes.

Cell lines – HeLa and SH-SY5Y cells were subcultured as previously described (Chapter 2). Human iPSC-derived neural progenitors (NPCs) were generated and subcultured as previously described (38). Briefly, NPCs were maintained in poly-ornithine (Sigma Aldrich, catalog #P3655) and laminin (Sigma Alridch, catalog #L2020) coated T-75 flasks in neurosphere medium. Neurosphere medium consists of 30% Ham's F12 (Mediatech, catalog #10-080-CV), 70% DMEM (Gibco, cat# 11995), 1% penicillin-streptomycin dual antibiotic solution (Fisher, #ICN1670249), 2% B27 (Gibco, catalog #17504-044) and was supplemented with 20 ng/mL epidermal growth factor (EGF; Sigma-Aldrich, prepared as 20 μg/mL stock

in DMEM), 20 ng/mL bFGF (Stemgent; prepared as 20 μg/mL stock in PBS), and 5 μg/mL heparin (Sigma Aldrich; prepared as 5 mg/mL stock in Ham's F12 media) just before use.

Western blot and CETSA with KDM-009 and KDM-093 - Western blotting of bulk H3K4me2 levels and CETSA were performed as previously described (Chapter 2). Briefly, SH-SY5Y cells were plated in 24-well plates (500 μL, 2 million cells/mL) and grown overnight, then treated with 10 μM or 25 μM test compound or vehicle control pre-diluted in warmed culture media such that the final concentration of DMSO did not exceed 0.1% w/w. Cells were harvested after 24 hours by aspiration of media and direct addition of 100 μL 1x sample loading buffer + DTT, and proteins were analyzed by western blotting exactly as previously described. Compounds were tested in duplicate and the experiment was repeated once (n=4). For CETSA, nearly confluent SH-SY5Y cells were gently scraped from a T-75 flask and the diluted to a density of 1 million cells per mL of culture media, then 1 mL of gently mixed suspension was transferred a 1.5-mL Eppendorf tube, with one tube per compound treatment. Test compounds or DMSO vehicle control were pre-diluted in 37 °C cell culture media then added to the cell suspension, with a final amount of DMSO not exceeding 0.1% v/v. Cells were treated for 30 minutes, then pelleted, washed twice with 37 °C PBS, then suspended at a density of 1 million cells per 0.1 mL of PBS. A 25 μL aliquot of this solution was added to each tube of a PCR strip, and samples were heated to the indicated temperatures for 3 minutes, followed by a 5-minute hold at room temperature, then finally 3 cycles of freeze-thawing to lyse the cells. The supernatant obtained after high speed centrifugation was analyzed by dot blotting exactly as previously described. Compounds were tested in duplicate, and the experiment was repeated once (n=4).

CellTiter Glo® assay – The assay was performed based on the manufacturer's recommendations. Briefly, freshly passaged SH-SY5Y cells were seeded into a 96-well plate (100 μL per well, 2 million cells per mL) and grown overnight. The media was gently removed by aspiration and replaced with pre-warmed media without FBS and containing test compounds or DMSO control diluted so that the final concentration

of DMSO did not exceed 0.1% w/w. Staurosporine (Sigma Aldrich, catalog #S5921) at a final concentration of 10 µM was used as a positive control. Cells were exposed to test compound for 24 hours, then 20 µL of the reconstituted CellTiter Glo® reagent (Promega, catalog #G7572) was added per well. After 30 minutes, luminescence was read using a PerkinElmer Wallac Envision 2103 Multilabel plate reader (emission filter: 570 nm). Compounds were tested in duplicate, KDM-009 and KDM-093 were tested once (n=2). Treatment with RN1 was repeated in independent experiments presented later (Chapter 4).

Wnt signaling reporter assay – Human iPSC-derived neural progenitors were generated and the reporter assay was run as previously described (38). These cells stably express a luciferase reporter consisting of tandem TCF/LEF binding sites and a minimal CMV promoter. Wnt3a-conditioned media was prepared exactly as previously described (38). Briefly, white 96-well (Corning, catalog #3903) microplates were coated with poly-ornithine/laminin, then cells were seeded at a density of 20,000 cells per well. After 24 hours, test compounds were pre-diluted in culture media and added so that the final concentration of DMSO did not exceed 0.1% w/w. Immediately following compound treatment, an additional 10 µL of media or Wnt3a-conditioned media was added to a final concentration of 5% v/v. This volume had been previously optimized as reported (38). The next day, plates were equilibrated to room temperature, then 30 µL of reconstituted SteadyGlo® reagent (Promega, catalog #E2550) was added per well. After 30 minutes, luminescence was read using a PerkinElmer Wallac Envision 2103 Multilabel plate reader (emission filter: 570 nm). For the data presented here, compounds were tested once in duplicate (n=2). The experiment was repeated one additional time at slightly different compound concentrations with qualitatively similar results (data not shown). For both assays, CHIR99021 (Sigma Aldrich, catalog # SML1046) at 10 µM was used as a positive control.

3.6 References

1. Zheng, Y. C., Ma, J., Wang, Z., Li, J., Jiang, B., Zhou, W., Shi, X., Wang, X., Zhao, W., and Liu, H. M. (2015) A Systematic Review of Histone Lysine-Specific Demethylase 1 and Its Inhibitors. *Medicinal research reviews* **35**, 1032-1071

2. Hayward, D., and Cole, P. (2016) LSD1 Histone Demethylase Assays and Inhibition. *Methods in Enzymology*

3. Stazi, G., Zwergel, C., Valente, S., and Mai, A. (2016) LSD1 inhibitors: a patent review (2010-2015). *Expert Opinion on Therapeutic Patents*, 1-16

4. Maes, T., Carceller, E., Salas, J., Ortega, A., and Buesa, C. (2015) Advances in the development of histone lysine demethylase inhibitors. *Current opinion in pharmacology* **23**, 52-60

5. Mohammad, H. P., Smitheman, K. N., Kamat, C. D., Soong, D., Federowicz, K. E., Van Aller, G. S., Schneck, J. L., Carson, J. D., Liu, Y., and Butticello, M. (2015) A DNA hypomethylation signature predicts antitumor activity of LSD1 inhibitors in SCLC. *Cancer cell* **28**, 57-69

6. Kalin, J., Wu, M., Hayward, D., Wang, L., Roberts, J., Prusevich, P., Hancock, W., Bradner, J., Ryu, B., and Alani, R. (2015) CoREST in Peace: Dual Action Inhibitors of Histone Deacetylase and Lysine Specific Demethylase. *The FASEB Journal* **29**, 723.728

7. Rotili, D., Tomassi, S., Conte, M., Benedetti, R., Tortorici, M., Ciossani, G., Valente, S., Marrocco, B., Labella, D., and Novellino, E. (2013) Pan-histone demethylase inhibitors simultaneously targeting Jumonji C and lysine-specific demethylases display high anticancer activities. *Journal of medicinal chemistry* **57**, 42-55

8. Fiskus, W., Sharma, S., Shah, B., Portier, B., Devaraj, S., Liu, K., Iyer, S. P., Bearss, D., and Bhalla, K. (2014) Highly effective combination of LSD1 (KDM1A) antagonist and pan-histone deacetylase inhibitor against human AML cells. *Leukemia* **28**, 2155-2164

9. Baell, J. B., and Holloway, G. A. (2010) New substructure filters for removal of pan assay interference compounds (PAINS) from screening libraries and for their exclusion in bioassays. *Journal of medicinal chemistry* **53**, 2719-2740

10. Huang, Y., Greene, E., Murray Stewart, T., Goodwin, A. C., Baylin, S. B., Woster, P. M., and Casero, R. A. (2007) Inhibition of lysine-specific demethylase 1 by polyamine analogues results in reexpression of aberrantly silenced genes. *Proceedings of the National Academy of Sciences* **104**, 8023

11. Huang, Y., Stewart, T. M., Wu, Y., Baylin, S. B., Marton, L. J., Perkins, B., Jones, R. J., Woster, P. M., and Casero, R. A. (2009) Novel oligoamine analogues inhibit lysine-specific demethylase 1 and induce reexpression of epigenetically silenced genes. *Clinical Cancer Research* **15**, 7217

12. Zhu, Q., Huang, Y., Marton, L., Woster, P., Davidson, N., and Casero, R. Polyamine analogs modulate gene expression by inhibiting lysine-specific demethylase 1 (LSD1) and altering chromatin structure in human breast cancer cells. *Amino Acids*, 1-12

13. Sharma, S. K., Wu, Y., Steinbergs, N., Crowley, M. L., Hanson, A. S., Casero, R. A., and Woster, P. M. (2010) (Bis)urea and (Bis)thiourea Inhibitors of Lysine-Specific Demethylase 1 as Epigenetic Modulators. *Journal of Medicinal Chemistry* **53**, 5197-5212

14. Schmidt, D. M. Z., and McCafferty, D. G. (2007) trans-2-Phenylcyclopropylamine Is a Mechanism-Based Inactivator of the Histone Demethylase LSD1†. *Biochemistry* **46**, 4408-4416

15. Neelamegam, R., Ricq, E. L., Malvaez, M., Patnaik, D., Norton, S., Carlin, S. M., Hill, I. T., Wood, M. A., Haggarty, S. J., and Hooker, J. M. (2011) Brain-Penetrant LSD1 Inhibitors Can Block Memory Consolidation. *ACS Chemical Neuroscience*

16. Forneris, F., Binda, C., Adamo, A., Battaglioli, E., and Mattevi, A. (2007) Structural basis of LSD1-CoREST selectivity in histone H3 recognition. *Journal of Biological Chemistry* **282**, 20070

17. Plant, M., Dineen, T., Cheng, A., Long, A. M., Chen, H., and Morgenstern, K. A. (2011) Screening for Lysine Specific Demethylase-1 Inhibitors Using a Label Free High Throughput Mass Spectrometry Assay. *Analytical Biochemistry*

18. Rye, P., Frick, L. LaMarr, W., Özbal, C. (2009) High-throughput Mass Spectrometric Detection of Histone 3 Demethylation. *In Society for Biomolecular Sciences Label Free Meeting, San Diego, CA*

19. Yu, V., Fisch, T., Long, A. M., Tang, J., Lee, J. H., Hierl, M., Chen, H., Yakowec, P., Schwandner, R., and Emkey, R. (2011) High-Throughput TR-FRET Assays for Identifying Inhibitors of LSD1 and JMJD2C Histone Lysine Demethylases. *Journal of Biomolecular Screening*

20. Gauthier, N., Caron, M., Pedro, L., Arcand, M., Blouin, J., Labonté, A., Normand, C., Paquet, V., Rodenbrock, A., Roy, M., Rouleau, N., Beaudet, L., Padrós, J., and Rodriguez-Suarez, R. (2011) Development of Homogeneous Nonradioactive Methyltransferase and Demethylase Assays Targeting Histone H3 Lysine 4. *Journal of Biomolecular Screening*

21. Amir, M., Kumar, H., and Javed, S. A. (2008) Condensed bridgehead nitrogen heterocyclic system: Synthesis and pharmacological activities of 1,2,4-triazolo-[3,4-b]-1,3,4-thiadiazole derivatives of ibuprofen and biphenyl-4-yloxy acetic acid. *European Journal of Medicinal Chemistry* **43**, 2056-2066

22. Mathew, V., Keshavayya, J., Vaidya, V. P., and Giles, D. (2007) Studies on synthesis and pharmacological activities of 3,6-disubstituted-1,2,4-triazolo[3,4-b]-1,3,4-thiadiazoles and their dihydro analogues. *European Journal of Medicinal Chemistry* **42**, 823-840

23. KATO, A., OGURA, M., and SUDA, M. (1966) Control mechanism in the rat liver enzyme system converting L-methionine to L-cystine. *The Journal of biochemistry* **59**, 40-48

24. Conner, J., and Russell, P. (1983) Elemental sulfur: a novel inhibitor of adenylate kinase. *Biochemical and biophysical research communications* **113**, 348-352

25. Pestana, A., and Sols, A. (1970) Reversible inactivation by elemental sulfur and mercurials of rat liver serine dehydratase and certain sulfhydryl enzymes. *Biochemical and biophysical research communications* **39**, 522-529

26. Mishanina, T. V., Libiad, M., and Banerjee, R. (2015) Biogenesis of reactive sulfur species for signaling by hydrogen sulfide oxidation pathways. *Nature chemical biology* **11**, 457-464

27. Vallari, R. C., and Pietruszko, R. (1982) Human aldehyde dehydrogenase: mechanism of inhibition of disulfiram. *Science* **216**, 637-639

28. Serafimova, I. M., Pufall, M. A., Krishnan, S., Duda, K., Cohen, M. S., Maglathlin, R. L., McFarland, J. M., Miller, R. M., Frödin, M., and Taunton, J. (2012) Reversible targeting of noncatalytic cysteines with chemically tuned electrophiles. *Nature chemical biology* **8**, 471-476

29. Dahlin, J. L., Nissink, J. W. M., Strasser, J. M., Francis, S., Higgins, L., Zhou, H., Zhang, Z., and Walters, M. A. (2015) PAINS in the assay: chemical mechanisms of assay interference and promiscuous enzymatic inhibition observed during a sulfhydryl-scavenging HTS. *Journal of medicinal chemistry* **58**, 2091-2113

30. An, W. F., Germain, A. R., Bishop, J. A., Nag, P. P., Metkar, S., Ketterman, J., Walk, M., Weiwer, M., Liu, X., and Patnaik, D. (2014) Discovery of potent and highly selective inhibitors of GSK3b.

31. Sinclair, D., and Fox, I. (1975) The pharmacology of hypouricemic effect of benzbromarone. *The Journal of rheumatology* **2**, 437-445

32. Shi, Y., Sawada, J.-i., Sui, G., Affar, E. B., Whetstine, J. R., Lan, F., Ogawa, H., Luke, M. P.-S., Nakatani, Y., and Shi, Y. (2003) Coordinated histone modifications mediated by a CtBP co-repressor complex. *Nature* **422**, 735-738

33. Willert, K., and Jones, K. A. (2006) Wnt signaling: is the party in the nucleus? *Genes & development* **20**, 1394-1404

34. Wexler, E., Geschwind, D., and Palmer, T. (2008) Lithium regulates adult hippocampal progenitor development through canonical Wnt pathway activation. *Molecular psychiatry* **13**, 285-292

35. Chubb, J., Bradshaw, N., Soares, D., Porteous, D., and Millar, J. (2008) The DISC locus in psychiatric illness. *Molecular psychiatry* **13**, 36-64

36. Gould, T. D., and Manji, H. K. (2002) The Wnt signaling pathway in bipolar disorder. *The Neuroscientist* **8**, 497-511

37. Haggarty, S. J., Singh, K., Perlis, R. H., and Karmacharya, R. Neuropsychiatric Disease-Associated Genetic Variation in the Wnt Pathway. *Wnt Signaling in Development and Disease: Molecular Mechanisms and Biological Functions*, 393-409

38. Zhao, W.-N., Cheng, C., Theriault, K. M., Sheridan, S. D., Tsai, L.-H., and Haggarty, S. J. (2012) A high-throughput screen for Wnt/β-catenin signaling pathway modulators in human iPSC-derived neural progenitors. *Journal of biomolecular screening*, 1087057112456876

39. Fang, M., Li, J., Blauwkamp, T., Bhambhani, C., Campbell, N., and Cadigan, K. M. (2006) C-terminal-binding protein directly activates and represses Wnt transcriptional targets in Drosophila. *The EMBO journal* **25**, 2735-2745

40. Wigle, T. J., Swinger, K. K., Campbell, J. E., Scholle, M. D., Sherrill, J., Admirand, E. A., Boriack-Sjodin, P. A., Kuntz, K. W., Chesworth, R., and Moyer, M. P. (2015) A High-Throughput Mass Spectrometry Assay Coupled with Redox Activity Testing Reduces Artifacts and False Positives in Lysine Demethylase Screening. *Journal of biomolecular screening* **20**, 810-820

41. Cyr, A. R., and Domann, F. E. (2011) The redox basis of epigenetic modifications: from mechanisms to functional consequences. *Antioxidants & redox signaling* **15**, 551-589

42. Neelamegam, R., Ricq, E. L., Malvaez, M., Patnaik, D., Norton, S., Carlin, S. M., Hill, I. T., Wood, M. A., Haggarty, S. J., and Hooker, J. M. (2011) Brain-penetrant LSD1 inhibitors can block memory consolidation. *ACS chemical neuroscience* **3**, 120-128

CHAPTER 4

4 Activity-Dependent Regulation of KDM1A by a Putative Thiol/Disulfide Switch

4.1 Abstract

Lysine demethylation of proteins such as histones is catalyzed by several classes of enzymes, including the FAD-dependent amine oxidases KDM1A/B. The KDM1 family shares significant homology to the mitochondrial monoamine oxidases MAO-A/B and produces hydrogen peroxide in the nucleus as a byproduct of demethylation. Here, we show KDM1A is highly thiol-reactive *in vitro* and in cellular models. Enzyme activity is potently and reversibly inhibited by the drug disulfiram and by hydrogen peroxide. Hydrogen peroxide produced by KDM1A catalysis reduces thiol labeling and inactivates demethylase activity over time. MALDI-TOF mass spectrometry indicates that hydrogen peroxide blocks labeling of cysteine 600, which we propose forms an intramolecular disulfide with cysteine 618 to negatively regulate the catalytic activity of KDM1A. This activity-dependent regulation is unique among histone-modifying enzymes but consistent with redox sensitivity of epigenetic regulators.

4.2 Introduction

Post-translational N-methylation of lysine residues in proteins such as histones plays a widespread role in normal and pathological biological processes, including transcriptional regulation, chromatin remodeling, cell signaling, and assembly of protein complexes, among other functions. Lysines can be mono-, di- or tri-methylated, with each modification resulting in different functional outcomes depending on the degree of methylation and its context (1). Oxidative removal of histone lysine N-methyl groups is catalyzed by two mechanistically-distinct classes of lysine-specific demethylases (KDMs) (2). Most

identified demethylases are JmjC domain-containing, iron (II) and α-ketoglutarate dependent oxygenases (KDM subfamilies 2-8). These enzymes hydroxylate the N-methyl group of their substrates producing a hemi-aminal intermediate that fragments to the demethylated lysine and formaldehyde, a catalytic mechanism capable of demethylating mono-, di-, or tri-methylated substrates (3). In contrast, the amine oxidase domain-containing demethylases utilize a flavin adenine dinucleotide (FAD) cofactor (KDM subfamily 1). These enzymes, KDM1A and KDM1B, couple the reduction of FAD to $FADH_2$ with the oxidation of the C-N methylamine bond to a hydrolytically labile iminium ion, a mechanism only compatible with mono- and di-methylated substrates (4-6). The KDM1 family features a catalytic amine oxidase (AO) domain with significant homology to the mitochondrial monoamine oxidases MAO-A and MAO-B, which have been pharmacological targets for antidepressants and neuroprotective agents for decades due to their function to catalyze the oxidative deamination of neurotransmitters (7).

All KDMs require molecular oxygen to demethylate their substrates. KDM subfamilies 2-8 generate a reactive Fe(IV) oxo species which inserts an oxygen atom into a substrate C-H bond, whereas the KDM1 family uses molecular oxygen to re-oxidize their flavin cofactor to the quinone species (3). Beyond the mechanistic requirement for oxygen, most JmjC domain-containing KDMs are inducible in hypoxic conditions and many are direct targets of the hypoxia inducible factor HIF-1 (8).The role of the KDM1 family in hypoxia is less well-established, but KDM1A has been shown to mediate hypoxia-induced histone lysine demethylation at the *BRCA1* and *RAD51* promoters in MCF-7 breast cancer cells and the *MLH1* promoter in RKO colon cancer cells (9,10). In addition to their requirement for molecular oxygen, all KDMs liberate the former N-methyl group as formaldehyde. The fate of formaldehyde and general mechanisms that protect KDMs from cross-linking damage remain unclear. However, KDM1A has been shown to bind tetrahydrofolate, which serves as the formaldehyde acceptor for the enzymes dimethylglycine dehydrogenase and sarcosine dehydrogenase and may play a similar role for KDM1A (11).

A key feature that distinguishes class 1 KDMs from class 2-8 KDMs is the production of hydrogen peroxide (H_2O_2), which is generated when oxygen accepts electrons to re-oxidize the $FADH_2$ cofactor. Production of H_2O_2 in the nucleus is significant as it is known to cause mutagenic changes to DNA, including formation of 8-oxo-7,8-dihydro-2'-deoxyguanosine (8-oxoG). This modified nucleobase is repaired by the base excision repair (BER) pathway (12), and recruitment of BER machinery to the 8-oxoG lesions caused by KDM1A catalytic activity has been linked to estrogen-, Myc-, and androgen-induced transcriptional activation (13-15). These examples suggest a critical role for H_2O_2 generation in the mechanism of KDM1A distinct from other classes of histone lysine demethylases. To the best of our knowledge, the importance of H_2O_2 in KDM1B-catalyzed lysine demethylation has yet to be described. Here, we describe an additional role for H_2O_2 in KDM1A biochemistry. We show that KDM1A is inactivated by cysteine oxidation, and that catalytically-generated H_2O_2 negatively regulates demethylase activity. We propose a mechanism where KDM1A utilizes a thiol/disulfide switch to sense H_2O_2, a unique auto-oxidation mechanism among histone modifiers but consistent with general mechanisms of redox sensing by epigenetic enzymes. This mechanism may also allow KDM1A to sense other cellular oxidants, such as the neurotransmitter dopamine.

4.3 Results and Discussion

4.3.1 KDM1A is reversibly inhibited by thiol-reactive compounds

Tranylcypromine (TCP; Parnate) inhibits FAD-dependent amine oxidases by forming covalent co-factor adducts (7). TCP derivatives, such as RN1, exploit the same mechanism of action but with improved selectivity for KDM1A over other enzyme family members such as the monoamine oxidases (16). Using these compounds as positive controls, a high-throughput screen followed by detailed secondary assays was used to identify novel KDM1A inhibitors, as described in Chapter 3. Notably, many of the small molecules initially identified as potent, structurally novel KDM1A inhibitors were found to have potential

for reactivity with thiol groups. Thiol-reactive small molecules are known to be promiscuous enzyme inhibitors, and are generally disfavored for therapeutic development due to metabolic liability (17). However, given our interest in the nuclear redox activity of KDM1A and emerging evidence for dynamic cysteine metabolism in other epigenetic regulators, including histone deacetylases (HDACs) that are known to complex with KDM1A, we sought to further characterize KDM1A's thiol-reactivity. Two mechanistic classes of thiol-reactive compounds were utilized: the FDA-approved drug disulfiram and the oxidizing agent 2,2'-dithiodipyridine (2,2'-DPS) form reversible disulfide bonds, whereas maleimides such as N-naphthylmaleimide (Np-Mal) or biotinylated maleimide (Biotin-Mal) form essentially irreversible sulfur-carbon thioether bonds and are selective for thiols at physiological pH (Figure 4.1, note that thiol-maleimide adducts can be reversed with extended incubation in reducing environments (18)). Both classes of small molecules inhibit KDM1A activity as measured by a thigh-throughput mass spectrometry assay (Figure 4.2A). Enzyme inactivation was measured after a 10-minute pre-incubation with compound followed by a 20-minute demethylation reaction; however, all compounds studied here are expected to form covalent adducts and so relative potencies may exhibit time-dependence. Under these conditions, all thiol-reactive inhibitors were measured to have apparent IC_{50} values of less than 1 µM.

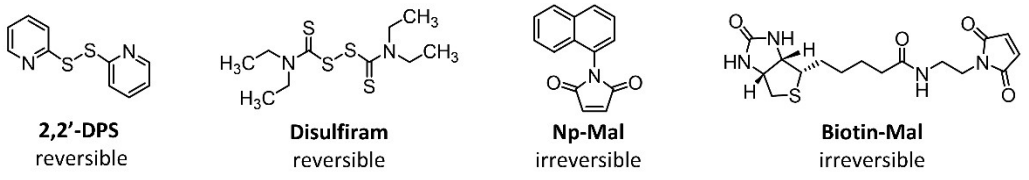

Figure 4.1 Chemical structures of thiol-reactive KDM1A inhibitors.
Thiol-reactive probes form disulfide bonds that are readily reversed in reducing environments, or essentially irreversible thioether bonds.

Based on this panel of inhibitors, we suspected that covalent modification of one or more cysteine residues on KDM1A resulted in enzyme inactivation. Consistent with this mechanism, inhibition by disulfide-forming compounds (10 µM, 10-minute pre-incubation) was reversed following addition of an

excess of the thiol-selective reducing agent DTT (1 mM, Figure 4.2B). In contrast, the thioether-forming Np-Mal and FAD-adduct forming RN1 were irreversible under these conditions. An LC-MS-based assay compatible with reducing agents such as DTT was critical to these and subsequent studies, and was developed after the initial observation that many thiol-reactive compounds interfered with the HRP-coupled assays we and others have previously used to profile KDM1A inhibition (Chapter 3 and (16,19)). Both MAO-A and MAO-B are known to be modified and inhibited by high concentrations of thiol-reactive compounds in a process competitive with substrate binding (20). To determine the relative thiol-reactivity among homologous FAD-dependent amine oxidases, a panel of mass spectrometry assays to monitor KDM1A/B activity and enzymatically-coupled assays for MAO-A/B activity were run. Even with longer reaction durations (60 minutes for KDM1B/MAO-A/B versus 20 minutes for KDM1A), thiol-reactive inhibitors were found to be 30-90 fold more potent against recombinant KDM1A versus the second-most inhibited enzyme (Figure 4.2A). In particular, MAO-B was not inhibited by thiol-reactive compounds under the conditions tested, consistent with hours-long treatment required for cysteine modification (20).

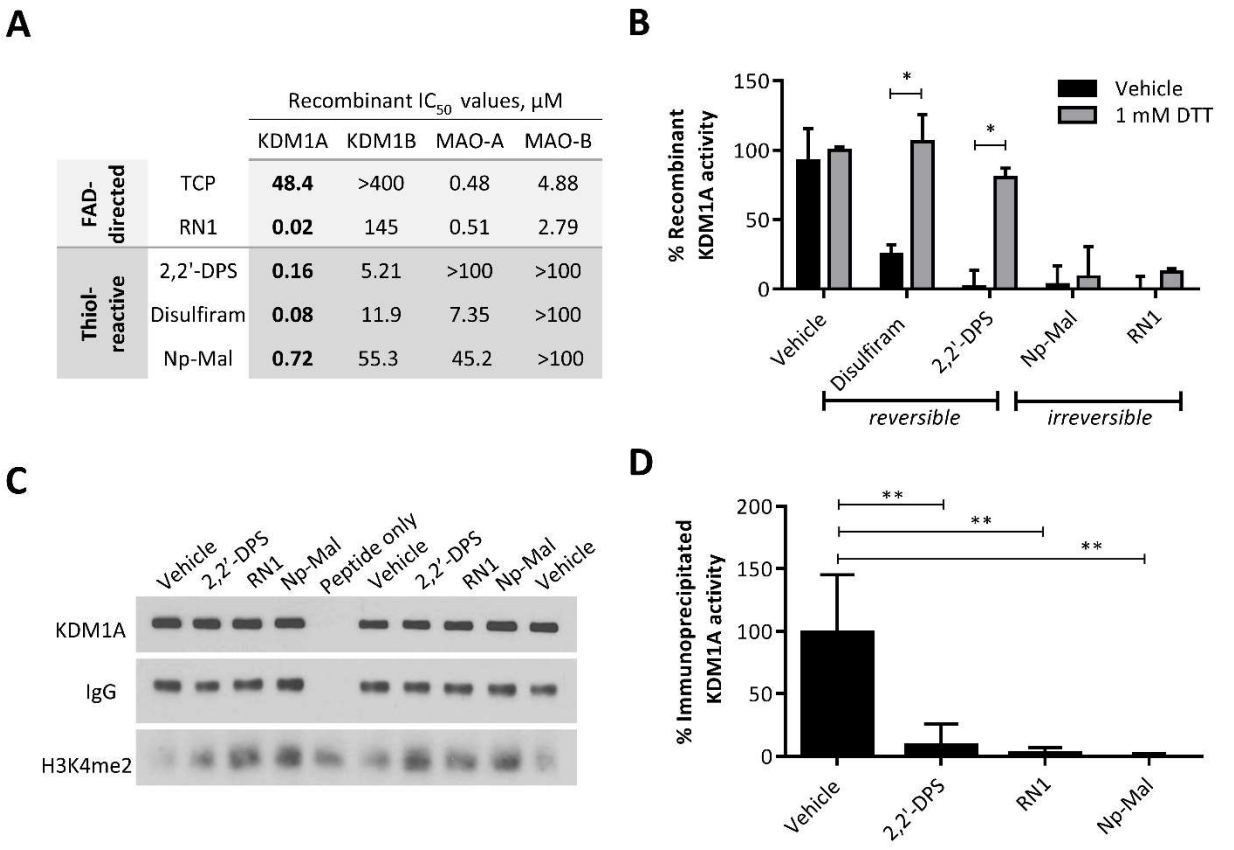

Figure 4.2 KDM1A is reversibly inhibited by thiol-reactive small molecules.
A. *In vitro* enzymatic assays with recombinant KDM1A/B or MAO-A/B reveal potent inhibition of KDM1A by reversible and irreversible thiol-reactive small molecules. Apparent IC_{50} values reported in μM for 20 minute (KDM1A) and 60 minute (KDM1B, MAO-A/B) reactions. **B.** Inhibition of KDM1A by disulfide forming thiol-reactive small molecules (disulfiram, 2,2'-DPS) is reversible by addition of DTT. Covalent modification by Np-maleimide or RN1 is not reversible by DTT. Compounds (1 μM) were pre-incubated with KDM1A for 10 min prior to reduction, and demethylation of H3K4me2 starting material was detected by LC-MS. Error bars indicate SD, * $p < 0.05$ by 2-tailed *t* test with correction for multiple comparisons. **C.** Full-length KDM1A immunoprecipitated from HeLa cells is inhibited by thiol-reactive inhibitors (10 μM) in a cell-free assay. Representative western blot indicates depletion of H3K4me2 starting material. **D.** Quantification of immunoprecipitated KDM1A activity in n = 4 assays from biological duplicates. Error bars indicate SD, ** $p < 0.01$ by 1-way ANOVA with correction for multiple comparisons.

The recombinant KDM1A used in this study contains all 9 cysteine residues encoded in the full-length protein and was purified with an N-terminal GST tag. To ensure consistency among reactions, recombinant KDM1A was pre-reduced with immobilized TCEP resin then desalted with buffer exchange immediately prior to each assay. Although the GST tag served as a useful surrogate marker for total

recombinant protein in several western blot-based experiments, as no commercially-available antibodies were found that detected the recombinant protein, GST itself can be modified by high concentrations of thiol-reactive compounds (21). We confirmed that His_6-tagged KDM1A is also inhibited by thiol-reactive compounds, but noted that this enzyme had significantly lower demethylase activity than the GST-tagged protein (data not shown). In addition, full-length KDM1A was immunoprecipitated from HeLa cells and demethylation of a synthetic 21-mer peptide substrate was monitored using western blotting (Figures 4.2C and 4.2D). Peptide demethylation was inhibited by the disulfide-forming 2,2'-DPS, the thioether-forming Np-Mal, and the FAD-directed inhibitor RN1, suggesting that full-length KDM1A is also inhibited by thiol-reactive compounds. These compounds reduced the production of H_2O_2 in immunoprecipitated reactions as measured by the HRP-coupled assay, consistent with inhibition of KDM1A as opposed to another, co-immunoprecipitated demethylase (data not shown). Finally, a biotinylated maleimide (Biotin-Mal, Figure 4.1) was used to further characterize the thiol-reactivity of the native enzyme. KDM1A from SH-SY5Y lysate was readily labeled by 10 µM Biotin-Mal and pulled down on streptavidin-agarose beads (Figure 4.4D). SH-SY5Y cells were selected as a model system due to their expression of all four homologous FAD-dependent amine oxidases. The lysis buffer used for this experiment was degassed by sonication under vacuum to minimize artefactual oxidation and adjusted to a relatively low pH (6.5) to bias the selectivity of maleimide labeling towards cysteine thiol nucleophiles (22). Under these conditions, KDM1A appears to be relatively more thiol-reactive than its homologues KDM1B and MAOA/B (Figure 4D), consistent with the *in vitro* activity observed with recombinant proteins (Figure 3A). However, these data do not exclude the possibility that KDM1B and MAO-A/B were not detected due to Biotin-Mal modification preventing epitope recognition by their respective antibodies.

4.3.2 Cysteine Modification alters KDM1A conformation

Both KDM1A and KDM1B were found to be inhibited by the FDA-approved drug disulfiram (Figure 4.2A). Disulfiram has been used clinically as an aldehyde dehydrogenase inhibitor, where it inhibits catalysis by modification of active-site cysteines. Notably, a class 2 KDM, JMJD2A, has also been reported to be inhibited by disulfiram, and the mechanism this inhibition is proposed to involve disruption of JMJD2A's cysteine-rich zinc-binding site (23). KDM1B contains a unique N-terminal zinc-finger domain consisting of a C4H2C2-type zinc finger and a CW-type zinc finger, and mutation of zinc-finger cysteine residues results in subtle conformational alterations that impair FAD binding and demethylase activity (24). We thus speculate that disulfiram inhibits KDM1B by a similar mechanism as JMJD2A, cysteine modification and ejection of zinc, but further work is required to test this mode of inactivation.

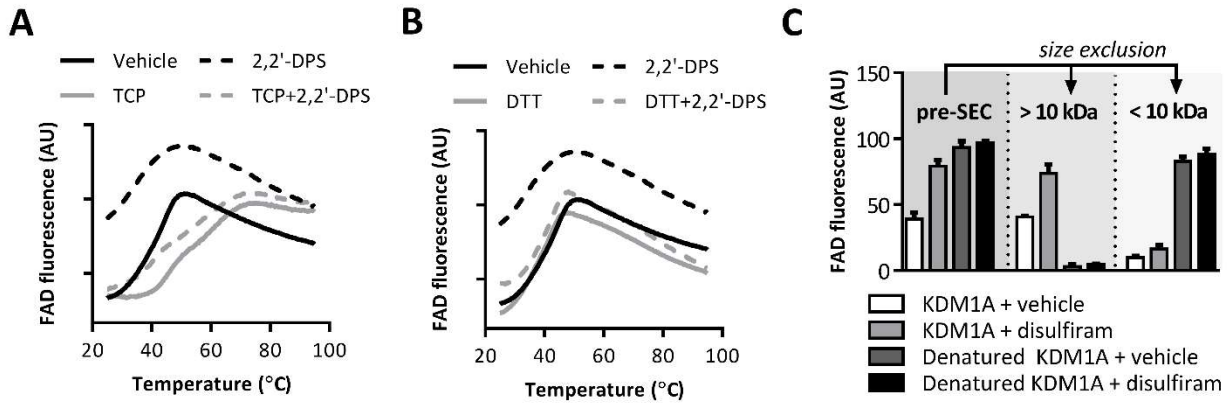

Figure 4.3 Thiol-reactive inhibitors increase the fluorescence of KDM1A-bound FAD.
A. ThermoFAD melting curves of recombinant KDM1A (5 µM) pre-treated with TCP (250 µM) or vehicle control for 10 minutes, followed by 2,2'-DPS (250 µM) or vehicle control. 2,2'-DPS increases FAD fluorescence only when the cofactor has not been inactivated by an FAD-directed inhibitor. In addition, 2,2'-DPS slightly thermally destabilized recombinant KDM1A. **B.** The increased FAD fluorescence of KDM1A pre-treated with 2,2'-DPS is reversed by addition of DTT (5 mM). For A and B, melting curves were averaged from technical replicates from 2 or 3 experiments (n=6 for vehicle and 2,2'-DPS, n=4 for other conditions, error bars not shown for clarity). **C.** Recombinant KDM1A was pre-treated with disulfiram (12.5 µM) or vehicle control, then a portion was heated to denature the protein and release FAD into solution. The FAD fluorescence of each solution was measured before and after size exclusion chromatography (SEC). Bound FAD is detected in the >10 kDa fraction, while free FAD is detected in the <10 kDa fraction. The experiment was run with technical triplicates and was repeated once (n=6, error bars indicate SD).

KDM1A does not contain a cysteine-rich zinc-binding motif; nonetheless, impaired FAD binding or destabilizing conformational changes following cysteine modification may be relevant to the mechanism of inhibition by disulfiram and other thiol-reactive compounds. The inherent fluorescence of the FAD cofactor was leveraged to test these hypotheses. Free FAD in solution fluoresces more strongly than bound FAD in the catalytic core of a flavoprotein. Applying this principle, the ThermoFAD assay measures the increase in FAD fluorescence as the test flavoprotein is heated and unfolded, releasing its cofactor into solution (25). Conveniently, this assay can be run in a standard RT-PCR instrument, as the emission and excitation wavelengths of FAD are closely matched to those of SYBR green. Thiol-reactive inhibitors thermally destabilized the T_M of recombinant KDM1A by 1-4 ° C (data quantification not shown). More notably, all classes of thiol-reactive inhibitors significantly increased FAD fluorescence at room temperature (Figures 4.3A-4.3C and data not shown). This effect was blocked when recombinant KDM1A was pre-treated with TCP, which alters the fluorescence properties of FAD (Figure 4.3A, this effect was also seen for RN1). Furthermore, FAD fluorescence is returned to baseline levels upon addition of DTT (Figure 4.3B). Possible explanations for this observation include a conformation change upon KDM1A cysteine modification resulting in either increased exposure of bound FAD to solvent and/or partial release of bound FAD into solution.

Many epigenetic modifiers are sensitive to fluctuations in the availability of their energetic cofactors by virtue of having a K_D for cofactor binding near physiological concentrations (26). To test if cysteine modification weakens KDM1A's affinity for FAD, several attempts were made to rescue KDM1A demethylase activity by addition of excess FAD (data not shown). However, the only conditions found to reverse inhibition were those including thiol-selective reducing agents. Finally, size-exclusion chromatography (SEC) was used to test if the observed increase in FAD fluorescence resulted from release of the cofactor into solution. Recombinant KDM1A was treated with disulfiram or vehicle control, then a portion was heated to denature the protein and release FAD into solution. Disulfiram-treated KDM1A had

increased FAD fluorescence relative to the vehicle control before SEC, and fluorescence remained associated with the protein-containing fraction (>10 kDa, Figure 4.3C). In contrast, the FAD liberated from KDM1A by thermal denaturation was detected in the small molecule fraction (<10 kDa). Finally, disulfiram does not affect FAD fluorescence when KDM1A is unfolded. Taken together, these data suggest that cysteine modification by thiol-reactive inhibitors results in a reversible conformational change of KDM1A associated with increased fluorescence of the bound FAD cofactor. Inhibition may result from changes in the active site configuration which increase cofactor exposure to solvent and ablate catalytic competency.

4.3.3 Cys600 is Modified by Biotin-Mal and Forms a Putative Disulfide with Cys618

To gain further insight into the mechanism and possible significance of KDM1A thiol-reactivity, we sought to identify which cysteine residue, or residues, were labeled with Biotin-Mal using mass spectrometry. Samples of recombinant KDM1A were labeled with Biotin-Mal or vehicle control, subjected to in-gel trypsin digestion, and the resulting tryptic digest peptides were measured with MALDI-TOF mass spectrometry. Under optimized conditions, 73% sequence coverage was obtained including peaks corresponding to all cysteine-containing peptides (Supplementary Tables A1 and A2). Of the nine cysteine residues in KDM1A, only Cys600 was unambiguously labeled by Biotin-Mal (Figure 4.4A). This residue is conserved in all mammalian forms of KDM1A and is located in the FAD-binding portion of the amine oxidase domain. The corresponding cysteine residues in MAO-A and MAO-B are the only to be modified by a related biotinylated maleimide (Cys266 of clorgyline-inactivated MAO-A and Cys5 of pargyline-inactivated MAO-B, respectively (20)).

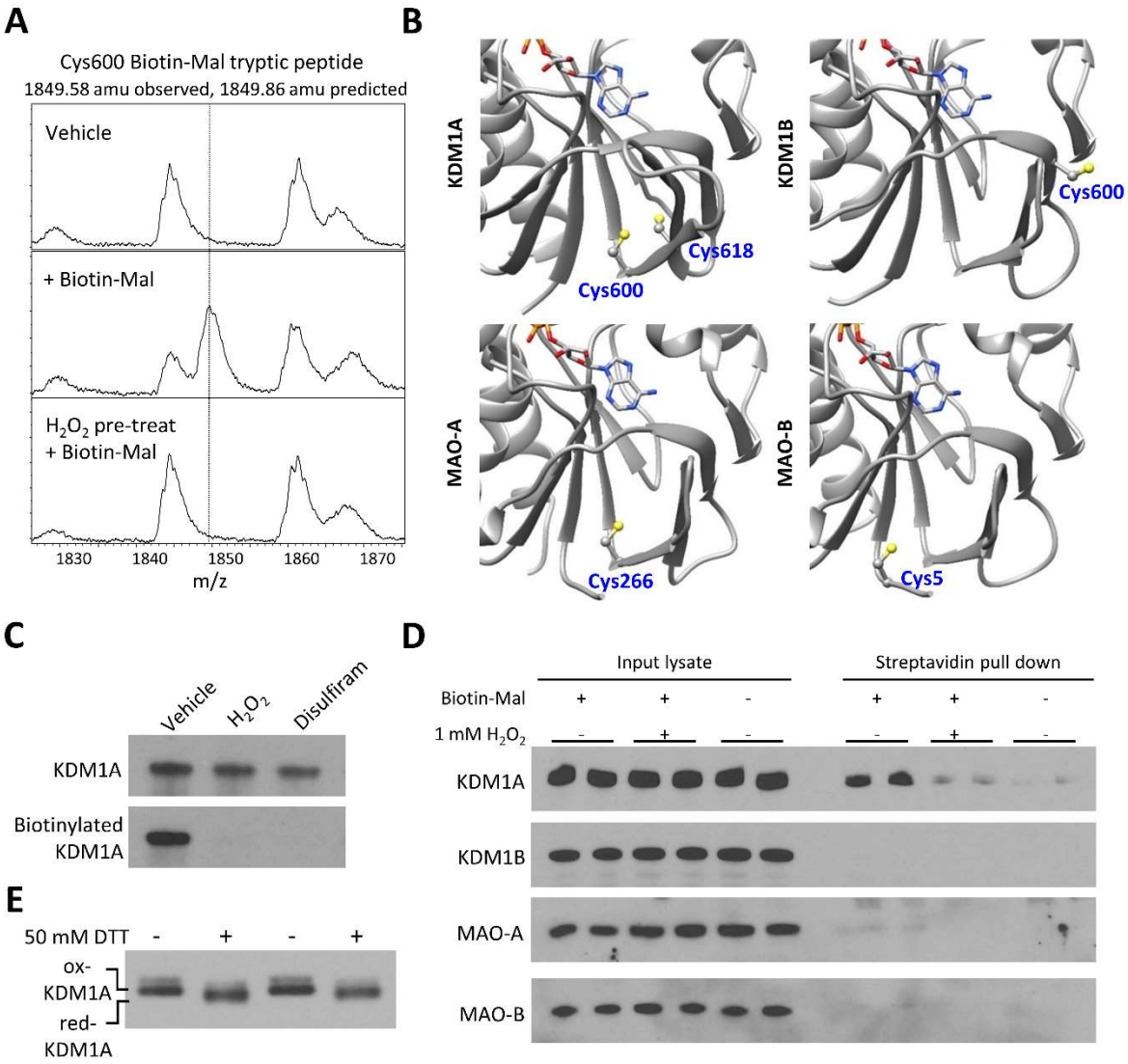

Figure 4.4 KDM1A forms a putative intramolecular disulfide bond.

A. MALDI-TOF analysis of KDM1A tryptic digests identifies Cys600 as a site of Biotin-mal labeling. Labeling of Cys600 is blocked when KDM1A is pre-treated with H_2O_2. **B.** Crystal structures of the FAD-binding amine oxidase domains of KDM1A/B and MAO-A/B indicate a unique pair of proximal cysteine residues in KDM1A which may be capable of disulfide bond formation (respective PDB accession codes: 2JER, 4GUU, 2BXR, and 2XFU, only residues in the amine oxidase domains are displayed). Cys600 is ~5 Å away from Cy618 in the crystal structure of KDM1A, and this pair of cysteines abuts the Rossmann fold responsible for FAD cofactor binding. **C.** Pre-treatment of recombinant KDM1A with H_2O_2 or disulfiram followed by desalting with buffer exchange blocks labeling with Biotin-Mal, as measured by blotting with a streptavidin-HRP conjugate. **D.** KDM1A is readily labeled with 10 µM Biotin-Mal in SH-SY5Y cell lysate, and labeling is blocked by pulse pre-treatment (10 min) of intact cells with 1mM H_2O_2. Other FAD-dependent amine oxidases do not appear to be as thiol-reactive. **E.** Oxidized and reduced forms of KDM1A from SH-SY5Y cell lysate migrate differentially by non-reducing SDS-PAGE followed by western blotting, consistent with intramolecular disulfide bond formation.

Examination of the crystal structures of KDM1A revealed the presence of Cys618 proximal to Cys600 (Figure 3B). Comparison of KDM1A/B and MAO-A/B indicates that only KDM1A contains a pair of cysteines in FAD-binding amine oxidase domain (Figure 4.4B). Although the Cys600/Cys618 sulfur atoms were not oriented towards one another in the solved structures, the average S-S distance was ~4.8 Å and the average Cb-Cb distance was ~5.1 Å in a sampling of available KDM1A structures (data not shown), raising the possibility of intramolecular disulfide formation (27). Notably, this pair of cysteines abuts the conserved Rossmann fold responsible for co-factor binding, suggesting that cross-strand disulfide bond formation may allosterically regulate FAD accessibility or redox potential, which may be consistent with the FAD fluorescence signature associated with cysteine modification (27-29).

4.3.4 KDM1A is reversibly inhibited by H_2O_2 in vitro

Production of H_2O_2 in the nucleus is a distinguishing feature of KDM1A/B biochemistry and may have important functional consequences; furthermore, proximal cysteine thiols can be reversibly oxidized by H_2O_2 to form disulfide bonds. On this basis, we were motivated to test the reactivity of KDM1A with H_2O_2. When oxidized, cysteine thiols are no longer nucleophilic and are thus do not readily react with electrophilic maleimides (22). Consistent with this mechanism, treatment of recombinant KDM1A with disulfiram or with 1 mM H_2O_2, followed by buffer exchange, blocked Biotin-Mal labeling as detected by blotting with a streptavidin-peroxidase conjugate (Figure 4.4C). MALDI-TOF analysis of tryptic peptides confirmed that pre-treatment of recombinant KDM1A with H_2O_2 blocked Biotin-Mal labeling of Cys600 (Figure 4.4A). To test if cysteine oxidation might be relevant to full-length KDM1A, intact SH-SY5Y cells were pulse treated with 1 mM H_2O_2 for 10 minutes, then collected and washed with PBS prior to lysis in degassed, pH 6.5 buffer containing Biotin-Mal. Under these conditions, pre-treatment with H_2O_2 reduced Biotin-Mal labeling of KDM1A to near background levels (Fig 4.4D). These data indicate that KDM1A thiol-reactivity is sensitive to H_2O_2.

Cysteine thiols can be reversibly oxidized by H_2O_2 to form sulfenic acids, which may further react with nearby thiols to form disulfide bonds. Several tool compounds have been developed to detect sulfenic acids based on their reactivity with 1,3-diones such as dimedone (22). Efforts to trap and detect sulfenic acid formation in H_2O_2-treated recombinant KDM1A or in SH-SY5Y cell lysate with dimedone or a biotinylated derivative (BP1) were unsuccessful in both western blotting and mass spectrometry experiments (data not shown), suggesting that this oxidized intermediate may be rapidly converted to a disulfide species. Under harsh conditions, thiols are oxidized by H_2O_2 to form sulfinic and sulfonic acids, modifications that are essentially irreversible by reducing agents such as DTT (22). No differences were observed between oxidized and control tryptic peptide MALDI-TOF spectra in the absence of Biotin-Mal labeling, suggesting that any oxidation caused by H_2O_2 was reversed during the reduction step of the in-gel digestion protocol (Supplementary Table A1). Two tryptic peptides were observed which may correspond to the hydrolyzed Biotin-Mal adduct of Cys195 and Cys665, respectively. Notably, formation of neither adduct was blocked by H_2O_2 oxidation (Supplementary Table A1). Non-reducing PAGE followed by western blotting provided no evidence for KDM1A intermolecular disulfide formation either *in vitro* or in SH-SY5Y cell (data not shown). However, subtle changes in the migration of KDM1A from SH-SY5Y lysate were observed in the presence or absence of DTT by non-reducing PAGE (Figure 4.E). Using this electrophoresis technique, two DTT-sensitive bands were resolved and detected by immunoblotting for KDM1A; we suspect that one band may be a KDM1A splice isoform important in SH-SY5Y neuronal differentiation, but additional work is needed to clarify this hypothesis (30). While other mechanisms cannot be excluded, these data are fully-consistent with formation of putative intramolecular disulfide between Cys600 and Cys618 in KDM1A.

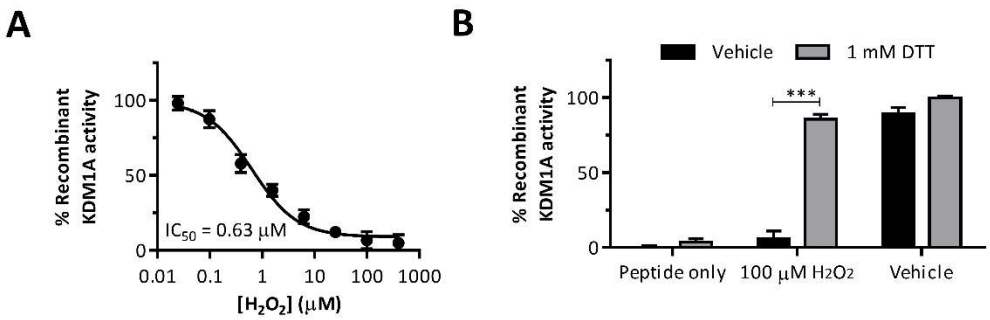

Figure 4.5 Recombinant KDM1A is inhibited by hydrogen peroxide.
A. Exogenously applied H_2O_2 inhibits recombinant KDM1A with an apparent IC_{50} value of 630 nM, error bars indicate SD. **B.** Inhibition of recombinant KDM1A by H_2O_2 is reversible by the addition of DTT. KDM1A was pre-incubated with H_2O_2 (100 μM) for 10 min prior to reduction. Error bars indicate SD, *** $p < 0.001$ by 2-tailed *t* test with correction for multiple comparisons. For both A and B, demethylation of H3K4me2 starting material was detected by LC-MS after 1-hour reaction.

4.3.5 Activity-dependent oxidation of KDM1A

Modification of KDM1A with thiol-reactive small molecules results in enzyme inhibition, and H_2O_2 pre-treatment blocks these modifications *via* proposed disulfide bond formation. We thus reasoned that H_2O_2 itself could inhibit KDM1A's enzyme activity. Indeed, exogenously applied H_2O_2 was found to inhibit the catalytic activity of recombinant KDM1A with an apparent IC_{50} value around 630 nM in an LC-MS assay, and inhibition was fully reversed by addition of the thiol-selective reducing agent DTT (Figure 4.5A and 4.5B). Concentrations of H_2O_2 required for complete inhibition of KDM1A were an order of magnitude greater than the enzyme concentration (200 nM). We postulated that the H_2O_2 produced by KDM1A as a byproduct of catalysis might negatively regulate enzyme activity by cysteine oxidation after several rounds of substrate conversion. To test this hypothesis, recombinant KDM1A was treated with a large excess of synthetic peptide substrate (1,000-fold) and substrate demethylation was monitored by LC-MS over time. The demethylase activity of vehicle-treated KDM1A plateaued after several hours, whereas catalysis continues unabated in the presence of DTT (Figure 4.6A).

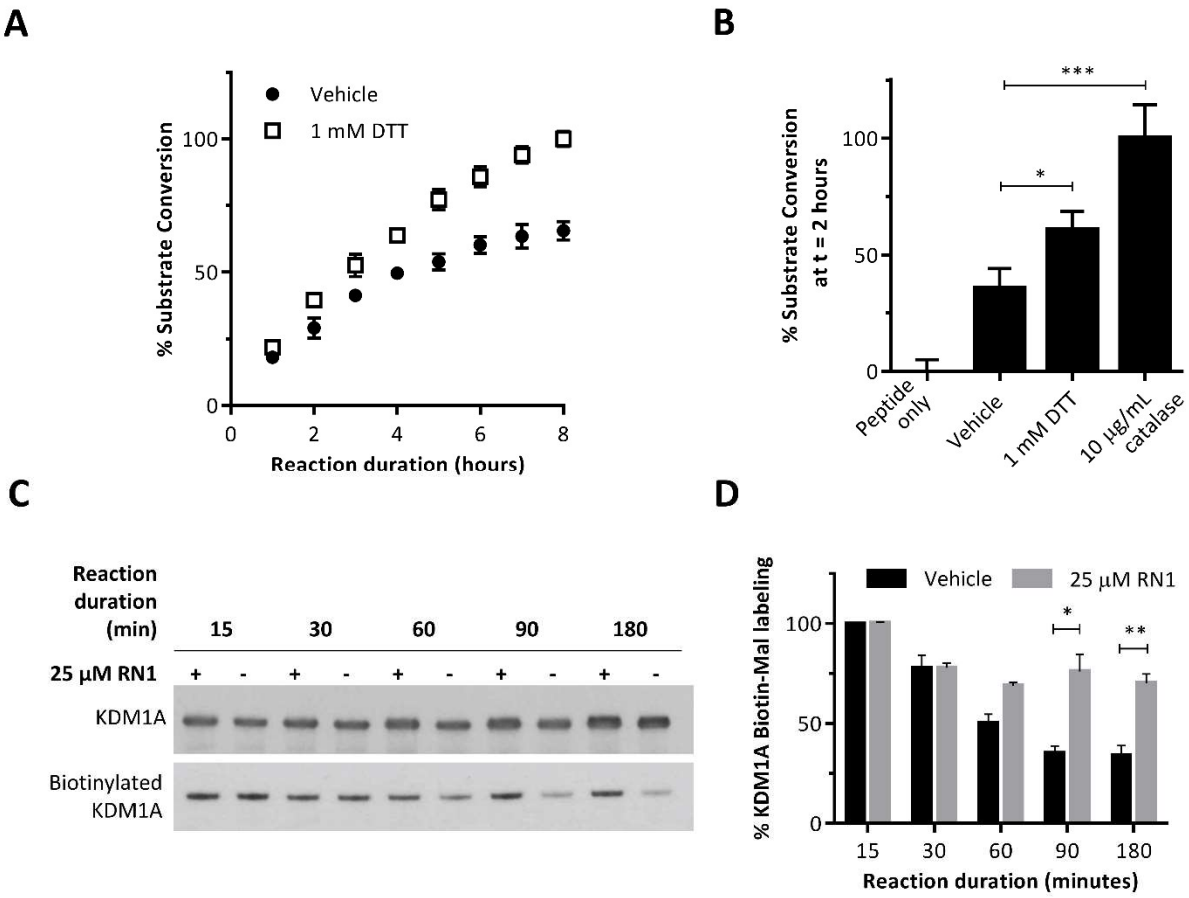

Figure 4.6 Activity-dependent regulation of KDM1A.
A. Demethylation of H3K4me2 peptide substrate by recombinant KDM1A is enhanced in the presence of DTT (1 mM), or **B.** the enzyme catalase (10 µg/mL). For both A and B, demethylation of H3K4me2 starting material was detected by LC-MS. Error bars indicate SD, * $p < 0.05$, *** $p < 0.001$ by 1-way ANOVA with correction for multiple comparisons. **C.** Labeling of recombinant KDM1A with Biotin-Mal (25 µM) is reduced with extended demethylation reaction durations. Addition of the FAD-directed inhibitor RN1 (25 µM) blocks the time-dependent reduction in labeling. **D.** Quantification of Biotin-Mal labeling as measured by blotting with a streptavidin-HRP conjugate and normalized to total recombinant KDM1A over 3 replicate experiments. Error bars indicate SD, * $p < 0.05$, ** $p < 0.01$, by 2-tailed *t* test with correction for multiple comparisons.

In addition to H_2O_2, molecular oxygen also oxidizes thiols to disulfide bonds and would be predicted to reduce KDM1A activity over time. To distinguish between these two oxidants, the enzyme catalase was added to decompose H_2O_2 before its concentration was sufficient to inhibit KDM1A. Addition of catalase to the KDM1A reaction with excess substrate significantly increased substrate demethylation, suggesting that H_2O_2 is the relevant inactivating oxidant (Figure 4.6B). Finally, we tested if KDM1A catalytic activity results in decreased thiol-reactivity over time. Recombinant KDM1A was treated with vehicle or

inactivated with the FAD-directed inhibitor RN1, then mixed with an excess of substrate. Thiol-reactivity was probed by Biotin-Mal labeling at various time intervals. Initial labeling efficiencies were comparable, indicating that RN1 inhibition is non-competitive with thiol labeling (Figure 4.6C and 4.6D). An initial drop in labeling efficiency was seen for both active and inactive forms of KDM1A, which may reflect oxidation by O_2. However, the labeling efficiency of RN1-inactivated KDM1A plateaus, whereas labeling of the catalytically-active protein diminishes over time. Under these conditions, we propose that KDM1A is feedback inhibited by the H_2O_2 byproduct of catalysis *via* a thiol/disulfide switch (Figure 4.7). As others have reported, the enzymatic activity of recombinant KDM1B was substantially lower than recombinant KDM1A *in vitro*, so further efforts will be necessary to determine if KDM1B is negatively regulated by its own H_2O_2 production (31).

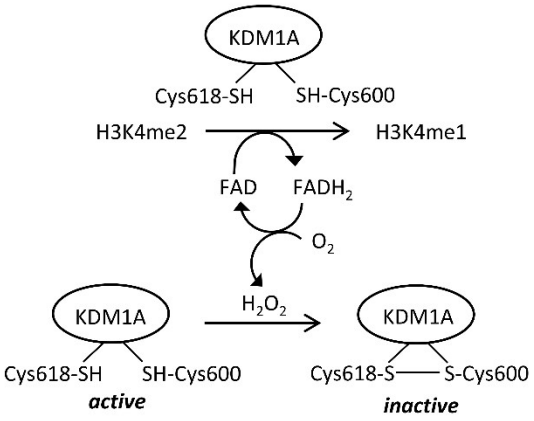

Figure 4.7 Working model of KDM1A activity-dependent regulation by a thiol/disulfide redox switch.

4.3.6 Exogenous dopamine synergizes with KDM1A inhibitors and oxidizes KDM1A

Neurons are particularly vulnerable to oxidative stress, and modification of proteins and lipids by reactive oxygen and nitrogen species (ROS/RNS) are broadly associated with neurodegenerative and neuropsychiatric diseases (32,33). Human SH-SY5Y cells are catecholaminergic and undergo autophagy and induction of α-synuclein upon exposure to exogenous dopamine, and have thus been used as a model

system to test the role of oxidative stress in the etiology of Parkinson's disease (34). Dopamine is readily oxidized to an *ortho*-quinone and/or cyclized aminochrome, producing free radicals as products (35). The cytotoxicity of dopamine is normally mitigated by sequestration into vesicles or metabolic clearance by the monoamine oxidases, with cell death occurring if these processes are exceeded by dopamine uptake (34). The trace amine tyramine is also metabolized by the monoamine oxidases, but is not a catechol and does not autoxidize. As an initial exploration of the role of KDM1A in dopamine cytotoxicity, SH-SY5Y cells were treated with tyramine or dopamine in conjunction with FAD-directed KDM1A inhibitors. SH-SY5Y cells treated with 50 μM tyramine produce hydrogen peroxide, and this production can be blocked by pre-treatment with TCP (data not shown), confirming monoamine oxidase activity in these cells. However, cells treated with 1 mM tyramine for 24 hours did not differ in cell viability from vehicle-treated cells (Figure 4.8A), suggesting that the ROS produced by MAO activity was sub-lethal. In contrast, application of exogenous dopamine resulted in significant cell death, which was potentiated by co-treatment with RN1. Notably, the concentrations of RN1 which potentiate dopamine cytotoxicity (25 μM) do not affect cell viability in the absence of the neurotransmitter. Synergistic toxicity was also observed for co-treatment of dopamine and TCP, as well as with application of exogenous H_2O_2 in conjunction with RN1 or TCP (data not shown). Based on dopamine's propensity for oxidation, we speculated that pulse-treatment of cells would result in KDM1A oxidation, as was observed with H_2O_2 application. Indeed, exposure of SH-SY5Y cells to 1 mM dopamine for 20 minutes, followed by washing of the cell pellet before lysis, significantly reduced biotin-maleimide labeling of KDM1A in the streptavidin pull-down assay (Figure 4.B). Although much additional work will be required to clarify these results and extend them to physiologically-relevant conditions, these data represent the first step towards understanding the redox regulation of KDM1A in a neurobiological context.

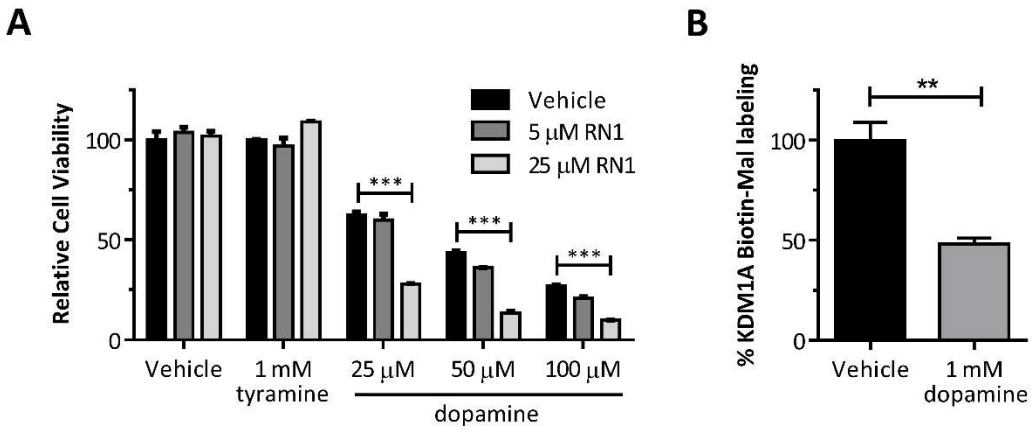

Figure 4.8 Exogenous dopamine synergizes with KDM1A inhibitors and oxidizes KDM1A.
A. RN1 potentiates the cytotoxicity of dopamine. SH-SY5Y cells were treated with RN1 (5 or 25 μM) or vehicle control in conjunction with tyramine, dopamine, or vehicle for 24 hours, then cell viability was assessed with the CellTiter Glo® assay. Error bars indicate SD, n=4 from biological duplicates, *** $p < 0.001$ by 1-way ANOVA with Dunnett correction for multiple comparisons. **B.** Biotin-maleimide labeling of KDM1A is blocked by pulse pre-treatment (20 min) of intact cells with 1mM dopamine as measured by streptavidin pull-down assay and western blotting. Error bars indicate SD, n=4 from biological duplicates, ** $p < 0.01$ by 2-tailed *t* test.

4.4 Conclusion

Epigenetic machinery is regulated by the cellular redox state through several mechanisms, including fluctuations in the availability of metabolites utilized as substrates and cofactors, interaction with redox-sensitive transcription factors, modification by redox-sensitive enzymes, and direct modification by ROS/RNS (36). The evolution of two mechanistically-distinct classes of histone lysine demethylases points towards important differences in their regulation, including by their enzymatic chemistries. Enzymes such as flavoproteins that produce ROS are rare in the nucleus, and oxidation of DNA by the H_2O_2 generated from KDM1A catalysis has been implicated in transcriptional regulation by BER (13-15). Given this context, we were intrigued to discover that KDM1A is highly thiol-reactive both *in vitro* and in cellular models.

While our data are fully consistent with a model of intramolecular disulfide bond formation, definitive assignment of cysteine reactivity and disulfide bond formation is challenging. Thiol-labeling of MAO-A and MAO-B is substantially reduced by competition with enzyme substrate, indicating that enzyme

conformations vary significantly in their cysteine reactivity and/or accessibility (20). Further complicating this analysis is the observation that TCP may form unstable adducts with MAO cysteine residues (37). Our data suggest that KDM1A thiol reactivity is non-competitive with RN1 inactivation, although other FAD-directed inhibitors remain to be tested. Prior to determination of its crystal structure, MAO-A was proposed to contain a redox-sensitive active-site disulfide bond (38). The solved structure of MAO-A later revealed a disulfide linkage between Cys321 and Cys323 (PDB ID: 2BXR), although these residues are not near the active site and are not conserved in KDM1A (39). Subsequent electrospray mass spectrometry experiments provided no evidence for intramolecular MAO-A disulfide bond formation, raising the possibility of artefactual oxidation during crystallization (20). Crystallography experiments on oxidized KDM1A may provide additional evidence for disulfide bond formation and clarify the mechanism of enzyme inactivation.

KDM1A is an attractive therapeutic target due to its elevated expression in many cancers and possible role in neurologic disease and viral pathogenesis, and numerous assays exist to profile inhibition by novel compounds (40). Our results as well as others' reports indicate that additional screening strategies are needed to overcome the predominant mode of inhibition *via* thiol-reactivity and general redox sensitivity to find more tractable, drug-like small molecule inhibitors (41). One potential avenue to circumvent unwanted thiol reactivity is to mutate candidate cysteine residues. This approach has led to mixed results with the monoamine oxidases; for example, site-directed mutagenesis of MAO-A Cys374 and the corresponding MAO-B Cys365 to serine resulted in loss of enzyme activity, whereas cysteine to alanine mutants remained active (42). Despite highly similar overall folds, the rate of thiol reactivity is vastly greater for MAO-A than MAO-B, and appears to be greater still for KDM1A, suggesting that subtleties in enzyme structure modulate reactivity. In light of these observations, we favored a chemical tool-based approach to study KDM1A cysteine reactivity.

In the presence of excess substrate, we found that the H_2O_2 generated by multiple rounds of KDM1A catalysis was linked with diminished enzyme activity and Biotin-Mal labeling, suggesting that auto-oxidation negatively regulates enzyme activity. To the best of our knowledge, this is the first example of an activity-dependent thiol/disulfide switch among epigenetic enzymes. The physiological relevance of this mechanism remains to be tested, but this chemistry fits within an emerging picture of cysteine-mediated redox regulation of chromatin biology. ROS-generating stimuli result in intramolecular disulfide bond formation between Cys667 and Cys669 of HDAC4, promoting nuclear exportation (43). Peroxide-sensitive, regulatory intermolecular disulfides have been proposed to form between the transcription factor FoxO and the p300/CBP acetyltransferase (44). Recently, the Sin3A-associated protein 30-like (SAP30L), a key protein in Sin3A repressive complexes, was found to form two intramolecular disulfide bonds with concomitant release of zinc from a Cys3His type zinc finger upon H_2O_2 treatment (45). In addition to cysteine-mediated regulation by ROS, critical cysteine residues on the histone deacetylase HDAC2, a component of KDM1A repressive complexes, appears to be regulated by RNS. Brain-derived neurotrophic factor (BDNF) triggers NO synthesis and induces S-nitrosylation of histone deacetylase 2 (HDAC2) at Cys262 and Cys274 in neurons, resulting not in altered enzymatic activity but rather in release from chromatin (46). These same cysteine residues and their homologs on HDAC1 and 3 are carbonylated upon exposure to cigarette smoke and other alkylating agents, resulting in enzyme inactivation (47). These findings collectively point to multiple mechanisms by which cysteine modification regulates chromatin-modifying complexes.

Our proposed mechanism of thiol/disulfide regulation of KDM1A raises several questions which remain to be addressed in a cellular context. What is the relevant reducing agent that opposes KDM1A oxidation? Notably, the nuclear glutathione and thioredoxin-1 systems responsible for reduction of many protein cysteines are controlled independently from their cytoplasmic counterparts, and are not in redox equilibrium with one another (48). Does KDM1A sense ROS (or RNS) resulting from hypoxia and other cell

signaling events, such as dopamine neurotransmission, or does cysteine oxidation result from an activity-dependent mechanism as seen in our *in vitro* studies? Negative feedback regulation may be relevant in bursts of highly-localized KDM1A activity, such as that resulting in 8-oxoG modification of target genes. Furthermore, does KDM1A oxidize any of its non-histone substrates? For example, exogenous H_2O_2 induces methylation of the transcription factor Sp1, a modification that strengthens its interaction with HDAC1 and that is sustained by KDM1A inhibition with pargyline or by KDM1A knock down (49). The H_2O_2 generated by KDM1A may play multiple roles in the biochemistry of this enzyme and its co-regulators. Finally, we expect that many cellular oxidants may regulate demethylation by KDM1A, both in and out of the brain.

4.5 Materials and Methods

Inhibitors and Reagents– TCP, disulfiram, and 2,2'-DPS were purchased from Sigma Aldrich. Np-Mal was purchased from ChemBridge (catalog #51332107). Biotin-Mal was purchased from Anaspec (catalog #AS-60643). RN1 was synthesized as previously described (16). Inhibitors were used without further purification and were stored as 25 mM stock solutions in DMSO at -20 °C. Dilutions in aqueous buffer were prepared immediately prior to use. Hydrogen peroxide (Sigma Aldrich, cat# 216763) was stored as a 37% solution at 4 °C. DTT (Sigma Aldrich), 2-iodoacetamide (Alfa Aesar), and dopamine hydrochloride (Sigma Aldrich) were stored as powders at 4 °C and solutions were prepared immediately before use.

Recombinant Enzymes and Substrates - Enzymes and substrates were prepared exactly as previously described (Chapter 2).

Cell lines- HeLa and SH-SY5Y cells were maintained exactly as previously described (Chapter 2).

Recombinant Amine Oxidase Assays (Figure 3A) - KDM1A (30 nM) was pre-incubated with inhibitors for 10 minutes in 50 mM pH 7.4 sodium phosphate buffer, followed by addition of H3K4me2

peptide substrate (5 μM) in a total reaction volume of 30 μL. The demethylation reaction was quenched with 1% formic acid after 20 minutes, then detection of substrate conversion to H3K4me1 and H3K4me0 was accomplished on an Agilent RF300 mass spectrometry system with RapidFire chromatography in line with a triple stage quadrapole mass spectrometer (RapidFire MS) as previously described (16). KDM1B (60 nM) was pre-incubated with inhibitors for 10 min in 50 mM pH 8.1 sodium phosphate buffer followed by addition of H3K4me2 peptide substrate (5 μM) in a total reaction volume of 15 μL. The demethylation reaction was quenched with 1% formic acid after 1 hour, then detection of substrate conversion to H3K4me1 and H3K4me0 was accomplished by LC-MS using an Agilent 6310 ion trap mass spectrometer with an ESI source connected to an Agilent 1200 series HPLC with isocratic elution of 5% acetonitrile (ACN) in 0.1% formic acid (FA) at a flow rate of 0.5 mL/min through an Agilent Eclipse XBD-C8 reversed-phase column. Percent enzyme activity was calculated from ratio of H3K4me1 and H3K4me0 peak areas to the H3K4me2 peak area in inhibited wells relative to control wells. MAO-A and MAO-B were pre-incubated with compounds for 10 minutes, then enzyme activity was assayed using the MAO-Glo assay kit (Promega #V1401) according to the manufacturer's protocol in Proxiplate 384 Plus plates (Perkin Elmer) with a miniaturization of the final assay volume to 20 μL as previously described (16). Reactions were quenched after 1 hour by adding reconstituted luciferin detection reagent, and fluorescence at 570 nm was measured on a Perkin Elmer Wallac Envision 2103 Multilabel plate reader. Percent enzyme activity was calculated from the fluorescence readings of inhibited wells relative to control wells. For all enzymes, the compound concentration resulting in 50% inhibition (apparent IC_{50}) was determined by 3-parameter non-linear regression of the plot of log[inhibitor] versus enzyme activity in GraphPad Prism 6 (GraphPad Software, Inc.).

Statistical analyses – Statistical analysis of enzyme activity and blot densitometry data were performed using unpaired, two-tailed Student's *t* tests with post hoc Holm-Sidak correction for multiple comparisons or 1-way ANOVA with post hoc Dunnett correction for multiple comparisons to determine *p*

values, as indicated in each figure legend. Statistical testing and graph preparation were performed using GraphPad Prism 6 (GraphPad Software, Inc.). All error bars indicate standard deviation (SD). A *p* value of <0.05 was considered significant. Relative degree of significance is indicated in figures by the number of asterisks and is defined in each figure legend.

Recombinant KDM1A activity assays – With the exception of the inhibition data in Figure 4.3A, KDM1A assays were run as follows: recombinant KDM1A was pre-reduced for 15 minutes on ice with immobilized TCEP resin (Thermo Scientific), which had been equilibrated in assay buffer, 50 mM, pH 7.4 sodium phosphate. Following reduction, the buffer was exchanged using Zeba spin desalting columns (7K molecular weight cut-off, Thermo Scientific) that had been pre-equilibrated with assay buffer. Demethylation reactions were quenched with 1% formic acid and detection of substrate conversion to H3K4me1 and H3K4me0 was accomplished by LC-MS as described for the KDM1B assay. For dithiothreitol (DTT) reversibility experiments and inhibition by H_2O_2, 1.5 µM KDM1A was reduced with an equal volume of TCEP resin, desalted, then diluted to a final [KDM1A] of 200 nM. KDM1A was pre-incubated with inhibitors for 10 minutes, followed by addition of 1 mM DTT or vehicle control. After a 10-minute reduction, H3K4me2 substrate was added to a final concentration of 10 µM in a final volume of 30 µL and the reaction was allowed to proceed for 1 hour. For feedback inhibition experiments, 5 µM recombinant KDM1A was reduced with an equal volume of TCEP beads, desalted, then diluted to a final [KDM1A] of 400 nM. DTT (final concentration of 1 mM), catalase (Sigma Aldrich, catalog #C1345, final concentration of 10 µg/mL) or vehicle control were added, followed by H3K4me2 substrate (final concentration of 500 µM) in total reaction volume of 10 µL. The demethylation reactions were quenched at various time points as indicated.

Immunoprecipitation assay – The immunoprecipitation assay was performed as described in Chapter 2. Briefly, HeLa cells were lysed in ice-cold PBS containing 0.15% Ipegal CA-630 1x protease inhibitors, then pre-cleared lysate was nutated with anti-KDM1A antibody (Abcam, catalog #129195, lot

#YI120618DS) for 1 hour, then immunoprecipitated overnight at 4 °C at a ratio of 12 million HeLa cells per 50 µL packed protein agarose A beads (Roche) per 5 µL antibody per tube. KDM1A-bound beads were pooled, washed three times with 50 mM phosphate buffer, pH 7.4 with 0.1% Brij-35, then divided into Eppendorf tubes (25 µL of 1:1 bead slurry per reaction). Immunoprecipitated KDM1A was pre-incubated with inhibitors (10 µM) or vehicle control for 10 minutes before addition of 10 µM H3K4me2 substrate for 1 hour at 37 ° C, then quenched by addition of sample loading buffer + DTT. Reactions were run in technical replicates, and the entire procedure was repeated twice. Proteins were detected and peptide demethylation reaction progression was assessed by western blotting exactly as previously described (Chapter 2).

FAD fluorescence experiments – *Thermo*FAD experiments were run essentially as previously described (25). Briefly, recombinant KDM1A was diluted to 5 µM in 50 mM sodium phosphate, pH 7.4, buffer. A volume of 0.25 uL of test compound or DMSO vehicle control for a final concentration of 250 µM was added to and mixed well with 25 µL of KDM1A solution per well of a MicroAmp Optical 96-well Reaction Plate (Life Technologies, catalog #N8010560). For combinatorial compound testing, TCP was added 10 minutes prior to addition of 2,2'-DPS, or 2,2'-DPS was added 10 minutes prior to addition of DTT. The plate was sealed with adhesive film and FAD fluorescence was measured using the SYBR green instrument settings (excitation filter: 485 nm; emission filter: 535 nm) with heating from 25 °C to 95 °C at a rate of 1 °C/minute and a fluorescence reading at every 0.5 °C. Compounds were tested in duplicate, and the experiment was performed three times, with some test compounds repeated in 2/3 replicates (n=4) or in all 3 replicates (n=6). For size exclusion chromatography experiments, recombinant KDM1A was diluted to 1 µM in 50 mM sodium phosphate, pH 7.4 buffer. To a volume of 300 µL was added disulfiram to a final concentration of 12.5 µM or vehicle control. After a 10-minute pre-incubation, each solution was split into two aliquots, and one aliquot was heated to 95 °C in a heat block for 10 minutes then cooled to room temperature. A 20 µL aliquot was removed from each sample to determine the pre-

size exclusion chromatography fluorescence, then the remainder was subjected to SEC in an Amicon Ultra centrifugal filter device with a 10 kDa molecular weight cutoff (EMD Millipore, catalog #UFC501024). Fluorescence measurements of the pre-SEC, the supernatant containing molecules larger than 10 kDa, and the flow-through containing molecules smaller than 10 kDa were performed simultaneously using a PerkinElmer Wallac Envision 2103 Multilabel plate reader (excitation filter: 485 nm; emission filter: 535 nm). The experiment was performed in with technical triplicates (three fluorescence readings from the same SEC fraction) and the experiment was repeated once (n=6).

KDM1A Biotin-Mal Labeling Assays - For differential labeling experiments, 3 μM recombinant KDM1A was reduced with 2 equivalent volumes of tris(2-carboxyethyl) phosphine (TCEP) resin, desalted with buffer exchange, then split into 3 aliquots, which were treated with 1 mM H_2O_2, 25 μM disulfiram, or vehicle control for 20 minutes. Each aliquot was then desalted with buffer exchange and labeled biotin-maleimide (Biotin-Mal) at a final concentration of 10 μM for 20 minutes. Excess maleimide was quenched with 40 mM DTT for 10 minutes, followed by addition of sample loading buffer for analysis by western blotting. Biotinylation was detected with a streptavidin-HRP conjugate (Millipore, catalog #18-152), then the membrane was stripped and re-probed for total recombinant protein with 1:10,000 anti-GST (Cell Signaling, catalog #2625P, lot #7) as no commercially-available KDM1A antibodies tested were able to recognize the recombinant protein. For activity-dependent labeling, 5 μM recombinant KDM1A was reduced with an equal volume of TCEP beads, desalted, then diluted to a final [KDM1A] of 400 nM. Recombinant KDM1A was pre-treated with 25 μM RN1 or vehicle control for 10 minutes before addition of H3K4me2 substrate (final concentration of 500 μM) in total reaction volume of 10 μL. At the time points indicated, 25 μM Biotin-Mal was added for 10 minutes, then excess maleimide was quenched with 40 mM DTT for 10 minutes followed by addition of sample loading buffer. Biotinylated and total protein was detected as described above and band intensities were quantified in ImageJ. Biotinylated KDM1A was normalized to total recombinant KDM1A for statistical analyses.

Streptavidin Pull-Down Assay- Lysis buffer (50 mM pH 6.5 sodium phosphate with 1% Ipegal CA-630 and 1x protease inhibitors), was degassed by sonication under vacuum for 20 minutes, then chilled on ice. SH-SY5Y cells were collected, washed with PBS, then pulse-treated with 1 mM H_2O_2, 1 mM dopamine, or vehicle control for 20 minutes. Cells were then pelleted and washed with PBS. Ice-cold lysis buffer was supplemented with 10 µM Biotin-Mal or vehicle control immediately prior to use, and cells were lysed at a density of 2 million SH-SY5Y cells/mL with sonication. After 20 minutes of labeling, input samples were reserved and 100 µL of pre-equilibrated 1:1 streptavidin-agarose slurry (Life Technologies catalog #951) was added per mL of lysate and nutated for 1 hour. The strepativin-agarose beads were washed three times in unsupplemented lysis buffer, then an equal volume of sample loading buffer + DTT was added to each bead slurry and samples were boiled prior to analysis by western blot. Technical replicates were run on adjacent lanes, and the experiment was repeated twice. Membranes were probed for KDM1A (1:5000, Cell Signaling, catalog #2184S, lot #1), KDM1B (1:5000, Abcam catalog #ab52001, lot #GR81275-1), MAO-A (1:1000, Santa Cruz, catalog #sc-20156, lot #D2710) or MAO-B (1:1000, Abcam catalog #ab125010, lot #GR188691-2).

Matrix Assisted Laser Desorption/Ionization (MALDI) Time-of-Flight (TOF) Mass Spectrometry – A solution of 5 µM recombinant KDM1A was reduced with 1 equivalent volume of TCEP resin, desalted with buffer exchange, then split into 2 aliquots, which were treated with 1 mM H_2O_2 or vehicle control for 20 minutes. Each sample was desalted with buffer exchange, then split into two aliquots and treated with 10 µM Biotin-Mal or vehicle control for 20 minutes. Excess maleimide was quenched with 40 mM DTT for 10 minutes, followed by addition of sample loading buffer. A total of 10 µg of recombinant protein sample was loaded per lane of a pre-cast 4-12% Bis-Tris Nu-PAGE gel (Invitrogen). The gel was stained with Coomassie Brilliant Blue R-250 staining solution (Bio-Rad) then destained overnight with 50:40:10 methanol/water/acetic acid. Bands were excised, washed with 50% ACN in 50 mM pH 8 ammonium bicarbonate, reduced with 100 µL of 10 mM DTT for 30 min at 80 °C, then alkylated with 55 mM

iodoacetamide for 20 min in the dark. Excised bands were washed again then incubated overnight with 10 ng/uL sequencing grade modified porcine trypsin (Promega) in 50 mM pH 8 ammonium bicarbonate at 37 °C. Peptides were extracted in 1% trifluoroacetic acid (TFA), mixed with an equal volume of 70 mg/mL 2,5-dihydroxybenzoic acid matrix (Sigma) in 7:3 ACN/0.1% TFA, then deposited on an MTP 384 polished steel BC target plate (Bruker) and analyzed with an autoflex speed LRF MALDI-TOF mass spectrometer (Bruker). The acquired spectra were manually referenced against a virtual digest (UCSF Protein Prospector MS-Digest) including variable oxidation states and missed cut sites. Samples were deposited in triplicate the experiment was repeated twice.

Non-reducing PAGE- Lysis buffer (50 mM pH 6.5 sodium phosphate with 0.15% Ipegal CA-630 and 1x protease inhibitors) was degassed by sonication under vacuum for 20 minutes, then chilled on ice. SH-SY5Y cells were collected, washed with PBS, then pulse-treated with 1 mM H_2O_2 for 20 minutes. Cells were then pelleted and washed with PBS then lysed at a density of 1 million SH-SY5Y cells/mL with sonication. The lysate was split into two aliquots and treated with 50 mM DTT or vehicle control for 10 minutes. Proteins were denatured with non-reducing sample loading buffer (Thermo Scientific) and brief heating to 70 °C, then separated on a pre-cast 3-8% Tris-Acetate Nu-PAGE gel with Tris-Acetate SDS running buffer supplemented with Nu-PAGE antioxidant at the cathode (Invitrogen) at 50 V overnight at 4 °C. The Nu-PAGE antioxidant maintains already reduced proteins in their reduced state and resulted in sharper reduced KDM1A bands (data not shown). Following gel electrophoresis, proteins were transferred and blotted for KDM1A (Cell Signaling, catalog #2184S, lot #1) as described above. Replicate samples were run within a gel, and the experiment was repeated three times.

CellTiter Glo® assay – The assay was performed as described in Chapter 3. Briefly, SH-SY5Y cells were seeded into a 96-well plate (100 µL per well, 2 million cells per mL) and grown overnight, then treated with test compounds or vehicle control to the final concentrations indicated in the figure and legend in pre-warmed media without FBS and using 10 µM staurosporine as a positive control. Cells were

exposed to test compound for 24 hours, then 20 µL of the reconstituted CellTiter Glo® reagent (Promega, catalog #G7572) was added per well and luminescence was read after 30 minutes using a PerkinElmer Wallac Envision 2103 Multilabel plate reader (emission filter: 570 nm). Compounds were tested in duplicate and the experiment was repeated twice (n=4).

4.6 References

1. Mosammaparast, N., and Shi, Y. (2010) Reversal of histone methylation: biochemical and molecular mechanisms of histone demethylases. *Annu. Rev. Biochem.* **79**, 155-179
2. Burg, J. M., Link, J. E., Morgan, B. S., Heller, F. J., Hargrove, A. E., and McCafferty, D. G. (2015) KDM1 class flavin-dependent protein lysine demethylases. *Peptide Science* **104**, 213-246
3. Walport, L. J., Hopkinson, R. J., and Schofield, C. J. (2012) Mechanisms of human histone and nucleic acid demethylases. *Curr. Opin. Chem. Biol.* **16**, 525-534
4. Gaweska, H., Henderson Pozzi, M., Schmidt, D. M., McCafferty, D. G., and Fitzpatrick, P. F. (2009) Use of pH and kinetic isotope effects to establish chemistry as rate-limiting in oxidation of a peptide substrate by LSD1. *Biochemistry* **48**, 5440-5445
5. Shi, Y., Lan, F., Matson, C., Mulligan, P., Whetstine, J. R., Cole, P. A., Casero, R. A., and Shi, Y. (2004) Histone demethylation mediated by the nuclear amine oxidase homolog LSD1. *Cell* **119**, 941-953
6. Karytinos, A., Forneris, F., Profumo, A., Ciossani, G., Battaglioli, E., Binda, C., and Mattevi, A. (2009) A novel mammalian flavin-dependent histone demethylase. *J. Biol. Chem.* **284**, 17775-17782
7. Yang, M., Culhane, J. C., Szewczuk, L. M., Jalili, P., Ball, H. L., Machius, M., Cole, P. A., and Yu, H. (2007) Structural basis for the inhibition of the LSD1 histone demethylase by the antidepressant trans-2-phenylcyclopropylamine. *Biochemistry* **46**, 8058-8065
8. Melvin, A., and Rocha, S. (2012) Chromatin as an oxygen sensor and active player in the hypoxia response. *Cell. Signal.* **24**, 35-43
9. Lu, Y., Chu, A., Turker, M. S., and Glazer, P. M. (2011) Hypoxia-induced epigenetic regulation and silencing of the BRCA1 promoter. *Mol. Cell. Biol.* **31**, 3339-3350
10. Lu, Y., Wajapeyee, N., Turker, M. S., and Glazer, P. M. (2014) Silencing of the DNA mismatch repair gene MLH1 induced by hypoxic stress in a pathway dependent on the histone demethylase LSD1. *Cell reports* **8**, 501-513
11. Luka, Z., Moss, F., Loukachevitch, L. V., Bornhop, D. J., and Wagner, C. (2011) Histone demethylase LSD1 is a folate-binding protein. *Biochemistry* **50**, 4750-4756
12. Li, J., Braganza, A., and Sobol, R. W. (2013) Base excision repair facilitates a functional relationship between Guanine oxidation and histone demethylation. *Antioxidants & redox signaling* **18**, 2429-2443

13. Perillo, B., Ombra, M. N., Bertoni, A., Cuozzo, C., Sacchetti, S., Sasso, A., Chiariotti, L., Malorni, A., Abbondanza, C., and Avvedimento, E. V. (2008) DNA oxidation as triggered by H3K9me2 demethylation drives estrogen-induced gene expression. *Science* **319**, 202-206

14. Amente, S., Bertoni, A., Morano, A., Lania, L., Avvedimento, E., and Majello, B. (2010) LSD1-mediated demethylation of histone H3 lysine 4 triggers Myc-induced transcription. *Oncogene* **29**, 3691-3702

15. Yang, S., Zhang, J., Zhang, Y., Wan, X., Zhang, C., Huang, X., Huang, W., Pu, H., Pei, C., and Wu, H. (2015) KDM1A triggers androgen-induced miRNA transcription via H3K4me2 demethylation and DNA oxidation. *The Prostate* **75**, 936-946

16. Neelamegam, R., Ricq, E. L., Malvaez, M., Patnaik, D., Norton, S., Carlin, S. M., Hill, I. T., Wood, M. A., Haggarty, S. J., and Hooker, J. M. (2011) Brain-penetrant LSD1 inhibitors can block memory consolidation. *ACS chemical neuroscience* **3**, 120-128

17. Dahlin, J. L., Nissink, J. W. M., Strasser, J. M., Francis, S., Higgins, L., Zhou, H., Zhang, Z., and Walters, M. A. (2015) PAINS in the assay: chemical mechanisms of assay interference and promiscuous enzymatic inhibition observed during a sulfhydryl-scavenging HTS. *J. Med. Chem.* **58**, 2091-2113

18. Baldwin, A. D., and Kiick, K. L. (2011) Tunable degradation of maleimide–thiol adducts in reducing environments. *Bioconj. Chem.* **22**, 1946-1953

19. Forneris, F., Binda, C., Vanoni, M. A., Battaglioli, E., and Mattevi, A. (2005) Human histone demethylase LSD1 reads the histone code. *J. Biol. Chem.* **280**, 41360-41365

20. Hubálek, F., Pohl, J., and Edmondson, D. E. (2003) Structural Comparison of Human Monoamine Oxidases A and B MASS SPECTROMETRY MONITORING OF CYSTEINE REACTIVITIES. *J. Biol. Chem.* **278**, 28612-28618

21. Tamai, K., Satoh, K., Tsuchida, S., Hatayama, I., Maki, T., and Sato, K. (1990) Specific inactivation of glutathione S-transferases in class Pi by SH-modifiers. *Biochem. Biophys. Res. Commun.* **167**, 331-338

22. Paulsen, C. E., and Carroll, K. S. (2013) Cysteine-mediated redox signaling: chemistry, biology, and tools for discovery. *Chemical reviews* **113**, 4633-4679

23. Rose, N. R., Thalhammer, A., Seden, P. T., Mecinović, J., and Schofield, C. J. (2009) Inhibition of the histone lysine demethylase JMJD2A by ejection of structural Zn (II). *Chemical Communications*, 6376-6378

24. Schroeder, F. A., Lewis, M. C., Fass, D. M., Wagner, F. F., Zhang, Y.-L., Hennig, K. M., Gale, J., Zhao, W.-N., Reis, S., and Barker, D. D. (2013) A selective HDAC 1/2 inhibitor modulates chromatin and gene expression in brain and alters mouse behavior in two mood-related tests. *PloS one* **8**, e71323

25. Forneris, F., Orru, R., Bonivento, D., Chiarelli, L. R., and Mattevi, A. (2009) ThermoFAD, a Thermofluor®-adapted flavin ad hoc detection system for protein folding and ligand binding. *FEBS journal* **276**, 2833-2840

26. Kaelin, W. G., and McKnight, S. L. (2013) Influence of metabolism on epigenetics and disease. *Cell* **153**, 56-69

27. Wouters, M. A., Fan, S. W., and Haworth, N. L. (2010) Disulfides as redox switches: from molecular mechanisms to functional significance. *Antioxidants & redox signaling* **12**, 53-91

28. Forneris, F., Binda, C., Adamo, A., Battaglioli, E., and Mattevi, A. (2007) Structural basis of LSD1-CoREST selectivity in histone H3 recognition. *J. Biol. Chem.* **282**, 20070-20074

29. Yang, M., Gocke, C. B., Luo, X., Borek, D., Tomchick, D. R., Machius, M., Otwinowski, Z., and Yu, H. (2006) Structural basis for CoREST-dependent demethylation of nucleosomes by the human LSD1 histone demethylase. *Mol. Cell* **23**, 377-387

30. Laurent, B., Ruitu, L., Murn, J., Hempel, K., Ferrao, R., Xiang, Y., Liu, S., Garcia, B. A., Wu, H., and Wu, F. (2015) A specific LSD1/KDM1A isoform regulates neuronal differentiation through H3K9 demethylation. *Mol. Cell* **57**, 957-970

31. Kakizawa, T., Mizukami, T., Itoh, Y., Hasegawa, M., Sasaki, R., and Suzuki, T. (2016) Evaluation of phenylcyclopropylamine compounds by enzymatic assay of lysine-specific demethylase 2 in the presence of NPAC peptide. *Bioorganic & Medicinal Chemistry Letters*

32. Jomova, K., Vondrakova, D., Lawson, M., and Valko, M. (2010) Metals, oxidative stress and neurodegenerative disorders. *Molecular and cellular biochemistry* **345**, 91-104

33. Tsaluchidu, S., Cocchi, M., Tonello, L., and Puri, B. K. (2008) Fatty acids and oxidative stress in psychiatric disorders. *BMC psychiatry* **8**, 1

34. Gómez-Santos, C., Ferrer, I., Santidrián, A. F., Barrachina, M., Gil, J., and Ambrosio, S. (2003) Dopamine induces autophagic cell death and α-synuclein increase in human neuroblastoma SH-SY5Y cells. *Journal of neuroscience research* **73**, 341-350

35. Sulzer, D., and Zecca, L. (1999) Intraneuronal dopamine-quinone synthesis: a review. *Neurotoxicity research* **1**, 181-195

36. Cyr, A. R., and Domann, F. E. (2011) The redox basis of epigenetic modifications: from mechanisms to functional consequences. *Antioxidants & redox signaling* **15**, 551-589

37. Silverman, R. B., and Zieske, P. A. (1986) Identification of the amino acid bound to the labile adduct formed during inactivation of monoamine oxidase by 1-phenylcyclopropylamine. *Biochem. Biophys. Res. Commun.* **135**, 154-159

38. Sablin, S. O., and Ramsay, R. R. (1998) Monoamine oxidase contains a redox-active disulfide. *J. Biol. Chem.* **273**, 14074-14076

39. De Colibus, L., Li, M., Binda, C., Lustig, A., Edmondson, D. E., and Mattevi, A. (2005) Three-dimensional structure of human monoamine oxidase A (MAO A): relation to the structures of rat MAO A and human MAO B. *Proceedings of the National Academy of Sciences of the United States of America* **102**, 12684-12689

40. Hayward, D., and Cole, P. (2016) LSD1 Histone Demethylase Assays and Inhibition. *Methods in Enzymology*

41. Wigle, T. J., Swinger, K. K., Campbell, J. E., Scholle, M. D., Sherrill, J., Admirand, E. A., Boriack-Sjodin, P. A., Kuntz, K. W., Chesworth, R., and Moyer, M. P. (2015) A High-Throughput Mass Spectrometry Assay Coupled with Redox Activity Testing Reduces Artifacts and False Positives in Lysine Demethylase Screening. *J. Biomol. Screen.* **20**, 810-820

42. Vintém, A. P. B., Price, N. T., Silverman, R. B., and Ramsay, R. R. (2005) Mutation of surface cysteine 374 to alanine in monoamine oxidase A alters substrate turnover and inactivation by cyclopropylamines. *Bioorganic & medicinal chemistry* **13**, 3487-3495

43. Ago, T., Liu, T., Zhai, P., Chen, W., Li, H., Molkentin, J. D., Vatner, S. F., and Sadoshima, J. (2008) A redox-dependent pathway for regulating class II HDACs and cardiac hypertrophy. *Cell* **133**, 978-993

44. Dansen, T. B., Smits, L. M., van Triest, M. H., de Keizer, P. L., van Leenen, D., Koerkamp, M. G., Szypowska, A., Meppelink, A., Brenkman, A. B., and Yodoi, J. (2009) Redox-sensitive cysteines bridge p300/CBP-mediated acetylation and FoxO4 activity. *Nat. Chem. Biol.* **5**, 664-672

45. Laitaoja, M., Tossavainen, H., Pihlajamaa, T., Valjakka, J., Viiri, K., Lohi, O., Permi, P., and Jänis, J. (2015) Redox-dependent disulfide bond formation in SAP30L corepressor protein: Implications for structure and function. *Protein Sci.*

46. Nott, A., Watson, P. M., Robinson, J. D., Crepaldi, L., and Riccio, A. (2008) S-Nitrosylation of histone deacetylase 2 induces chromatin remodelling in neurons. *Nature* **455**, 411-415

47. Doyle, K., and Fitzpatrick, F. A. (2010) Redox signaling, alkylation (carbonylation) of conserved cysteines inactivates class I histone deacetylases 1, 2, and 3 and antagonizes their transcriptional repressor function. *J. Biol. Chem.* **285**, 17417-17424

48. Go, Y.-M., and Jones, D. P. (2010) Redox control systems in the nucleus: mechanisms and functions. *Antioxidants & redox signaling* **13**, 489-509

49. Chuang, J.-Y., Chang, W.-C., and Hung, J.-J. (2011) Hydrogen peroxide induces Sp1 methylation and thereby suppresses cyclin B1 via recruitment of Suv39H1 and HDAC1 in cancer cells. *Free Radical Biol. Med.* **51**, 2309-2318

APPENDIX A

Supplementary Material

Supplementary Table A.2 Summary of thiol-reactive properties of KDM1A inhibitors
The apparent IC_{50} values after a standard demethylation assay were determined by the HRP-coupled assay and/or the RapidFire MS assay. All compounds with an IC_{50} value below 1 µM are thiol-reactive. The most potent compounds were analyzed by LC-MS to determine sulfur-contamination status. In addition, several compounds identified by screening have been previously determined to be thiol-reactive. Finally, the DTT counterscreen revealed two lower potency inhibitors of KDM1A that were not inactivated by addition of DTT. These compounds were selected for further study.

Compound ID KDM-	Synonym	Rapid Fire MS IC_{50} (µM)	HRP-coupled IC_{50} (µM)	Sulfur in LC-MS	Thiol-reactive	Inactive + DTT
094	Disulfiram	0.034	0.22	N	Y	Y
112	Sulfur	0.099	0.10	-	Y	Y
005	6049-1254	0.22	0.11	Y		-
096	STK448931	0.31	0.59	Y		-
011	E157-3451	0.36	0.38	Y		-
002	3394-0341	0.41	0.73	Y		-
037	N-Naphthylmaleimide	0.42	0.14	N	Y	Y
007	7009-0641	0.44	0.21	Y		-
113	2,2'-Dithiodipyridine	0.47	0.22	N	Y	Y
014	G786-0574	0.60	0.32	Y		-
057	Sanguinarine	1.9	0.39	N		Y
028	CB8879597	4.7	0.69	N	Y	-
012	E906-0437	6.5	2.1	N		Y
093	Benzbromarone	16	1.0	N		N
043	LDN-0114193	-	2.2	-	-	Y
015	G786-0684	-	4.3	-	-	Y
009	C202-1767	-	8.0	-	-	N
085	Nifedipine	-	11	-	-	Y
052	Amrinone	-	13	-		Y
090	LDN-0072418	-	25	-	-	Y
016	G786-0767	-	43			Y

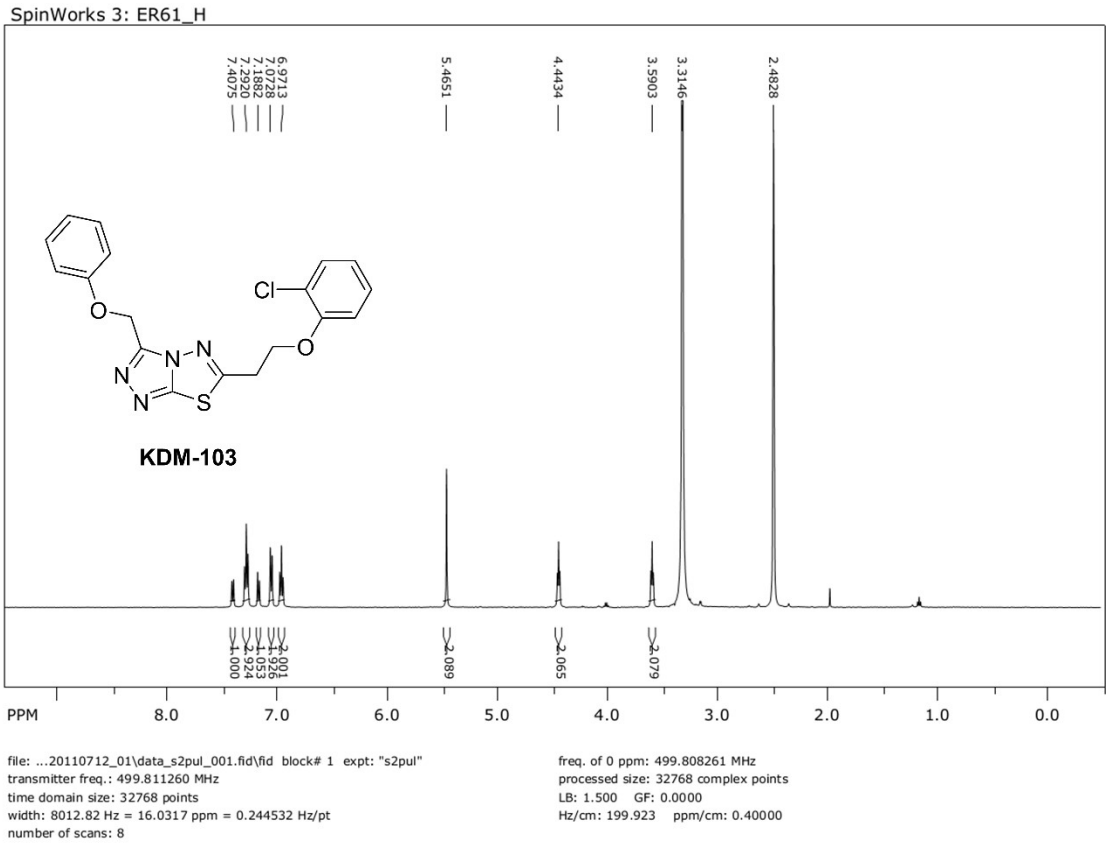

Supplementary Figure A.1 ^{1}H NMR spectrum of KDM-103

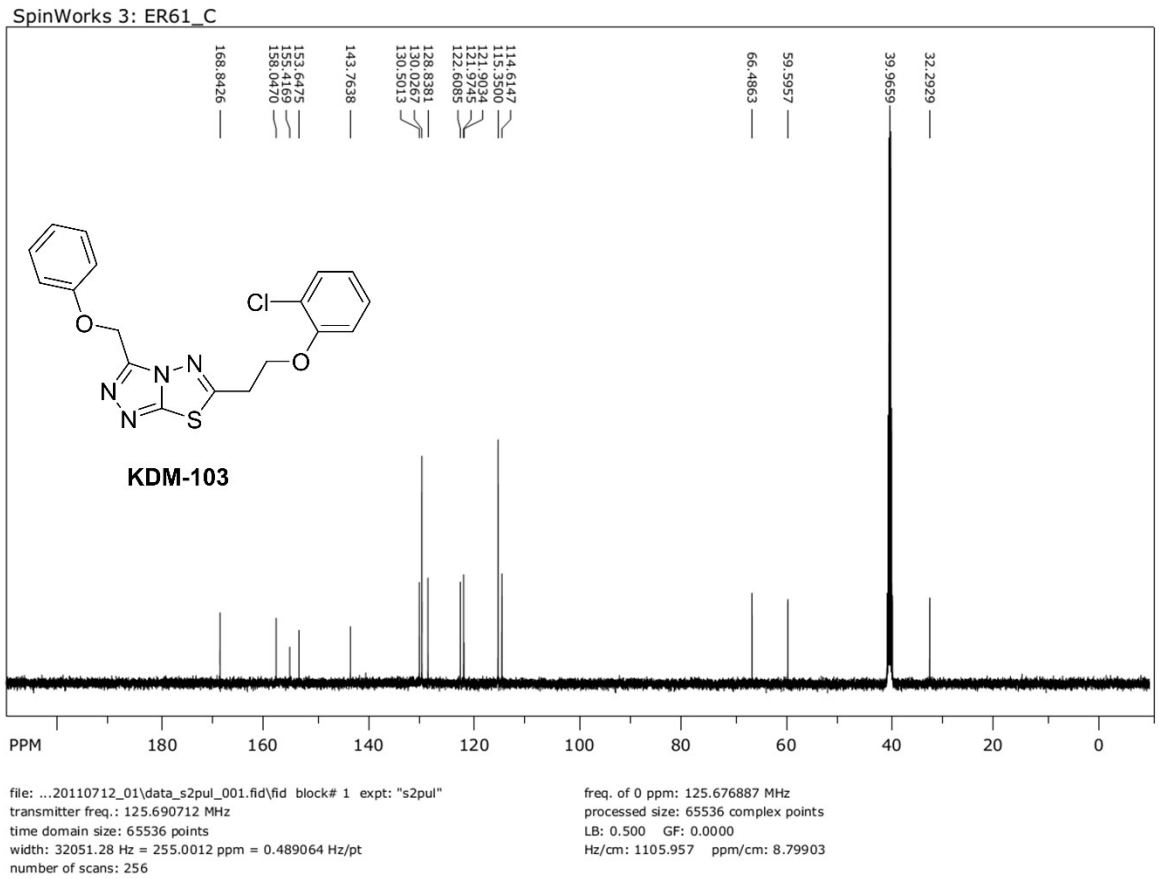

Supplementary Figure A.2 ^{13}C NMR spectrum of KDM-103

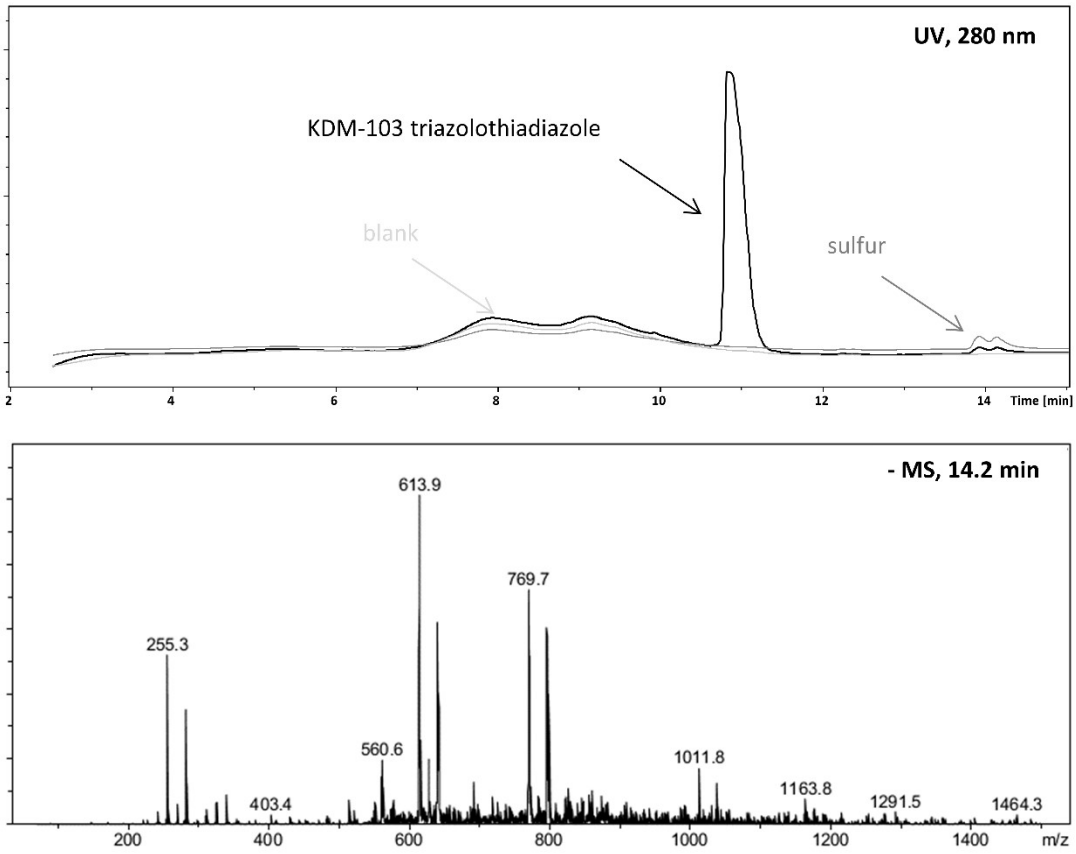

Supplementary Figure A.3 LC-MS of KDM-103 and elemental sulfur standard

Supplementary Table A.3 KDM1A tryptic peptides identified by MALDI-TOF

Samples of recombinant KDM1A were pre-treated with vehicle or 10 mM H_2O_2 followed by desalting with buffer exchange, labeling with vehicle or 10 µM Biotin-Mal, and in-gel trypsin digestion. Free cysteines were capped with iodoacetamide as part of the digestion procedure. The monoisotopic masses of the observed peptides (m/z) and their peak intensities (arbitrary units, AU) are listed for each experimental condition. The corresponding predicted peptides masses, residue numbers, and sequences are listed for each peptide that was identified.

Vehicle pre-treat - Biotin-Mal observed peaks		Vehicle pre-treat + Biotin-Mal observed peaks		H_2O_2 pre-treat + Biotin-Mal observed peaks		H_2O_2 pre-treat - Biotin-Mal observed peaks		Predicted mass	Peptide first residue	Peptide last residue	Missed Cuts	Sequence of predicted peptide
m/z	*AU*	*m/z*	*AU*	*m/z*	*AU*	*m/z*	*AU*	*m/z*				
593.4	12593	593.5	1659	593.5	3274	593.5	1015	593.3	317	321	0	(R)VATFR(K)
690.5	2218	690.4	3569	690.7	3101	691.3	3361	690.4	745	750	0	(K)ETVVSR(W)
715.6	13078	716.7	4830	715.7	4269	716.7	5174	717.4	727	732	0	(R)C(carbamidomethyl)LAILK(G)
794.8	100139	795.6	58878	794.9	68413	795.6	73198	794.5	209	214	0	(K)VFLFIR(N)
821.1	1546	821.4	2325	820.9	1545	821.6	1942	820.4	486	492	0	(R)DLTALC(carbamidomethyl)K(E)
851.7	710	852.3	1445	851.7	549	852.4	508	851.4	662	668	0	(K)VVLCFDR(V)
880.7	3394	881.2	4007	880.6	1890	881.2	2644	880.4	654	661	0	(R)MGFGNLNK(V)
903.8	31613	904.3	34539	903.8	19228	904.2	22355	903.5	252	258	0	(R)VHSYLER(H)
908.7	22983	909.1	5354	908.7	3171	909.1	10072	908.5	662	668	0	(K)VVLC(carbamidomethyl)FDR(V)
945.6	710	946.1	1201	945.8	225	946.1	352	945.5	457	463	0	(K)ELHQQYK(E)
		952.1	894									
1012.7	4108	1012.8	9695	1012.7	1876	1012.8	3172	1012.5	464	472	0	(K)EASEVKPPR(D)
1032.7	7515	1033.0	6242	1032.7	3893	1032.8	7294	1032.6	745	752	1	(K)ETVVSRWR(A)
1057.7	780	1057.8	1285	1057.8	415	1057.7	621	1057.5	751	758	1	(R)WRADPWAR(G)
1074.6	1927	1074.7	2180	1074.6	802	1074.7	1441	1074.5	609	617	0	(R)STSQTFIYK(C)
1084.6	426	1084.6	542	1084.7	261	1084.7	377	1084.5	425	432	0	(K)DEQIEHWK(K)
1094.6	1226	1094.7	2615	1094.7	733	1094.7	914					
		1104.8	1204									
1110.6	454	1110.8	858	1110.6	358	1110.7	519					
1138.6	1254	1138.6	13681	1138.6	186	1138.5	521					
1149.6	552	1149.6	3095	1149.6	206	1149.5	369					
1161.7	8914	1161.5	7769	1161.7	4601	1161.6	7599	1161.6	259	268	0	(R)HGLINFGIYK(R)
1182.8	8996	1182.7	5731	1182.7	3291	1182.6	6953					
1187.6	5082	1187.6	4476	1187.5	1992	1187.4	3926	1187.6	733	744	0	(K)GIFGSSAVPQPK(E)
1190.7	60738	1190.7	68604	1190.7	32278	1190.6	54632	1190.6	796	805	0	(R)LFFAGEHTIR(N)
		1197.4	941									
1209.6	1315	1209.6	1265	1209.5	321	1209.5	588					
1227.6	2825	1227.5	1936	1227.6	798	1227.5	1432	1227.7	217	226	0	(R)TLQLWLDNPK(I)
		1235.5	7921	1235.5	1553				662	668	0	(K)VVLC(Biotin-Mal+H_2O) FDR(V)
		1263.5	1060									
1282.5	931	1282.5	1327	1282.6	537	1282.4	706	1282.6	493	503	0	(K)EYDELAETQGK(L)
1296.6	153	1296.6	268	1296.4	147	1296.8	175	1296.6	375	384	0	(K)DEMVEQEFNR(L)
		1306.4	1250									
1318.4	154	1318.7	101	1318.2	114	1318.5	178	1317.7	259	269	1	(R)HGLINFGIYKR(I)
1344.6	536	1344.4	152	1344.7	200	1344.2	458	1344.7	437	447	1	(K)TQEELKELLNK(M)

Supplementary Table A.2, continued

Vehicle pre-treat - Biotin-Mal observed peaks		Vehicle pre-treat + Biotin-Mal observed peaks		H_2O_2 pre-treat + Biotin-Mal observed peaks		H_2O_2 pre-treat - Biotin-Mal observed peaks		Predicted mass	Peptide first residue	Peptide last residue	Missed Cuts	Sequence of predicted peptide
m/z	*AU*	*m/z*	*AU*	*m/z*	*AU*	*m/z*	*AU*	*m/z*				
1383.7	44509	1383.7	27638	1383.9	25054	1383.7	40378	1383.8	281	295	0	(K)VIIIGSGVSGLAAAR(Q)
1429.5	872	1429.5	880	1429.6	663	1429.5	915	1429.8	689	699	0	(R)GELFLFWNLYK(A)
1446.3	185	1446.2	285	1446.3	246	1446.3	371	1446.7	360	372	0	(K)C(carbamidomethyl)PLYEANGQAVPK(E)
1448.5	1891	1448.4	687	1448.4	423	1448.3	817	1448.7	422	432	1	(K)HVKDEQIEHWK(K)
1464.5	345	1464.5	510	1464.4	145	1464.4	327					
1483.5	488	1483.3	488	1483.4	327	1483.4	470	1483.7	595	608	0	(R)YTASGCEVIAVNTR(S)
1516.5	7458	1516.5	8086	1516.5	4007	1516.4	6805					
1540.6	8742	1540.7	4222	1540.5	3856	1540.6	6724	1540.7	595	608	0	(R)YTASGC(carbamidomethyl)EVIAVNTR(S)
1553.5	12734	1553.5	13089	1553.5	4005	1553.3	9239	1553.7	373	384	1	(K)EKDEMVEQEFNR(L)
1568.7	41371	1568.7	38063	1568.6	23200	1568.6	41444	1568.9	806	820	0	(R)NYPATVHGALLSGLR(E)
1569.4	59373	1569.4	58839	1569.3	35716	1569.4	59997	1569.7	373	384	1	(K)EKDEM(ox)VEQEFNR(L)
1595.6	38305	1595.6	18085	1595.7	24870	1595.7	39624	1595.8	825	838	0	(R)IADQFLGAMYTLPR(Q)
1611.5	432	1611.5	352	1611.6	480	1611.6	709	1611.8	825	838	0	(R)IADQFLGAM(ox)YTLPR(Q)
		1625.5	265									
1690.6	4500	1690.6	2134	1690.6	4923	1690.5	5935					
1707.5	4570	1707.4	1105	1707.5	2198	1707.5	3239	1707.9	296	310	0	(R)QLQSFGMDVTLLEAR(D)
1801.7	681	1801.6	184	1801.6	551	1801.7	730					
1806.4	1007	1806.4	223	1806.3	550	1806.3	794	1805.9	569	585	0	(R)NGYSC(carbamidomethyl)VPVALAEGLDIK(L)
1829.3	199	1829.4	178	1829.2	92.4	1829.4	108	1829.0	727	744	1	(R)CLAILKGIFGSSAVPQPK(E)
1843.6	516	1843.6	271	1843.6	419	1843.5	398					
		1849.6	916					1849.9	595	608	0	(R)YTASGC(Biotin-Mal)EVIAVNTR(S)
1865.3	384	1866.2	311	1866.3	267	1865.8	324	1866.9	592	608	1	(R)QVRYTASGCEVIAVNTR(S)
1860.5	700	1860.4	725	1860.5	617	1860.4	723	1861.0	632	647	0	(K)QQPPAVQFVPPLPEWK(T)
		1894.1	497									
1918.4	40185	1918.5	37626	1918.4	22291	1918.4	38827	1918.0	508	524	0	(K)LQELEANPPSDVYLSSR(D)
1939.3	100	1939.6	85	1939.4	63.8	1939.5	73	1939.0	457	472	1	(K)ELHQQYKEASEVKPPR(D)
		2015.8	222									
2025.4	145	2025.2	36.3	2025.3	57.2	2025.2	76.9	2025.0	821	838	1	(R)EAGRIADQFLGAM(ox)YTLPR(Q)

Supplementary Table A.2, continued

Vehicle pre-treat - Biotin-Mal observed peaks		Vehicle pre-treat + Biotin-Mal observed peaks		H_2O_2 pre-treat + Biotin-Mal observed peaks		H_2O_2 pre-treat - Biotin-Mal observed peaks		Predicted mass	Peptide first residue	Peptide last residue	Missed Cuts	Sequence of predicted peptide
m/z	*AU*	*m/z*	*AU*	*m/z*	*AU*	*m/z*	*AU*	*m/z*				
		2088.6	438									
2177.9	10172	2177.8	2025	2177.5	7027	2177.5	6835	2177.1	669	688	0	(R)VFWDPSVNLFGHVGSTTASR(G)
2193.5	1241	2193.5	1195	2193.5	1677	2193.6	2124					
2205.6	12177	2205.9	2149	2205.5	5708	2205.5	5590	2205.0	551	568	0	(K)HWDQDDDFEFTGSHLTVR(N)
2221.5	1946	2221.8	3323	2221.4	1793	2221.6	3028					
2269.8	5137	2269.9	331	2269.7	1765	2269.8	5163					
2326.7	2128	2326.8	270	2326.6	966	2326.5	976					
2337.4	1081	2337.7	284	2337.5	299	2337.4	647	2337.1	188	208	0	(R)MTSQEAAC(carbamidomethyl)FPDIISGPQQTQK(V)
2342.8	756	2342.7	446	2342.5	739	2342.6	913					
2353.4	76.1	2353.4	44.6	2353.3	41.1	2353.4	61.8	2353.1	188	208	0	(R)M(ox)TSQEAAC(carbamidomethyl)FPDIISGPQQTQK(V)
2358.4	607	2358.1	391	2357.8	561	2357.5	666					
2420.4	85.2	2420.5	77.7	2420.4	99.3	2420.3	101	2420.2	323	347	0	(K)GNYVADLGAMVVTGLGGNPMAVVSK(Q)
2548.5	148	2548.6	117	2548.4	159	2548.6	188	2548.3	322	347	1	(R)KGNYVADLGAMVVTGLGGNPMAVVSK(Q)
		2664.7	294	2664.5	76.9			2664.2	188	208	0	(R)MTSQEAAC(Biotin-Mal+H2O)FPDIISGPQQTQK(V)
2708.1	2033	2708.0	587	2708.3	1363	2707.8	2288	2707.5	700	726	0	(K)APILLALVAGEAAGIMENISDDVIVGR(C)
2724.0	73	2724.4	59.4	2724.4	69.9	2724.1	110	2723.5	700	726	0	(K)APILLALVAGEAAGIM(ox)ENISDDVIVGR(C)
2730.1	188	2730.0	79.4	2730.1	125	2729.6	216	2729.4	527	550	0	(R)QILDWHFANLEFANATPLSTLSLK(H)
2887.8	6449	2887.5	4004	2887.7	5669	2887.5	9540	2886.5	227	251	0	(K)IQLTFEATLQQLEAPYNSDTVLVHR(V)
3286.6	11.1	3285.4	47	3285.8	11	3286.9	9.66	3286.8	618	647	1	(K)CDAVLCTLPLGVLKQQPPAVQFVPPLPEWK(T)

Supplementary Table A.4 Summary of sequence coverage of KDM1A tryptic peptides.
Bolded residues correspond to tryptic peptides observed by MALDI-TOF. Strikethrough residues are absent in the truncated recombinant protein. Cysteine residues are highlighted.

10	20	30	40	50
~~MLSGKKAAAA~~	~~AAAAAAAATG~~	~~TEAGPGTAGG~~	~~SENGSEVAAQ~~	~~PAGLSGPAEV~~
60	70	80	90	100
~~GPGAVGERTP~~	~~RKKEPPRASP~~	~~PGGLAEPPGS~~	~~AGPQAGPTVV~~	~~PGSATPMETG~~
110	120	130	140	150
~~IAETPEGRRT~~	~~SRRKRAKVEY~~	~~REMDESLANL~~	~~SEDEYYSEEE~~	~~RNAKAEKEKK~~
160	170	180	190	200
~~LPPPPPQAPP~~	EEENESEPEE	PSGVEGAAFQ	SRLPHDR**MTS**	**QEAACFPDII**
210	220	230	240	250
SGPQQTQKVF	**LFIRNRTLQL**	**WLDNPKIQLT**	**FEATLQQLEA**	**PYNSDTVLVH**
260	270	280	290	300
RVHSYLERHG	**LINFGIYKR**I	KPLPTKKTGK	**VIIIGSGVSG**	**LAAARQLQSF**
310	320	330	340	350
GMDVTLLEAR	DRVGGR**VATF**	**RKGNYVADLG**	**AMVVTGLGGN**	**PMAVVSK**QVN
360	370	380	390	400
MELAKIKQ**KC**	**PLYEANGQAV**	**PKEKDEMVEQ**	**EFNR**LLEATS	YLSHQLDFNV
410	420	430	440	450
LNNKPVSLGQ	ALEVVIQLQE	K**HVKDEQIEH**	**WK**KIVK**TQEE**	**LKELLNKM**VN
460	470	480	490	500
LKEKIK**ELHQ**	**QYKEASEVKP**	**PR**DITAEFLV	KSKHR**DLTAL**	**CKEYDELAET**
510	520	530	540	550
QGKLEEK**LQE**	**LEANPPSDVY**	**LSSR**DR**QILD**	**WHFANLEFAN**	**ATPLSTLSLK**
560	570	580	590	600
HWDQDDDFEF	**TGSHLTVRNG**	**YSCVPVALAE**	**GLDIK**LNTAV	R**QVRYTASGC**
610	620	630	640	650
EVIAVNTRST	**SQTFIYKCDA**	**VLCTLPLGVL**	**KQQPPAVQFV**	**PPLPEWK**TSA
660	670	680	690	700
VQR**MGFGNLN**	**KVVLCFDRVF**	**WDPSVNLFGH**	**VGSTTASRGE**	**LFLFWNLYKA**
710	720	730	740	750
PILLALVAGE	**AAGIMENISD**	**DVIVGRCLAI**	**LKGIFGSSAV**	**PQPKETVVSR**
760	770	780	790	800
WRADPWARGS	YSYVAAGSSG	NDYDLMAQPI	TPGPSIPGAP	QPIPR**LFFAG**
810	820	830	840	850
EHTIRNYPAT	**VHGALLSGLR**	**EAGRIADQFL**	**GAMYTLPR**QA	TPGVPAQQSP
852				
SM				